APPROVAL SHEET

Title of Dissertation: Synthesis, Characterization, and Plasmonic Enhancement of Fluorescent Carbon Nanodots

Name of Candidate: Rachel Danielle Schmitz
Doctor of Philosophy, 2016

Dissertation and Abstract Approved: _____
Dr. Christopher Geddes
Professor
Chemistry and Biochemistry

Date Approved: _____

# ABSTRACT


| | |
|---|---|
| Title of Document: | SYNTHESIS, CHARACTERIZATION, AND PLASMONIC ENHANCEMENT OF FLUORESCENT CARBON NANODOTS.<br><br>Rachel Danielle Schmitz, Doctor of Philosophy, 2016. |
| Directed By: | Dr. Christopher Geddes,<br>Professor of Chemistry and Biochemistry.<br>Director of Institute of Fluorescence. |



Carbon nanodots are fluorescent nanoparticles that have unique photophysical properties that make them ideal candidates as luminescent probes for various fields of study. Although the synthetic routes of carbon nanodots have been extensively investigated, many of them produce carbon nanodots with low fluorescence quantum yields and/or require surface modifications to obtain fluorescent nanoparticles. This research discusses the development of a combustion-based method to synthesize carbon nanodots along with the characterizations and modifications of the nanodots photophysical properties.

First, the synthetic aspect of this research investigated two combustion-based synthetic pathways of the carbon nanodots. The first pathway (candle-based) utilized the oxidation of candle soot with nitric acid followed by multiple neutralization and separation steps that resulted in carbon nanodots with low quantum yields (~2%). The second pathway (methane-based), utilizing methane gas, produced, and collected the carbon nanodots directly from a flame, which resulted in significantly less experimental time and carbon nanodots with higher quantum yields (~30%). The

photophysical characterizations of the synthesized carbon nanodots revealed an excitation wavelength dependent fluorescence, a broad absorption, good photostability, and complex intensity decays.

The photophysical properties of the methane-based nanodots were further investigated for a more in-depth understanding of the fluorescence-based structural architecture, utilizing fluorescence quenching methods. These experiments revealed that the fluorescence quenching of the nanodots can occur through both dynamic and static quenching mechanisms depending on the type of quencher utilized. Also, these experiments helped to elucidate the origin of the luminescence of carbon nanodots.

While carrying out the quenching experiments, a novel temperature dependent fluorescence property was observed and analyzed, which showed an increase of the emission intensity as a function of increased temperatures.

The last aspect of this research was intended to modify the carbon nanodots with bromide for the generation of singlet oxygen ($^1O_2$) and to utilize Metal-Enhanced Fluorescence (MEF) to improve the fluorescence and phosphorescence signals from the nanodots. The bromination experiments revealed that the brominated carbon nanodots had some phosphorescence character and could generate low amounts (~1-4%) of singlet oxygen. The MEF experiments showed that both the fluorescence and phosphorescence signal of carbon nanodots could be enhanced when in the presences of silver nanoparticles.

# SYNTHESIS, CHARACTERIZATION, AND PLASMONIC ENHANCEMENT OF FLUORESCENT CARBON NANODOTS.

By

Rachel Danielle Schmitz

Dissertation submitted to the Faculty of the Graduate School of the
University of Maryland, Baltimore County, in partial fulfillment
of the requirements for the degree of
Doctor of Philosophy
2016

# Dedication

To my sister, Leah, and to my husband, Michael, who both supported and encouraged me through my dissertation. I love you both with all that I am.

# Acknowledgements

I would like to thank my mentor, Dr. Chris Geddes for his support and guidance while completing my work. I would not be where I am today without your expertise and encouragement. Also, thank you to Dr. Lisa Kelly, Dr. Katherine Seley-Radtke, Dr. Marie-Christine Daniel-Onuta and Dr. Richard Thompson, for your support, encouragement, and expertise throughout my dissertation. You all have helped me become a better scientist by imparting your knowledge and wisdom to me over the past 5 years.

I would like to thank past and present members of the Geddes lab and the Institute of Fluorescence. I greatly appreciate Dr. Johan Melendez, Tonya Santaus and Buddha Mali for all their help and support over the past 5 years. Thank you all for being there when I needed it the most. I do not believe I could have survived this journey without any of you.

Also, I would like to thank all the faculty and staff of the chemistry department and the graduate students who have helped throughout my thesis. Especially, thank you to Dr. Lauren Schoukroun-Barnes, DeLauren McCauley, and Nicole Carbonaro, all of whom supported, listened, and encouraged me since the very beginning.

Finally, thank you to all my family and friends who have been by my side through everything and supported and pushed me to become the best scientist I can be. I would not be here today without all your love and encouragement.

# Table of Contents

# List of Tables

# List of Figures

# List of Acronyms and Symbols

| | |
|---|---|
| AUC | Area Under the Curve |
| DLS | Dynamic Light Scattering |
| DF | Delayed Fluorescence |
| FRET | Forster Resonance Energy Transfer |
| FT-IR | Fourier Transform Infrared |
| FWHM | Full Width, Half Maximum |
| IC | Internal Conversion |
| IRF | Instrument Response Function |
| ISC | Intersystem crossing |
| MB | Methylene Blue |
| MEF | Metal-Enhanced Fluorescence |
| MEF EVE | Metal-Enhanced Fluorescence Excitation Volumetric Effect |
| MEP | Metal-Enhanced Phosphorescence |
| P | Phosphorescence |
| PEG | Polyethylene glycol |
| RPM | Rotations Per Minute |
| SG | Singlet Oxygen Sensor Green Reagent |
| TADF | Thermally Activated Delayed Fluorescence |
| TCSP | Time-Correlated Single Photon Counting |
| UV | Ultra-violet |
| Vis | Visible |
| Z | Atomic Number |
| $^1O_2$ | Singlet Oxygen |
| $\lambda$ | Wavelength |
| $S_n$ | Singlet Energy State |
| $v_n$ | Vibrational energy state |
| $T_n$ | Triplet Energy State |
| $\Phi$ | Quantum Yield |
| $\tau$ | Lifetime |
| $\bar{\tau}$ | Average Lifetime |
| r | Anisotropy |
| $k_q$ | Biomolecular quenching constant |
| $^3O_2$ | Molecular Oxygen |
| $X^2$ | Chi-Squared, Goodness of Fit |
| $\eta$ | Viscosity |
| $\Delta G_{ST}$ | Singlet-Triplet State Energy Gap |

# Chapter 1: Introduction and Motivation

## 1.1 Overview

Carbon nanodots are a new class of carbon-based nanomaterials that were discovered in 2004 from purified carbon nanotubes by Scrivens *et al.*[1] Carbon nanodots are naturally fluorescent nanoparticles that have several unique photophysical characteristics, which make them an attractive and versatile as luminescent probes for many techniques in biomedicine and analytics over the traditional quantum dots or organic fluorophores.[2–12] These nanodots are typically less than 10 nm in diameter, display excitation wavelength dependent emission, demonstrate little to no toxicity in cells and can be synthesized using a variety of approaches.[2–6] However, the carbon nanodots synthesized in many of the approaches tend to have low quantum yields (< 10%) and/or require surface modification in order to have emissive properties.[2–5] This thesis is subsequently focused on the development of a simple and inexpensive combustion method to synthesize carbon nanodots, characterization the optical properties, and modification the nanodots to further enhance their optical properties.

To accomplish the synthetic aspect of this research, two pathways of synthesis of carbon nanodots are investigated and discussed in Chapters 2 and 3. Also, detailed within these two chapters are several fluorescence-based characterizations, which are used to help understand the possible origin of luminescence of the synthesized nanodots. Chapter 4 is focused on a more in-depth understanding of the fluorescence-based structural architecture of the nanodots by utilizing fluorescence quenching

methods. While carrying out the experiments described in Chapter 4, a novel temperature dependent fluorescence property was observed and is detailed in Chapter 5. Chapter 6 and 7 of this research are intended to discuss the modification of carbon nanodots with bromide for the generation of singlet oxygen ($^1O_2$), by increasing the triplet character of the nanodots, and the usage of Metal-Enhanced Fluorescence (MEF) to improve the fluorescence and phosphorescence signals from the nanodots, respectively.

## 1.2 Carbon Nanodots

Carbon nanodots are quasi-spherical shaped carbon-based nanomaterials that have been extensively studied since their discovery in 2004.[1–5,9–36] Carbon nanodots display many attractive features that have made them of great interest to researchers compared to quantum dots or organic fluorophores.[2–5] For example, their surface composition, believed to be composed of organic compounds and carboxylic acid groups, confers their water solubility and allows for surface functionalization with other molecules.[1–5,9–36] Also, carbon nanodots can be inexpensively synthesized and are thought to have a natural bio-compatibility and potentially low cell toxicity; however, the unique fluorescence characteristics are reported to be their most notable feature.[1–5,9–36] Carbon nanodots' fluorescence has been shown to be excitation wavelength dependent, highly photostable coupled with generally low quantum yields and multifaceted lifetimes.[1–5,9–36] All these features make carbon nanodots an attractive new option for applications in the analytical and biomedical fields.

Carbon nanodots were discovered by Scriven, *et al*. in 2004, when they were trying to purify single walled carbon nanotubes by gel electrophoresis, which were

produced from the arc-discharge soot.[1] When analyzing the gels, they noted three distinct bands, one of which was fluorescent when exposed to UV light.[1] The fluorescent material was shown to contain size-dependent fluorescent properties that were further separated into three colored bands.[1] After this first report of carbon nanodots, there has been extensive literature reporting on the various synthetic methods and the characterization of these novel fluorophores.

### *1.2.1 Synthesis of Carbon Nanodots*

Several methods to synthesize carbon nanodots, which are genreally organized into *Top-Down* and *Bottom-Up* approaches, have been previously described.[2–5] Top-down approaches involve producing carbon nanodots from a larger carbon substrate whereas bottom-up approaches create carbon nanodots from a molecular precursor.[2] Since the synthetic methods of carbon nanodots have been extensively described, only three methods from each of the top-down and bottom-up approaches will be discussed here. Figure 1.1 illustrates these six synthetic methods, with the right side (laser ablation, electrochemical, and arc-discharge) representing the top-down pathway and the left side (microwave, thermal, and combustion) representing the bottom-up pathways.

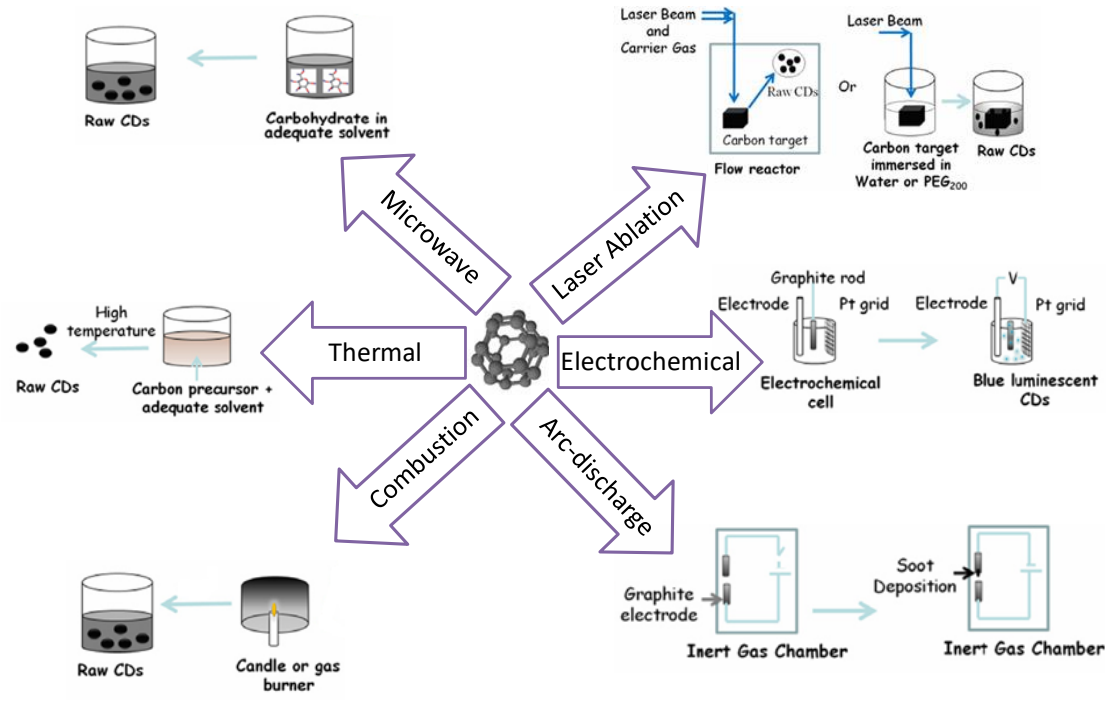


**Figure 1.1** The various top-down and bottom-up synthetic approaches to produce carbon nanodots. Bottom-Up approaches are shown on the right and Top-Down approaches on the left. Adapted from reference 4.

## Top-Down Approaches

The arc discharge method involves the vaporization of graphite electrodes by passing a current through the electrodes creating an arc between them.[1–5] The resulting soot from the vaporization was oxidized with nitric acid, neutralized and size separated by electrophoresis.[1] The resulting nanodots exhibited size-dependent fluorescent properties, when molecular weight cut-off filtration devices were used.[1–4]

Laser ablation synthesis involves the breaking down of a carbon target with a high-powered laser. The resulting product was oxidized with nitric acid and then an organic compound, such as polyethylene glycol (PEG), was added, to modify the surface of the resulting carbon nanodots.[2–5,11,12,22,23,30,31] Electrochemical synthesis generates carbon nanodots from an electrochemical cell that contains the carbon

source, as an electrode (graphite rod or carbon nanotube), reference electrode and electrolyte solution.[2–5,16,20,23–25,32] Both synthetic routes resulted in small sized carbon nanodots that had excitation wavelength dependent emission and low quantum yields (< 10%).[2–5,11,12,22,23,37]

Overall, the top-down approaches produced small fluorescent carbon nanodots that exhibit excitation wavelength dependent emission, good photostability, and relatively low quantum yields.[2–5] Along with these top-down methods, bottom-up approaches have been successful in synthesizing carbon nanodots.

**Bottom-Up Approaches**

Microwave and thermal syntheses are both one step processes that use high temperatures to produce carbon nanodots. For the microwave synthesis, a carbon source and an organic molecule, used for surface modification, are combined together and then exposed to microwaves for a set time period.[17,18,28,35–37] The resulting carbon nanodots displayed size and fluorescence properties that were related to the microwave exposure time.[2–5,18,28,35–37] Thermal methods involve similar methodology to the microwave synthesis, but thermal methods use higher temperatures (>200°C) instead of microwaves to produce carbon nanodots.[2–5,26,27,29] The carbon nanodots produced by this method displayed small diameters, 5-20 nm, and fluorescence that was excitation-wavelength dependent.[17,26,27,29,38] The final synthetic approach and the one employed in this research is the combustion method.

The combustion method involves the use of a carbon soot that is reacted with nitric acid followed by neutralization and purification of the carbon nanodot solution.[2–5,13,15,19,21,29,39–41] The carbon soot can be obtained from activated carbon,

natural gas burners, oil lamps, or candles[2–5,13,15,19,21,29,39–41] Ray, *et al*. and Liu, *et al.* both used candle soot to produce fluorescent carbon nanodots but vary in their purification processes.[13,15] Ray, *et al* uses a series of dilutions and centrifugation to purify the nanodots,[13] whereas Liu, *et al.* reported the use of an electrophoretic process to purify the carbon nanodots.[15] Both authors reported < 10 nm sized particles, excitation wavelength dependence emission of the carbon nanodots, and low quantum yields.[13,15]

One of the disadvantages of both the top-down and bottom-up methods is that the carbon nanodots produced have relatively low quantum yields, as previously reported. However, other groups have reported increased quantum yield after modification of carbon nanodot's surface by organic molecules.[1–4,13,15,22,23] Even with the increase in quantum yield following surface modification, the quantum yields are still relatively low (< 10%).[1–4,13,15,22,23] Therefore, there is a need for a synthetic method that can produce carbon nanodots with higher quantum yields without requiring a surface modification.

### *1.2.2 Origin of Carbon Nanodots' Luminescence*

The origin of the luminescence for carbon nanodots has not been elucidated, but the reported literature supports the notion that the synthetic method employed can influence the luminescence properties.[2,3,5,6,42,43] The luminescence properties were thought to be due to either size, different emissive sites/traps with a core structure, or multiple emissive centers on the surface of the carbon nanodots, but recent research suggests that the luminescence can originate from a combination of two mechanisms: core/surface traps and molecular fluorophores.[5,6,42–47]

The size-dependent emission of semiconductor nanoparticles is a well-known process, referred to as electron-hole recombination. This mechanism occurs when an electron from the valence band is excited to the conduction band causing a hole in the valence band and radiative recombination occurs to annihilate the resulting hole.[4,6,48] This mechanism is how all semiconductor nanoparticles emit light and is characterized by size-dependent emission, a narrow emission band and excitation wavelength independent emission.[6,48] Since carbon nanodots are not semiconductors and do not tend to display all these properties, this mechanism is less probable for the luminescence of carbon nanodots.

The next probable mechanism of fluorescence for carbon nanodots is the presence of surface traps on the nanodots. This emission mechanism is due to two sequential emission processes with different sources: the core and surface structures (impurities, surface defects, functional groups) of carbon nanodots.[5,6,47] Like the recombination mechanism, an electron/hole pair is formed from the core, but the pair can become trapped on the surface structures causing the radiative recombination to occur at longer wavelengths. This mechanism is typically characterized by excitation-wavelength dependent emission and broad emission bands.[6] Another possible mechanism of luminescence is the presence of multiple emissive centers (molecular fluorophores) on the surface of the carbon nanodots. This mechanism is generally characterized by excitation wavelength dependent emission and very broad emissive bands as well.[6]

The synthetic method utilized to produce the carbon nanodots can be used to distinguish between the surface traps and multiple emissive centers mechanisms.

According to Cayuela, *et al*, the presence of multiple emissive centers occurs from bottom-up approaches at low temperatures (<200°C), while the formation of a core structure only starts to arise at temperatures greater than 230°C.[5,6,42] However, it is possible to have a combination of both mechanisms (surface traps and emissive centers) present, depending on the synthetic route utilized.[5,6,42] Therefore, it can be concluded that the luminescence origins of carbon nanodots significantly depend on the synthetic method, conditions used during the synthesis, and the functionalization of the nanodots surface.

## 1.3 Photophysical Theory

To understand the characterization analysis that will be discussed in this research, a fundamental understanding of the theory of photophysical processes is necessary. This section will discuss the general background theory of the three photophysical processes of interest to this research notably, absorption, fluorescence, and phosphorescence.

### *1.3.1 Absorption*

Absorption occurs when a photon causes an electron to be promoted from the ground-state to the excited-state. The transitions between energy states (ground and excited-state) occur instantaneously ($10^{-15}$ s), which is not enough time for the nuclei to be displaced and is the reason why vertical lines are used to show the transition between energy states (Frank-Condon principle).[49–52]

To measure this transition, the absorption spectrum of a molecule is recorded using an UV-Vis spectrophotometer. This instrument measures the intensity of light

before and after it is passed through the sample over a wavelength range resulting in an absorbance (y-axis) versus wavelength (x-axis) plot. This plot reveals the range of wavelengths at which the respective molecule can absorb light, which can ultimately result in fluorescence. Absorption can also give information on concentration (c) and molar absorption coefficient (ε) through Beer-Lambert law (A=εcb). A block diagram of this instrument is shown in Figure 1.2.[49–52]

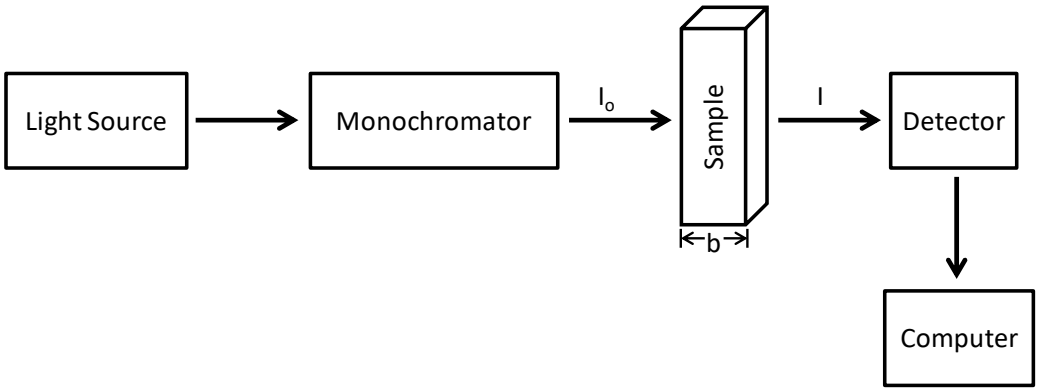


**Figure 1.2** Block diagram of general UV-Vis spectroscopy, where $I_o$ and I are the intensity of light before and after absorption, b is the path length of the sample. The arrows show the path the light travels in the instrument.

Along with absorption, the incident light can also be either scattered in an elastic or inelastic manner. The majority of the light is scattered at the same frequency as the incident light (elastic) but, some of the light can be scattered at different frequencies (inelastic).[53] Elastic scattering includes Rayleigh and Mie scattering, in which Rayleigh scattering occurs from molecules that are smaller than the wavelength (λ) of the photons and shows a $\lambda^{-4}$ dependence. In contrast, Mie scattering occurs from molecules that are same size or larger than the wavelength of photons used for excitation.[54] Raman scattering is an example of inelastic scattering, in which the light scattered occurs at longer wavelengths (Stokes scattering) or

shorter wavelengths (anti-Stokes scattering) than the incident light.[53] Rayleigh and Raman scatter can be spectral artifacts in this research, as they can be observed in the absorption or emission spectrum of the carbon nanodots synthesized, respectively, within this research.

### *1.3.2 Fluorescence*

Fluorescence is a spontaneous process where a photon of light is emitted from the lowest vibrational level of the excited-state (predominantly $S_1$ but occasionally a higher state) of a fluorophore, following the absorption of light.[49–52] Figure 1.3 is a Jablonski diagram that depicts some of the photophysical process that a fluorophore can undergo after the absorption of a photon. There are non-radiative and radiative pathways, which can deactivate the excited-state ($S_1$) of a fluorophore. Non-radiative pathways include internal conversion (IC) and intersystem crossing (ISC), whereas radiative pathways include fluorescence, delayed fluorescence, and phosphorescence and are characterized by the emission of a photon.[49–52]

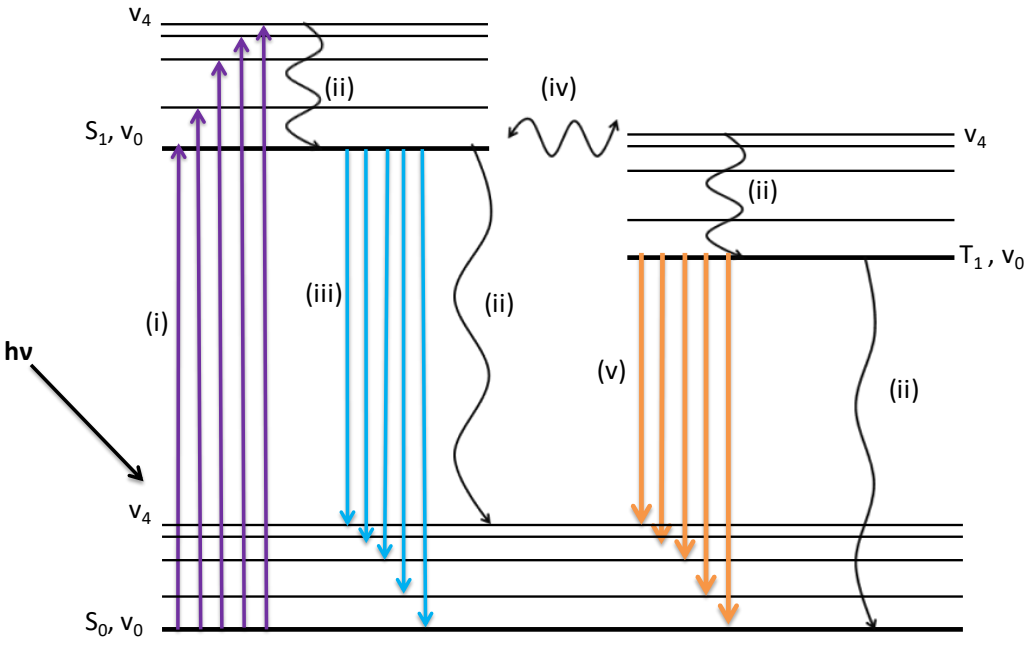


**Figure 1.3** Jablonski diagram of photophysical processes. (i) absorption, (ii) internal conversion, (iii) fluorescence, (iv) intersystem crossing, (v) phosphorescence. The ground-state, singlet and triplet excited-states are noted as $S_o$, $S_1$, and $T_1$ respectively and the vibrational energy levels within each state are labeled as $v_{0\text{-}4}$.

Immediately after absorption (i), rapid relaxation ($10^{-12}$ s) of the electron to the lowest vibrational energy state ($v_0$) of the $S_1$ occurs through IC.[49–52] From the $S_1$, $v_0$ state, the emission of a photon (fluorescence) can occur to any of the vibrational energy states of the $S_0$ at a slower rate ($10^{-9}$ s).[49–52] Overall, there is a loss of energy due to the relaxation from higher vibrational energy levels to the lowest vibrational energy level, which is the reason why fluorescence occurs at longer wavelengths than the absorption process (Stokes' shift).[49–52] Another general property of fluorescence is described by Kasha's rule, which states that fluorescence occurs from the lowest excited-state of a fluorophore ($S_1v_0$).[49–51] This means the fluorescence emission spectrum of a fluorophore will be observed no matter the wavelength of excitation making the emission spectrum independent of excitation wavelength, in essence the fluorescence spectrum is a mirror image of the absorption band of least frequency.[49–51]

Fluorescence quantum yield and lifetimes are two significant measurable characteristics of a fluorophore. Quantum yield (Φ) is denoted as a ratio of the number of photons emitted per photons absorbed, with the brightest fluorophore having quantum yield near unity (1).[49–52,55,56] Lifetimes (τ) reveal the time a fluorophore can exist in the excited-state ($S_1$), prior to its depopulation to the ground-state ($S_0$), which determines the time for possible excited-state interaction between fluorophore and the environment.[49–52] Equations 1.1 and 1.2 define quantum yield and lifetime:

$$\Phi = \frac{k_F}{k_{NR} + k_F} \quad \textbf{(1.1)}$$

$$\tau = \frac{1}{k_{NR} + k_F} \quad \textbf{(1.2)}$$

where $k_F$ is the fluorescence radiative rate constant of the fluorophore and $k_{NR}$ is the non-radiative rate constant.[49–52] Both rate constants depopulate the $S_1$ state and in order to have a quantum yield near unity, the $k_{NR}$ must be significantly smaller than $k_F$.[49–51] It is important to note that a fluorophore with longer fluorescence lifetime has more time to interact with their surrounding environment, which makes them more susceptible to non-radiative deactivation processes such as photobleaching and diffusional quenching.[49–51]

Fluorescence anisotropy is another important variable that can be readily measured. This measurement can reveal information on the size and shape of a molecule and the viscosity of the environment.[49–51] Anisotropy is based on this

selective absorption of light by a fluorophore based on its transition moment.[49–51] When a solution of randomly oriented fluorophores is excited with polarized light, it results in a partially polarized emission from the fluorophores. Anisotropy (r) is defined as

$$r = \frac{I_{\parallel} - I_{\perp}}{I_{\parallel} + 2I_{\perp}} \qquad \textbf{(1.3)}$$

where $I_{\parallel}$ and $I_{\perp}$ are the fluorescence intensities of the vertical and horizontally polarized emission, respectively.[49–51]

There are two temporal techniques used to collect the fluorescence data described: steady-state and time-resolved.[49,51,52] Steady-state measurements use constant illumination and average over all times, while the emission spectrum or intensity is recorded.[49–52] Time-resolved measurements use a pulsed illumination source whose duration is much smaller than the decay time of the fluorophore, which allows for lifetime and anisotropy decays to be measured in a time dependent manner.[49–52] Figures 1.4 and 1.5 show block diagrams of steady-state and time-resolved instrumentation in this research. Both types of instrument will be utilized to characterize the photophysical properties of the carbon nanodots synthesized in this research.

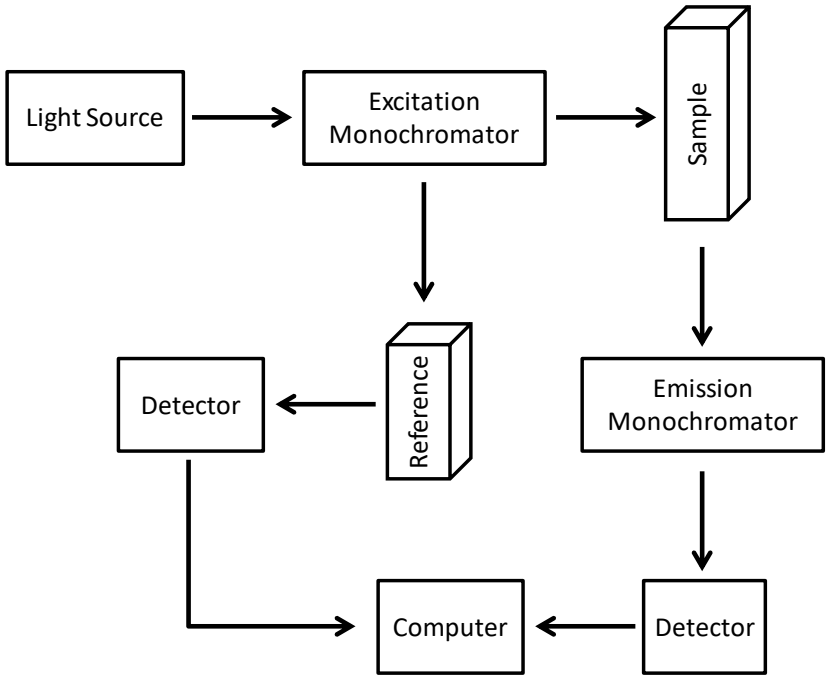


**Figure 1.4** Block diagram of general steady-state fluorescence spectroscopy.

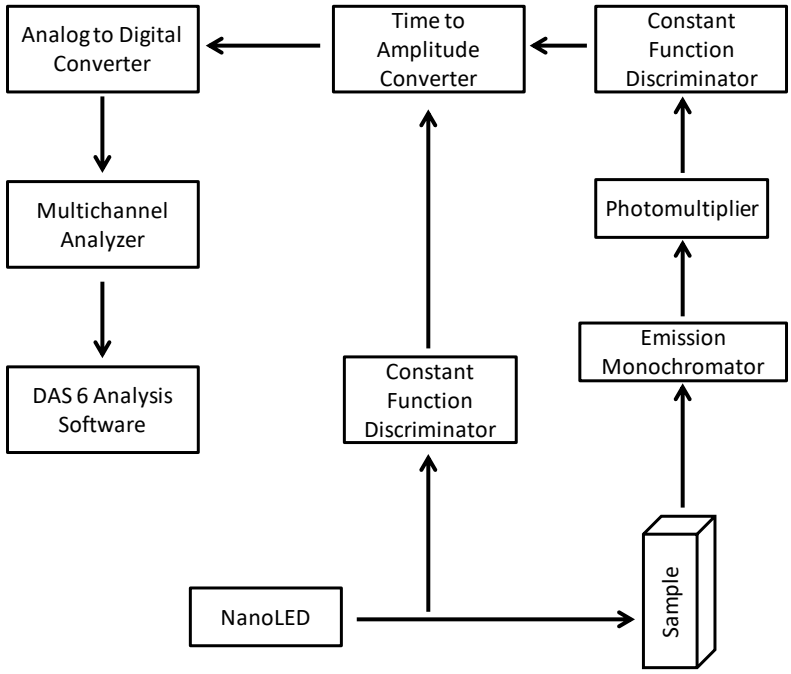


**Figure 1.5** Block diagram of time-resolved Time-Correlated Single Photon Counting (TCSP) fluorescence spectroscopy.

### *1.3.3 Fluorescence Quenching*

In addition to the previously described deactivation processes (1.3.2), the excited states of a fluorophore can be deactivated by bimolecular processes, known as quenching. [49–51,57] Quenching occurs mainly by dynamic (collisional) and static (ion-pair or molecular association) quenching mechanisms. Dynamic quenching is a diffusion controlled process that happens when an excited fluorophore collides with another molecule called a quencher.[49–51,57] Following the collision with a quencher, the fluorophore returns to the ground-state without emitting a photon.[49–51,57] Figure 1.6 shows this mechanism through a modified Jablonski diagram.

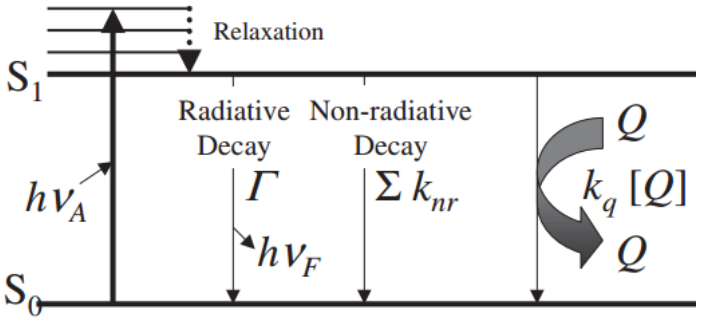


**Figure 1.6** Modified Jablonski diagram show dynamic quenching in relation to fluorescence ($h\nu_F$) and non-radiative pathways ($k_{NR}$). Where $k_q$ is the bimolecular rate constant and [Q] is the quencher concentration. Modified from reference 45.

In its simplest form, dynamic (collisional) quenching is described by the Stern-Volmer equation:[49–51,57]

$$\frac{I_0}{I} = 1 + k_q \tau_0 [Q] = 1 + K_{sv}[Q] \qquad \textbf{(1.4)}$$

where $I_0$ and I are the fluorescence intensities in absence and presence of quencher (Q), respectively, $k_q$ is the biomolecular quenching constant, $\tau_0$ is the lifetime of the

fluorophore in absence of quencher, [Q] is the concentration of quencher and $K_{SV}$ is the Stern-Volmer constant.[49–51,57] Stern-Volmer plots are typically presented as $I_0/I$ versus [Q], with the linearity of plots representing a single class of fluorophore being accessible to a single quencher. However, some deviations from linearity can be caused by presence of two fluorophore populations, where one is not accessible to the quencher.[49–51,57] This is usually seen as a deviation towards the x-axis.[49–51,57]

Static quenching occurs by the formation of a non-fluorescent ground-state complex between the fluorophore and quencher.[49–51,57] In this mechanism, the Stern-Volmer constant is considered an association constant for the complex formation as described by

$$\frac{I_0}{I} = 1 + K_s[Q] \qquad K_s = \frac{[F-Q]}{[F][Q]} \qquad \textbf{(1.5)}$$

where $K_S$ is the association constant, [Q] is quencher concentration, [F-Q] is the complex concentration, [F] is the fluorophore concentration.[49–51,57] The Stern-Volmer plot for static quenching is the same as dynamic quenching. It is important to acknowledge that both dynamic and static quenching can result in a linear plot of $I_0/I$ versus [Q] and by further analyzing the fluorescence lifetimes, differentiation between the two mechanism can be made. Dynamic quenching causes a decrease in fluorescence lifetimes, as the $S_1$ state is depopulated quicker, whereas static quenching does not typically affect a fluorophore's lifetime.[49–51,57] Chapter 4 will discuss the use of fluorescence quenching to determine structural and emission properties of carbon nanodots.

### *1.3.4 Metal-Enhanced Fluorescence (MEF)*

Metal-Enhanced Fluorescence (MEF) is a near-field fluorescence phenomenon that challenges both our basic thinking and principles of classical fluorescence.[58] In MEF, when a fluorophore comes into close proximity to noble metal nanoparticles, the fluorophore can be coupled in both the excited and ground-state to the surface plasmon electrons of the nanoparticles.[33,49,58–69] This ultimately results in the non-radiative energy transfer from the fluorophore to the surface plasmons (a mirror dipole), which rapidly radiate the coupled quanta themselves. Similar to classical fluorescence, which involves both an absorption and emission event, MEF is underpinned also by two main processes: an *enhanced absorption* and an *enhanced emission*. [58–60,65,67,70–72]

The enhanced absorption is a function of the increased electric field surrounding and in between metal nanoparticles.[58–60,65,67,70–74] When the fluorophore is in close proximity with these electric fields, the fluorophore effectively absorbs more light, in essence the fluorophore-metal absorption cross section is significantly increased leading to an increased excitation rate.[58–60,65,67,70–72] The enhanced emission is due to coupling and subsequent energy transfer from the fluorophore to the nanoparticles, followed by the nanoparticles radiating the energy through their scattering mode, i.e. radiating the coupled quanta. Since the nanoparticles emit the light usually under very favorable and rapid conditions, the resulting emission signal is enhanced.[58–60,65,67,70–72] Figure 1.7 illustrates the mechanism of MEF, highlighting the enhanced absorption and emission, as compared to classical far-field fluorescence.

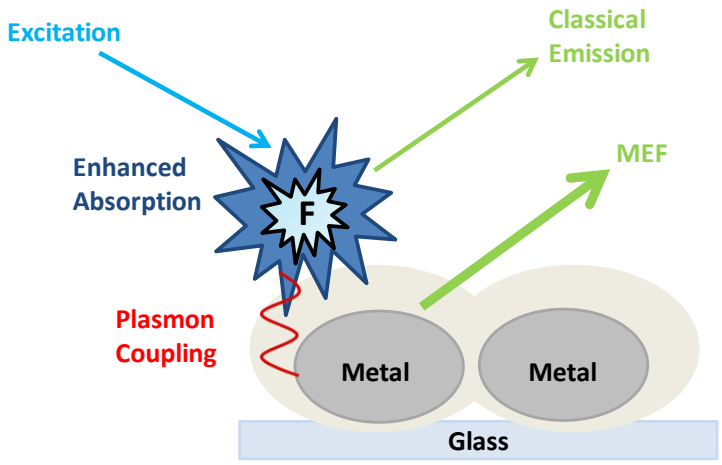


**Figure 1.7** Metal-enhance fluorescence diagram showing the enhanced absorption and emission (MEF) from a fluorophore in close proximity (~10 nm) to metal nanoparticles. Adapted from reference 58.

As a result of MEF, the coupled system fluorescence quantum yield (Φ) is increased and the fluorescence lifetime (τ) decreased, ultimately improving the photostability of the fluorophore.[58–60,65,67,70–72] The increase in the systems' fluorescence quantum yield can be thought as being due to the addition of a very rapid secondary radiative pathway due to the coupled system, $k_m$. The quantum yield, as previously described, is the number of photons emitted versus the number of photons absorbed and the addition of this new radiative pathway, $k_m$, increases the number of photons emitted, thus leading to an increase in the coupled system quantum yield. The fluorescence lifetime is inversely influenced by $k_m$ because of the addition of a new deactivation pathway of the excited-state. The fluorescence quantum yield and lifetime equations, 1.1 and 1.2, are modified by the addition of this secondary radiative pathway ($k_m$). The coupled systems' fluorescence quantum yields and lifetime equations are described by:

$$\Phi_m = \frac{k_F + k_m}{k_{NR} + k_F + k_m} \quad \textbf{(1.6)}$$

$$\tau_m = \frac{1}{k_{NR} + k_F + k_m} \quad \textbf{(1.7)}$$

where $k_F$ is the fluorescence rate constant of the fluorophore, $k_m$ is the coupled system (fluorophore + metal) fluorescence rate constant and $k_{NR}$ is the non-radiative rate constant. It has been hypothesized that the coupled system may have some influence on the non-radiative pathways as well as the radiative pathways.[58] Therefore, the $k_{NR}$ rate constant also represents the non-radiative pathways for the coupled system along with the other traditional, non-radiative pathways seen in fluorescence, i.e., internal conversion and intersystem crossing.

Some other notable properties of MEF are the wavelength dependence, distance dependence, and MEF Excitation Volumetric Effect (MEF EVE).[59,65,69,71,72,75,76] MEF is a wavelength dependent process that results from the overlap of the fluorophore's absorption and emission spectra with the absorption and scattering spectra of the metal nanoparticles.[59] Having good overlap of the spectra results in an increase of the MEF enhancement factor.[59,71] The need for the overlap of spectra for MEF is similar to that of the donor and acceptor pair in Forster Resonance Energy Transfer (FRET).[58,59] Also, the MEF enhancement factor is wavelength dependent and correlates with the scattering spectrum of the nanoparticles.[59,71,72] The distance between the fluorophore and metal nanoparticles is crucial as a result of the varying electric fields around the nanoparticles.[59,69,71,75] It has also been demonstrated that the electric fields around the nanoparticles are influenced by increasing power of

the excitation source through MEF EVE.[75] The increase in power results in an increase of the electric fields around the nanoparticles leading to a greater enhancement of signal.[75]

MEF has been reported in the literature to enhance the emission of different fluorophores, including carbon nanodots produced by laser ablation.[33] The laser ablated carbon nanodots showed an increased emission signal (10x) and photostability and a decrease lifetime when near-to silver nanoparticle coated surfaces.[33] Metal-enhanced phosphorescence (MEP) has also been reported to occur when a phosphorescent fluorophore is within close proximity to metal nanoparticles.[66–70] Zhang *et al.* and Mishra *et al.* reported MEP from Rose Bengal at low temperatures and eosin in glycerol when in close proximity to silver nanoparticles.[67,68] MEF appears to be a suitable method to enhance the emissive signals and in some cases the phosphorescence signal of fluorophores.

#### *1.3.5 Phosphorescence*

Phosphorescence is an emissive process that typically occurs from an excited triplet state ($T_1$) of a fluorophore to a singlet ground state ($S_0$) (Figure 1.3, v).[49–52] After absorption, the electron relaxes to lower vibrational levels of the $S_1$ state, however, instead of fluorescence, the electron can intersystem cross (ISC) into the triplet excited-state ($T_1$), if the energy gap is favorable between the singlet and triplet states.[49–51] Once in the $T_1$ state, the electron relaxes to the lowest vibrational level of the $T_1$ from where emission of a photon can occur (phosphorescence).[49–51] Due to ISC and IC, phosphorescence is a longer-lived process than fluorescence ($10^{-3}$ s as compared to $10^{-9}$s) and it is further Stokes' shifted than fluorescence because of the

loss of energy.[49–51] Phosphorescence typically happens from molecules that contain halides such as bromine and iodine because these atoms facilitate intersystem crossing from singlet state to the triplet state, the so called "Heavy atom effect".[49–51] Phosphorescence spectra are collected on a steady-state spectrofluorometer, but the instrument has to operate in a phosphorescence mode. This mode uses a pulsed light source and off-gated collection time to prevent the fluorescence spectrum from being collected, essentially the phosphorescence is collected after the fluorescence has decayed away. Figure 1.8 shows the typical data acquisition process and times for phosphorescence measurements in the spectrofluorometer.

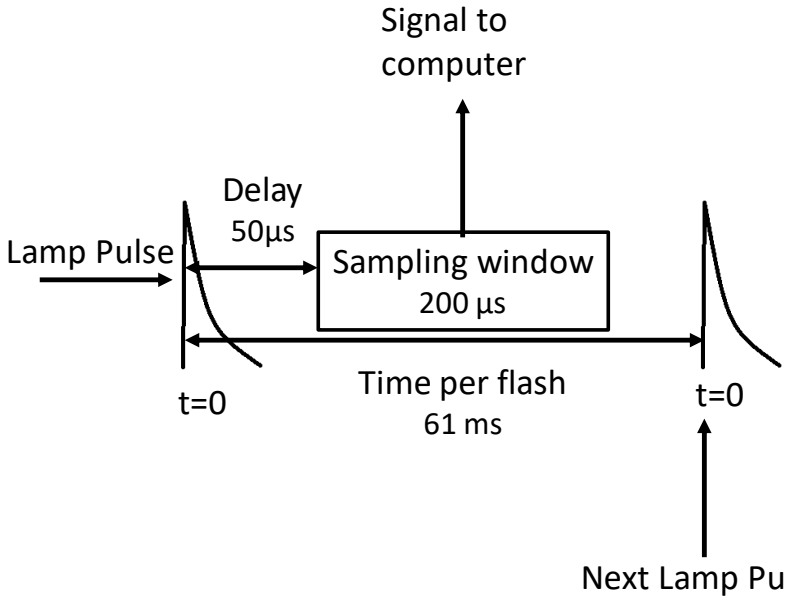


**Figure 1.8** Sequence of data acquisition for phosphorescence spectrum. The delay is time between the start of the lamp pulse and start of sample widow (~50 µs). Sampling window is time the signal is counted and measured. Time per flash is cycle length between lamp pulses.

### *1.3.6 Singlet Oxygen*

Molecular oxygen ($^3O_2$) has been of interest because of its unique electronic structure and the role it plays in life maintenance and destruction.[77–82] Unlike many

molecules, the ground-state for molecular oxygen is a triplet state and it has two excited singlet states, where the lowest excited-state generates singlet oxygen ($^1O_2$).[77–79,83] Singlet oxygen is a highly reactive species that can react in biological systems causing cell death, which is one of the main reasons it is of interest within this research.[77,79] Production of $^1O_2$ can be accomplished in a variety of ways but for this research the method of electronic energy transfer from the excited-state of fluorophore (sensitizer) to molecular oxygen will be investigated. This method, known as photosensitization, is shown in the modified Jablonski diagram in Figure 1.9. Generally, a fluorophore in the triplet state interacts with molecular oxygen resulting in an energy transfer from the fluorophore to the oxygen, generating $^1O_2$.[77,79,83]

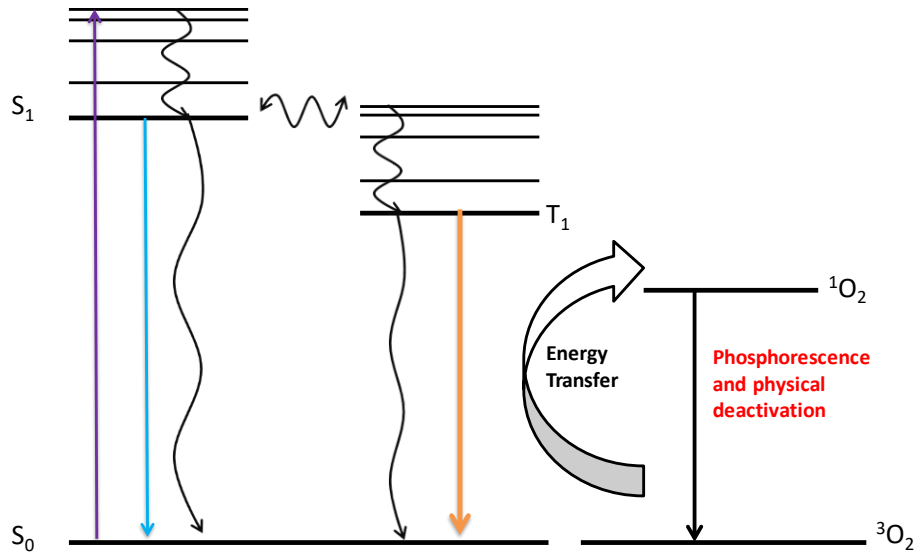


**Figure 1.9** Modified Jablonski diagram showing the production of singlet oxygen, $^1O_2$.

Detection of singlet oxygen can be accomplished by monitoring the phosphorescence emission of the $^1O_2$ state ($^1\Delta_g$) or by using a fluorescent probe that is specific for $^1O_2$.[77,79] The phosphorescence of the singlet oxygen is monitored at 1270 nm and is typically a weak signal.[68,77–79] The fluorescent probes usually have an emission signal in the visible region that can readily be detected by optical molecular detectors such as Singlet oxygen sensor green (SG). When in solution, the emission signal of SG is weak but in the presence of singlet oxygen, the emission signal is increased due to a structural change i.e., an un-quenching of the molecular fluorophore.[68,77–79] Figure 1.9 shows SG emission and structure in the absence and presence of singlet oxygen. For this research, SG combined with carbon nanodots will be used to study the $^1O_2$ generation.

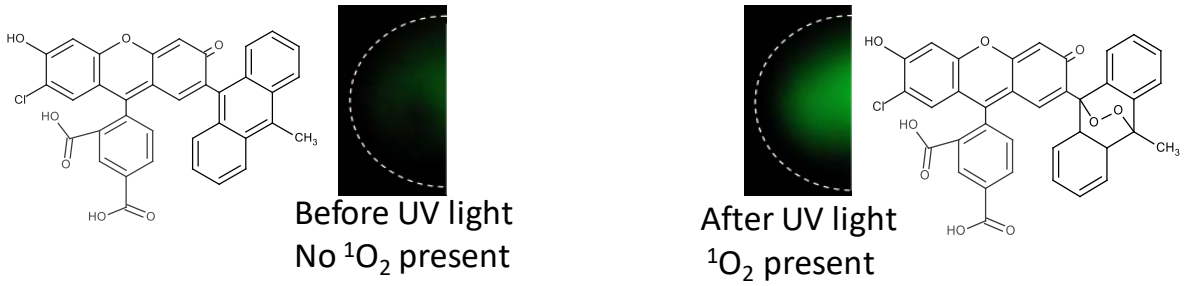


**Figure 1.10** (A) Singlet oxygen sensor green (SG) reagent before UV light exposure and no $^1O_2$ present. (B) SG after UV light exposure and $^1O_2$ present. Adapted from 59.

# Chapter 2: Synthesis and Photophysical Characterization of Candle-Based Carbon Nanodots

## 2.1 Introduction

Carbon nanodots can be synthesized from various pathways as seen in Chapter 1, but some of the pathways required surface passivation in order to obtain fluorescent nanodots and all of the pathways produced carbon nanodots with low quantum yields.[2–5] This research is focused on using the combustion pathway, via oxidation of candle soot, because it is a simple, straightforward, and cost-effective method to synthesize carbon nanodots. Carbon nanodots have been previously synthesized from candle soot by oxidizing the soot with nitric acid for 12 hours followed by multiple neutralization and purification steps.[13,15] This chapter aims to discuss the synthesis of carbon nanodots by two similar combustion methods utilizing candle soot, followed by the analysis of the photophysical properties of the resulting nanodots.

The two synthetic methods described herein involved the oxidation of candle soot with nitric acid for 12 hours, but utilize different approaches for the neutralization of the carbon nanodots. The first method was completed by following a previously published protocol by Ray, *et al*.[13] This method was used to gain an understanding of the synthetic procedures and the photophysical properties of the carbon nanodots. However, while replicating the procedures from Ray, *et al*, there was difficultly in reproducing experimental procedures and photophysical properties previously observed of these carbon nanodots. Also, the experimental procedures

involved multiple steps, were time-consuming and required multiple solvents to neutralize and separate, based on size, the carbon nanodots. These limitations led to the development of a second combustion-based synthesis approach aimed at reducing and simplifying the neutralization and size separation steps. The synthesis of carbon nanodots using the two-described methods, along with the analysis of the photophysical properties of the resulting carbon nanodots will be discussed in this chapter.

## 2.2 Experimental Details

### *2.2.1 Synthesis of Candle-Based Carbon Nanodots via Ray and co-workers*[13]

***Candle Soot Collection.*** Candle soot was collected by burning a white, unscented wax candle for several hours and using a Pyrex container to collect the soot as shown in Figure 2.1. The Pyrex container was cool to room temperature and then the soot was removed from the container using a metal spatula. The soot was stored in a 20-mL glass vial until needed.


**Figure 2.1** Experimental set-up for candle soot collection.

***Synthesis.*** Candle soot (25 mg) was combined with 15 mL of 5 M nitric acid ($HNO_3$, Sigma Aldrich, St. Louis, MO) in a three-necked round bottom flask. The solution was then refluxed for 12 hours at 100°C with the aid of magnetic stirring. Figure 2.2 shows the reflux experimental setup. After the reflux, the solution was allowed to cool overnight to room temperature and 12 mL of solution was recovered. The solution was then aliquoted into two 6 mL portions for neutralization and size separation as described below.

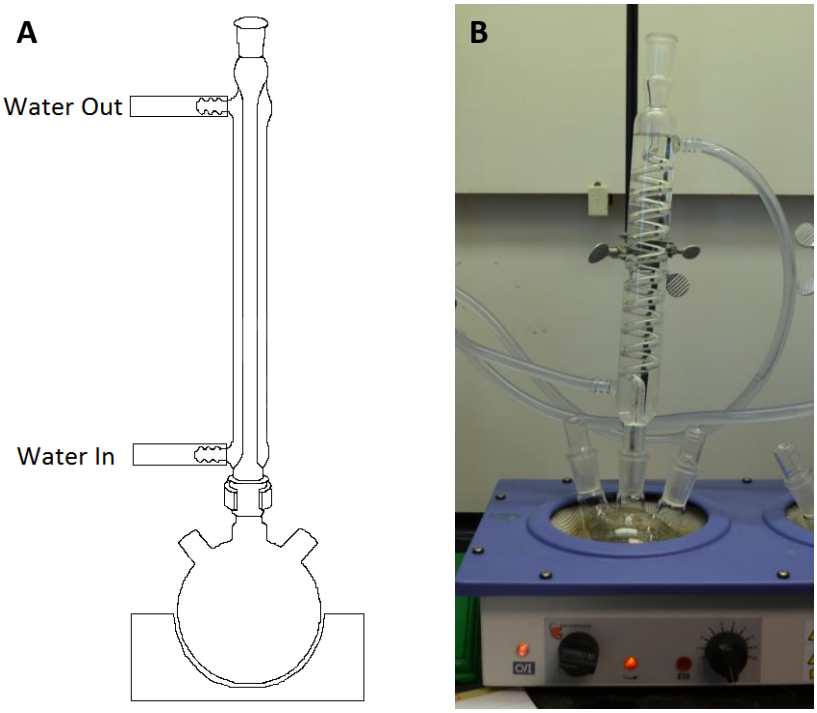


**Figure 2.2** A) Cartoon depiction of candle carbon nanodot reflux and B) Photograph of candle carbon nanodot reflux experimental set-up.

***Neutralization.*** This first aliquot of the refluxed solution (6 mL) was transferred to a 15-mL centrifuge tube and centrifuged at 3,000 RPM (1,046 RCF) for 10 minutes to separate the un-reacted candle soot from the solution. The supernatant (5.5 mL) was carefully removed using a pipette and placed in a 50-mL centrifuge tube and mixed with 3:1 ratio of acetone/water solution (16.5 mL acetone: 5.5 mL water). The resulting solution was divided into two centrifuge tubes and centrifuged at 14,000 RPM (24,446 RCF) for 10 minutes. Approximately 10 mL of the neutralized solution was taken from each centrifuge tube and used to separate the carbon nanodots by size as described below.

***Size Separation.*** The neutralized carbon nanodot solution was size separated at four centrifugation speeds with the aid of a water/ethanol/chloroform (1:1:3 ratio) solvent mixture. The solution was sequentially separated using the four centrifugation speeds (4,000/1,860, 5,000/2,907, 6,000/4,186, and 8,000/7,441 RPM/RCF), using the supernatant from the previous separation as the solution for next centrifugation. For example, the supernatant from the 4,000 RPM was used for 5,000 RPM centrifugation. The neutralized solution was aliquoted into two 5 mL portions and combined with the water/chloroform/ethanol solution (5 mL/5 mL/15 mL) followed by size separation as described in Figure 2.3. The resulting four solutions (each centrifugation speed) contained the fluorescent carbon nanodots. Photophysical characterizations were examined on each of the centrifugation fractions.

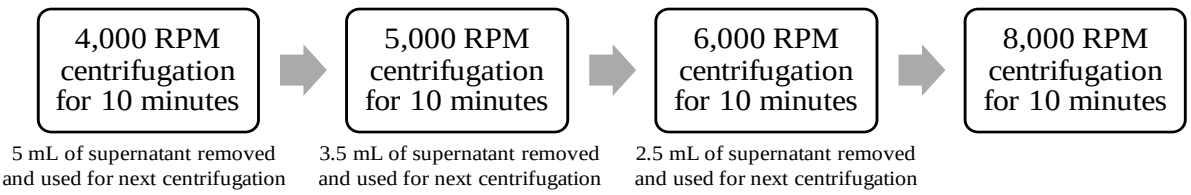


**Figure 2.3** Flow diagram of the size separation methods used for carbon nanodots synthesis via Ray, *et al.*[13]

### *2.2.2 Adapted Synthesis of Candle-Based Carbon Nanodots*

This section describes the second combustion-based approach used to synthesize carbon nanodots. Candle carbon nanodots were synthesized following the same procedures described in the previous section, however the neutralization and size separations methods were modified to reduce the number of steps and time required to obtain carbon nanodots.

***Synthesis.*** Briefly, 25 mg of candle soot was mixed with 15 mL of 5M $HNO_3$ in a three-necked round bottom flask and the resulting solution was refluxed for 12 hours at 100°C with magnetic stirring as shown in Figure 2.2. The solution was cooled overnight and 12 mL of a solution was collected and neutralized and separated as described below.

***Neutralization with NaOH.*** Neutralization of carbon nanodots was achieved by using two sodium hydroxide (NaOH) solutions, ~0.8 M and ~4 M, and universal indicator to assess the pH (Sigma Aldrich, St. Louis, MO). Two 50 mL burettes were used to titrate 0.8 M and 4 M of NaOH into 5 mL of the refluxed solution. After each addition of the base, the pH was tested with universal indicator, in a centrifugation tube, by adding one drop of solution to two drops of indicator and this process was repeated until a neutral pH (green indicator color) was achieved. After neutralization, the solution was stored over night at 4°C and the pH was re-tested the following day. To acquire enough sample for the size separation, the neutralization process was completed on the second 5 mL portion of refluxed sample.

***Size Separation by Centrifugation.*** The neutralized carbon nanodot solution was first size separated by utilizing four different centrifugation speeds: 3,000, 5,000, 10,000,

and 14,500 RPM (1,046, 2,907, 11, 627, and 24,446 RCF). The neutralized solution (two 4 mL portions divided in two centrifugation tubes) was centrifuged at each centrifugation speed three times to remove un-reacted soot.

Briefly, the first centrifugation was for 10 minutes then the supernatant was transferred to a new centrifugation tube and re-centrifuged for second 10 minutes. Following the second centrifugation, the supernatant was transferred again and centrifuged, for the third time, for 20 minutes. The two 10-minute centrifugations were used separated out un-reacted soot from the carbon nanodots and the 20-minute centrifugation was carried out to ensure that all un-reacted particles were removed. The four speeds were used to size separate the carbon nanodots, where the highest speed (14,500/24,446 RPM/RCF) would contain the smaller sized nanodots. After the last centrifugation (20-minute), the resulting solution contained the neutralized and size separated carbon nanodots.

***Size Separation with a Column.*** A secondary size separation method of carbon nanodots, after centrifugation, was completed using GE Healthcare PD midiTrap G-25 sample preparation columns (Exclusion limit of 5,000 $M_r$, Thermo Fisher Scientific, Waltham, MA). The columns were washed with water over night to ensure that all the preserving fluid was removed from the column. After washing, 1 mL of carbon nanodot solution was added to the column and eluted with water. The filtration was monitored by UV-light (365 nm) and 0.5-1 mL fractions were collected from the column over an hour and half period. The fluorescence properties of all the fractions were undertaken in a 1 mm quartz cuvette.

### *2.2.3 Photophysical Characterization of Candle-Based Carbon Nanodots*

***Absorption Measurements.*** Absorption measurements were carried out on a Cary 50 UV-Vis spectrophotometer (Agilent Technologies, Santa Clara, CA) equipped with a full spectrum xenon pulse lamp (190-1100 nm). Samples and solvent blanks (water) were measured in a 1-cm quartz or glass cuvette with a scan rate of 300 nm/min**.**

***Steady-State Fluorescence.*** Steady-state fluorescence measurements were carried out on a FluoroMax-4 or FluoroMax-4P spectrofluorometer (Horiba Scientific, Edison, NJ). The instrument was equipped with ozone-free xenon arc lamp, R928P photon counting photomultiplier tube for emission and a reference photodiode for lamp output monitoring. Experiments were undertaken using the FluorEssence software with samples measured in 1-cm glass or quartz cuvette. All spectra were corrected for the lamp by setting the software to divide the signal of the sample by the reference signal ($S_1/R_1$). The excitation and emission monochromators were adjusted to obtain the appropriate wavelengths to collect emission data from an excitation wavelength range of 300 nm to 700 nm.

***Time-Resolved Fluorescence.*** Time-resolved fluorescence intensity decays were obtained using the reverse start-stop time-correlated single photon counting (TCSPC) technique on a FluoroCube system™ (Horiba Scientific, Edison, NJ). An instrument response function (IRF) was taken using a dilute scattering solution of Ludox® AS-30 colloidal silica. The IRF and carbon nanodot samples were excited using NanoLEDs™ centered at 311, 351 and 474 nm, (Horiba Scientific, Edison, NJ) and the emission wavelength was selected with a monochromator. Subsequently the signal was detected on a TBX-04 detector (Horiba Scientific, Edison, NJ).

The IRF times of 800, 700, and 900 ps were determined by using the full width, half maximum (FWHM) of the IRF decay at the NanoLEDs$^{TM}$ 311, 351, and 474 nm, respectively. Table 2.1 shows the system hardware parameters used for the IRF and decay of carbon nanodots when using 311 nm NanoLED$^{TM}$ light source. The same parameters were used for all the light sources with only the monochromator settings changing.

**Table 2.1** Typical experimental parameters for time-resolved fluorescence decay measurements for the Instrument response function (IRF) and carbon nanodots excited with 311 nm NanoLED$^{TM}$.

| Parameter | IRF | Carbon Nanodots |
|---|---|---|
| Emission Monochromator | 311 nm | 450 nm |
| Excitation Polarizer | 0° | 0° |
| Emission Polarizer | 54.75° | 54.75° |
| TAC Range | 50 ns | 50 ns |
| Counts | 10,000 | 10,000 |
| Repetition Rate | 1 MHz | 1 MHz |

Decay traces were taken on the DataStation V 2.7.2 software and the fitting of the decays were completed using the DAS 6 Analysis software. The emission intensity decays were described, as shown in equation 2.1, by a sum of exponential terms

$$i(t) = \sum_{i=1}^{k} \alpha_i \exp\left(-\frac{t}{\tau_i}\right) \quad \textbf{(2.1)}$$

where k is the number of fluorescence decay components in the total decay function, $\alpha_i$ are the amplitudes, with their sum totaling to 1.0, and $\tau_i$ are the decay times. The fractional contribution of each component to the steady-state intensity is given as

$$f_i = \frac{\alpha_i \tau_i}{\sum_j \alpha_j \tau_j} \quad \textbf{(2.2)}$$

The mean lifetime of the carbon nanodot's excited-state was calculated using the equation 2.3.

$$\bar{\tau} = \sum_i f_i \tau_i \quad \textbf{(2.3)}$$

The values of the amplitudes and decay times were determined using nonlinear least-squares impulse re-convolution with a goodness-of-fit $\chi^2$ criterion.

***Maximum Entropy Method Analysis.*** The maximum entropy method was performed using a sequential quadratic programming method written in C-code.[84–86] For stability of the fitting algorithm (goodness of fit), the time-resolved data was collected to 100,000 counts at the peak of the fluorescence decay ($\lambda_{ex}$ = 474 nm and $\lambda_{em}$= 530 nm).

***Photostability Measurements.*** Photostability measurements were collected on a black polystyrene 96-well plate (Thermo Fisher Scientific, Waltham, MA) using either a 473 nm or 532 nm laser line (Lasermate, Walnut, CA) connected to an OceanOptics spectrometer utilizing the SpectraSuite software, through a bi-truncated 600 µM, 0.22

NA optical fiber. The spectra were taken in the strip graph setting with an integrated time of 50 ms and wavelength max at 583.74 nm. For each laser source, the appropriate notch or laser line filter was used to remove the excitation from the emission signal. 80 µL of carbon nanodot solution was analyzed for 20 minutes with each laser line.

***Elemental Analysis.*** Elemental analysis was carried out by Atlantic Microlab, Inc. (Norcross, GA). Carbon nanodots samples were dried in an oven at 40°C for one week. The dried samples (5-10 mg) were stored in glass vials and sent for analysis. However, it appeared that the samples were un-combustible based on the low, inconsistent results obtained.

***Quantum Yield.*** Relative free-space quantum yields were determined by comparing the corrected integrated emission intensity, optical density, and refractive index of the carbon nanodots to a suitable reference in 1 cm quartz cuvette at 20°C. The reference fluorophore used was quinine sulfate (0.1M $H_2SO_4$, $\lambda_{ex}$= 350 nm). The optical densities of the references and carbon nanodots were matched at the excitation wavelength (350 nm) and the steady-state emission spectra were integrated using SigmaPlot™ 11.0 software. Quantum yields were calculated using equation 2.5 where Φ is the quantum yield, I is the integrated emission intensity, OD is the optical density and n is the refractive index for carbon nanodots (CD) and reference (R), respectively.[49–51,56]

$$\Phi_{CD} = \Phi_R \left(\frac{I_{CD}}{I_R}\right)\left(\frac{OD_R}{OD_R}\right)\left(\frac{n_{CD}^2}{n_R^2}\right) \qquad \textbf{(2.5)}$$

## 2.3 Results and Discussion

### *2.3.1 Synthesis of Candle-Based Carbon Nanodots via Ray and co-workers.*[13]

In order to gain an understanding of the synthesis and photophysical properties, the protocol described in section 2.2.1 was utilized. After the reflux and first centrifugation at 3,000 RPM, the carbon nanodot solution showed an orange fluorescence under UV light, whereas Ray, *et al.*, [13] reported a green emission from their solution (Figure 2.5). These differences could be attributed to carbon nanodots with different photophysical properties being formed during the oxidation of the soot. As previously described, carbon nanodots can be generated in a variety of pathways, all of which produce slightly different luminescent particles.

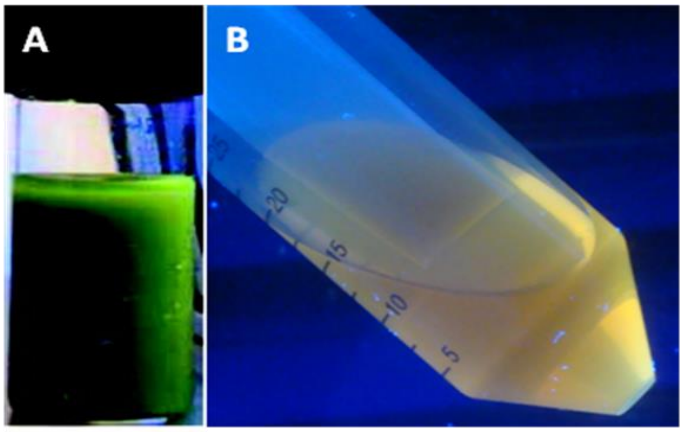


**Figure 2.4** Comparison of carbon nanodots synthesized from the oxidation of candle soot by A) Ray and co-workers and B) this research. Adapted from reference 7.

The separation methods described by Ray, *et al.*, reported the formation of a precipitate after each centrifugation except for 8,000 RPM, however, when replicating their steps, this research was unable to form a precipitate.[13] This difference can be related to the candle and soot and well as the volumes of solvents used for

neutralization and size separation. The soot used in this research came from a white, unscented wax candle, whereas, Ray and coworkers do not report the type of candle used, which could introduce variances between this work and literature. Also, the exact volumes of solvents used are not reported, only ratios are described, which could also lead to discrepancies in the results. These inconsistencies make a true replication of their work difficult, therefore only the absorption and fluorescence properties of the carbon nanodots synthesized in this method were characterized.

**Absorption and Fluorescence Characterization**

The absorbance and emissive properties of the synthesized nanodots were similar to those reported in literature. A broad absorption that tails off in the visible region was observed and an excitation wavelength-dependent emission, with the greatest emission seen at 517 nm when excited at 460 nm. Figure 2.6 shows the emission spectra for the 4,000 RPM and 8,000 RPM centrifugation fractions.

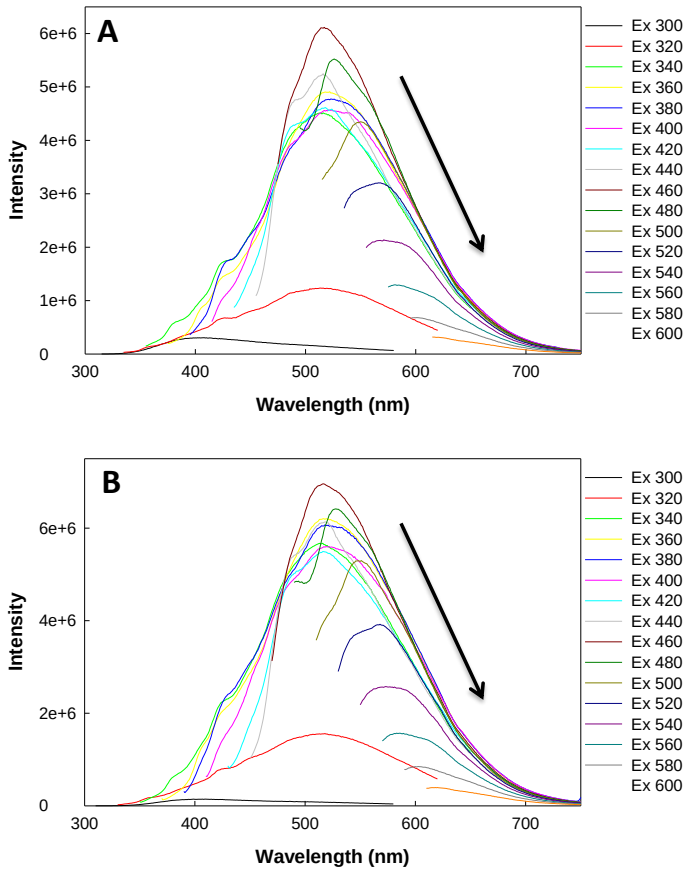


**Figure 2.5** Emission spectra of carbon nanodots separated at A) 4,000 rpm and B) 8,000 rpm excited at various wavelengths ranging from 300 to 600 nm.

It was reported by Ray, *et al.,* that various sized nanodots could be obtained by using different centrifugation speeds, with the smallest sizes (2-6 nm) attained at the highest speeds.[13] This was described as an increase in intensity and hypsochromic shift (blue shift) in the emission spectrum, however, this was not the case for this work. When comparing the four centrifugation fractions synthesized, there was no hypsochromic shift and only a slight increase in the intensity of the emission spectra (Data not shown). The reason for these differences is thought to be caused by the inability to generate a precipitate in the size separation steps, however size analysis was not carried out. The precipitate contained the smaller sized nanodots and by

isolating it from each centrifugation, various sized carbon nanodots would be obtained. Therefore, when no precipitate formed, the size separation by centrifugation resulted in four fractions of carbon nanodots with similar photophysical properties. Due to the inability to reproduce literature protocols, a secondary combustion synthetic method, by modifying the neutralization and size separation procedures, was developed to generate carbon nanodots.

### *2.3.2 Adapted Synthesis of Candle-Based Carbon Nanodots*

New neutralization and separation methods were undertaken to improve and simplify steps from the previous methods. The neutralization was carried out by using NaOH to neutralize the carbon nanodot solution to eliminate the multi-step process previously described. The separation was achieved by using various centrifugation speeds and G-25 columns, however size determination was not carried out. Following centrifugation separation, four fractions of fluorescent carbon nanodots were collected: 3,000, 5,000, 10,000 and 14,500 RPM. The column separation technique was implemented to further help segregate sizes of carbon nanodots. The photophysical characterizations of all fractions were carried out as previously described.

## Absorption Characterization

The absorption spectra of each fraction of carbon nanodots showed a high absorption in the UV region with a tail extending in to the visible region, which is commonly reported in literature.[2–5] Figure 2.7A shows the absorption spectra for each centrifugation fraction of carbon nanodots, whereas, Figure 2.7B compares the

normalized absorption for each fraction to Rayleigh light scatter. When compared to scattered light, the carbon nanodots appear to have little to no scatter light in their spectra, which means that the broad absorption is probably due to the nature of the carbon nanodots.

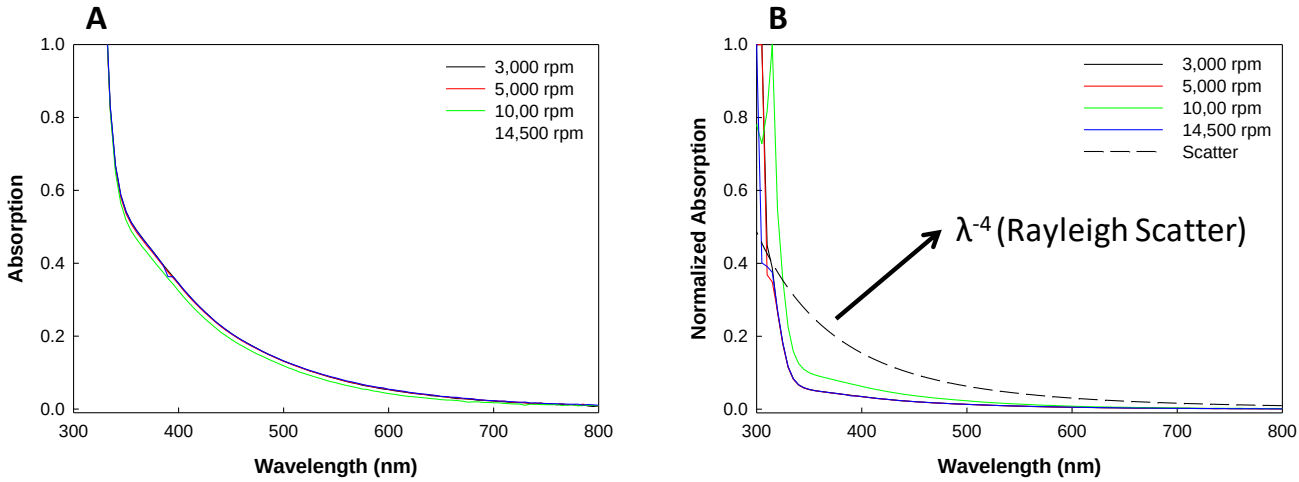


**Figure 2.6** A) Absorption spectra of carbon nanodots at various centrifugation speeds B) Normalized absorption spectra of carbon nanodots at various centrifugation speeds and Rayleigh scattering ($\lambda^{-4}$ trace).

## Fluorescence Characterization

The emission of all the carbon nanodots fractions were excitation wavelength dependent, as shown in Figures 2.8-2.11. The emission intensity significantly decreases at longer wavelengths (> 500 nm). The normalized spectra (Figure 2.8B-2.11B) display the excitation wavelength dependence observed by the carbon nanodots fractions. Similar emission characteristics were seen for numerous carbon nanodots solutions produced by this synthetic method. The excitation wavelength dependence and the decrease in emission intensity properties are commonly reported fluorescence properties in literature.[2–5]

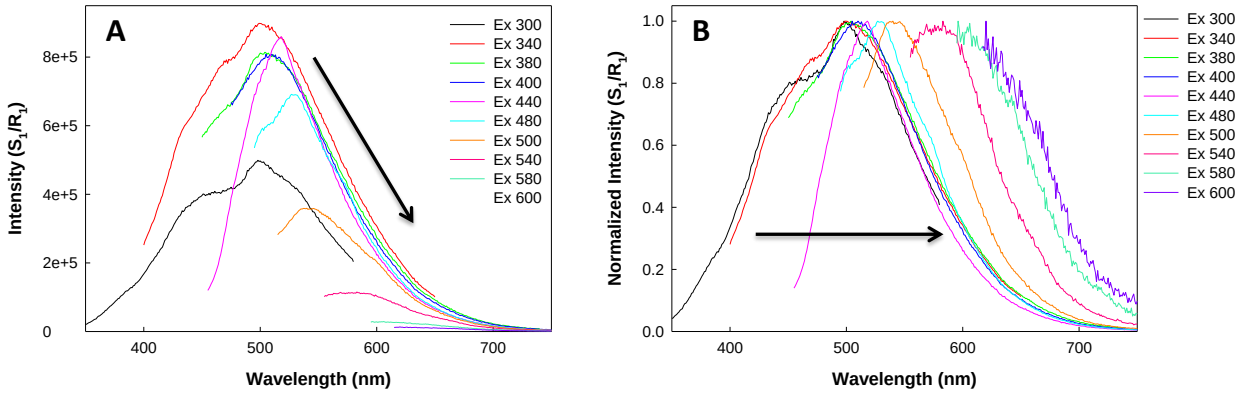


**Figure 2.7** (A) Emission spectra of carbon nanodots after 3,000 RPM (B) Normalized emission spectra of carbon nanodots after 3,000 RPM.

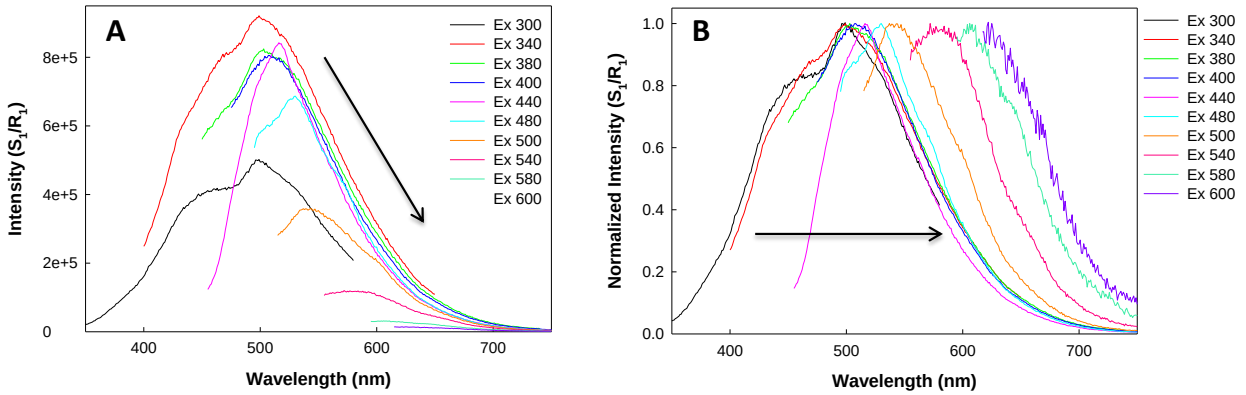


**Figure 2.8** (A) Emission spectra of carbon nanodots after 5,000 RPM (B) Normalized emission spectra of carbon nanodots after 5,000 RPM.

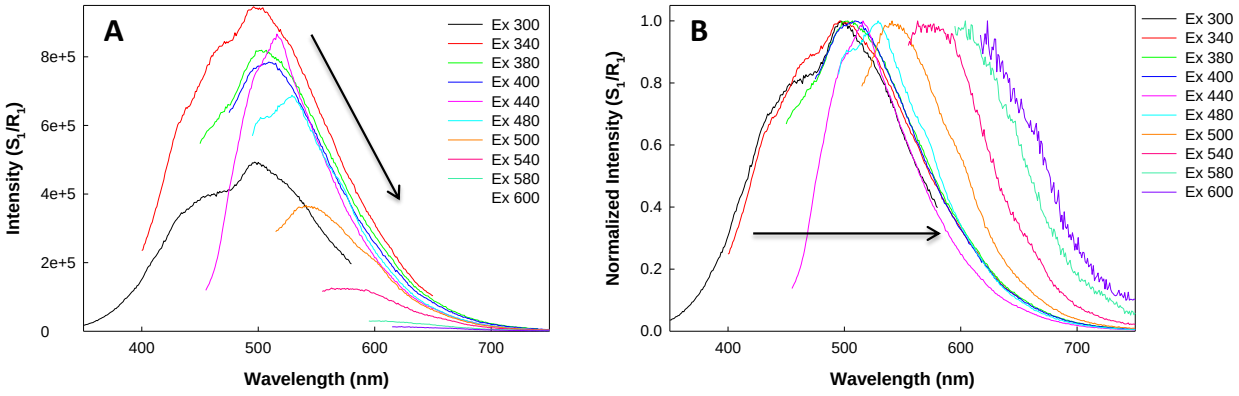


**Figure 2.9** (A) Emission spectra of carbon nanodots after 10,000 RPM (B) Normalized emission spectra of carbon nanodots after 10,000 RPM.

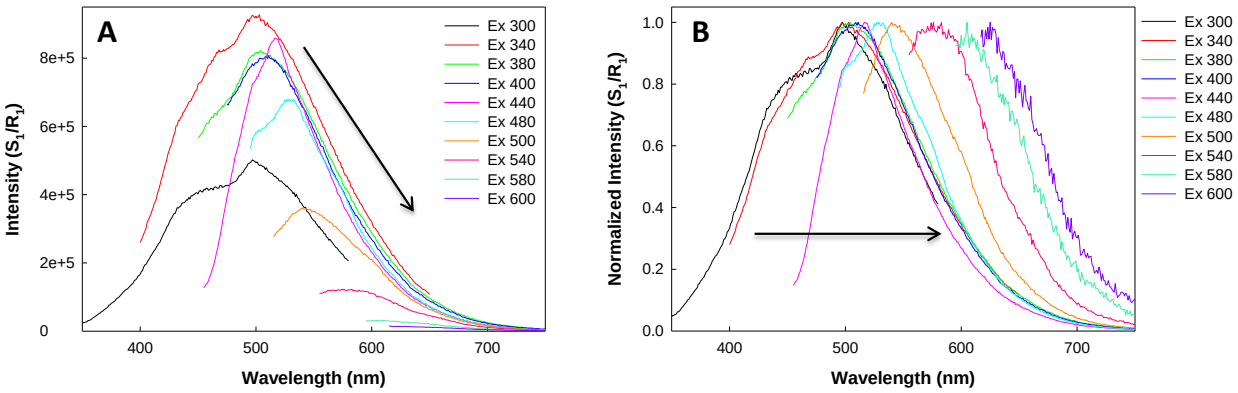


**Figure 2.10** (A) Emission spectra of carbon nanodots after 14,500 RPM (B) Normalized emission spectra of carbon nanodots after 14,500 RPM.

The origin of fluorescence for carbon nanodots is not completely understood to date, but the probable mechanism for these carbon nanodots is several diverse emitter centers present within carbon nanodots. The emissive centers are due to molecular fluorophores or functional groups on the surface of the nanodots.[5,6] According to Cayuela, *et al.*, diverse emitting centers are predominated at experimental temperatures less than 230°C and have broad, excitation wavelength dependent emission spectra.[6,42,87] The experimental and photophysical properties of the synthesized carbon nanodots support this mechanism of fluorescence. Also, fluorescence mechanism is further supported by complex time-resolved data that will be discussed later in this section.

Centrifugation was utilized as a method to separated carbon nanodots based on size. It was reported that high centrifugation speeds (16,000 RPM) could separate small sized carbon nanodots and this was characterized as an increase in the emission intensity and hypsochromic shift in the emission spectrum.[13] However, for this work, when comparing the emission spectra of the four centrifugation fractions (Figure 2.8-

2.11), the spectra were similar, if not identical. Subsequently, centrifugation was effective at removing the large, un-reacted particles, but has little to no effect in separating out the smaller sized particles. As a result of the lack of size separation from centrifugation, a secondary separation technique, utilizing size exclusion columns, was utilized. Figure 2.12 demonstrates the change of the emission properties of the early fractions collected from the column. Comparing the emission spectra of first fraction collected (Figure 2.12A) and the seventh fraction (Figure 2.12D), there is a hypsochromic shift of emission from 500-550 nm and 400-450 nm for the fractions, respectively. This shift in the emission spectra is telling of carbon nanodots, with different properties and/or sizes, being collected.[13] Fractions 1-10 were collected every three minutes and showed the greatest emission intensity. A total of 40 fractions were collected, but there was no significant emission signal after the 15$^{th}$ fraction. By utilizing two separation techniques, several fractions of carbon nanodots were obtained and their luminescence properties were characterized.

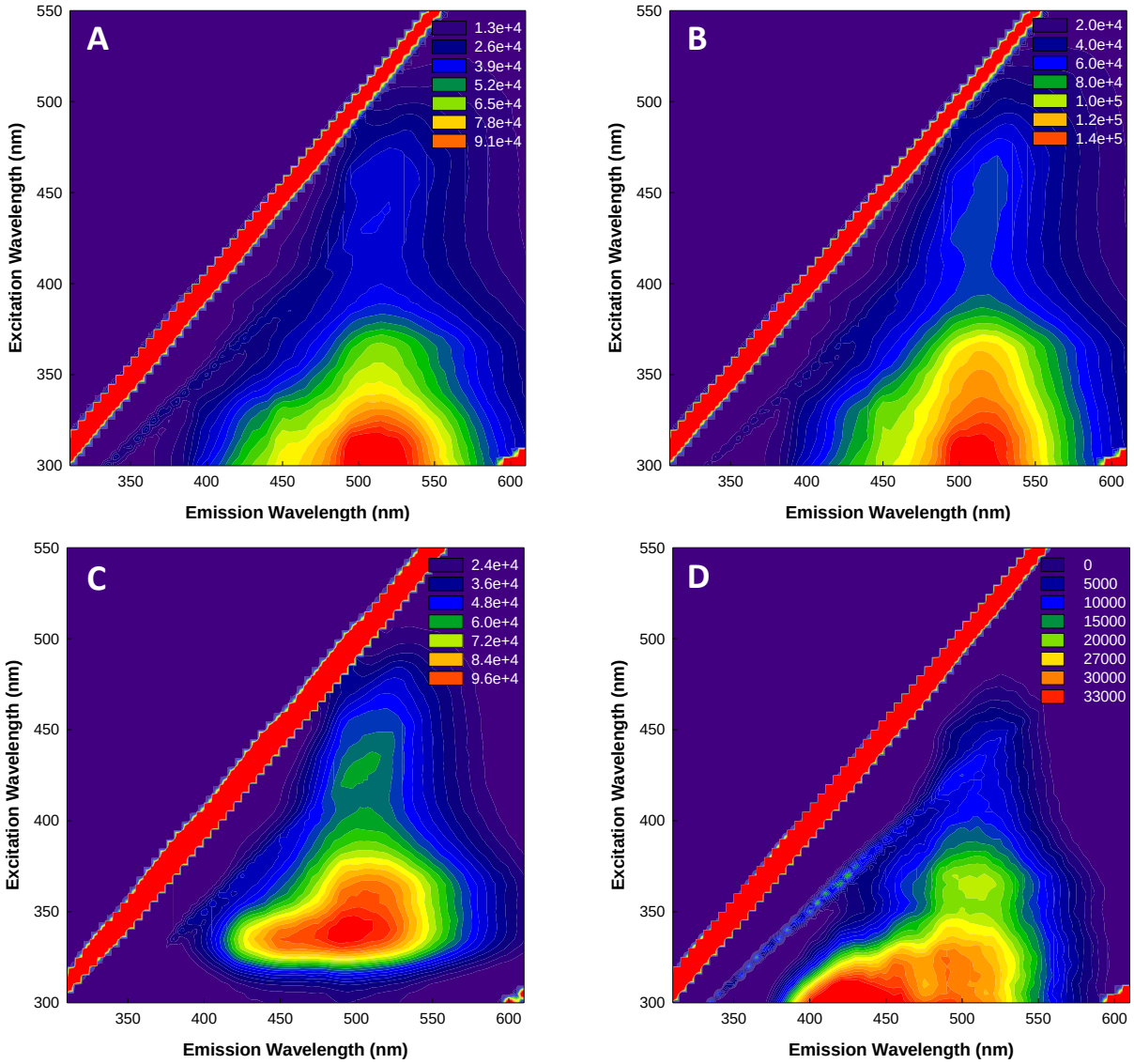


**Figure 2.11** Contour plot of 3D emission spectra of carbon nanodots fractions separated on column A) Fraction 1 B) Fraction 3 C) Fraction 5 D) Fraction 7. The intensity band shown in red for each spectrum is the zero order overtone bands.

### Fluorescence Quantum Yields Determination

The relative fluorescence quantum yields of carbon nanodots were determined by utilizing a known fluorophore standard, quinine sulfate. The relative quantum yields of carbon nanodots were determined to be < 2%. When comparing the different centrifugation fractions, the quantum yields of the higher spin speeds (14,500 RPM)

were consistently slightly higher than the quantum yields of lower spin speeds, as shown in Table 2.1. This table, also, illustrates the variation of the quantum yields between syntheses, i.e. 14,500 RPM 1.94% versus 4.49%. These differences in quantum yields are thought to be due to concentration variations and/or particle inhomogeneity that occurs when replicating the synthetic procedures described in section 2.2.2.

**Table 2.2** Relative and approximate quantum yield calculations of carbon nanodots, synthesized in 2.2.2, at two separate times, at different centrifugation speeds.

| Sample (rpm) | Average Φ (%) Synthesis 1 | Average Φ (%) Synthesis 2 |
|---|---|---|
| 3000 | 1.49 ± 0.14 | 1.71 ± 0.07 |
| 5000 | 1.28 ± 0.11 | 3.11 ± 0.06 |
| 10000 | 1.92 ± 0.11 | 3.08 ± 0.16 |
| 14500 | 1.94 ± 0.04 | 4.49 ± 0.22 |

*Each average quantum yield calculation is from triplicate measurements within same batch of nanodots.

**Photostability Characterization**

The photostability of carbon nanodots were studied over a 20-minute period to determine the stability of the emission when exposed to a constant excitation source. When exposed to an extremely high laser power (~250 mW), the emission intensity of carbon nanodots is stable over a 20-minute period with only about ≈ 50% loss. Figure 2.13 shows the normalized data for all four carbon nanodot fractions over this time. Carbon nanodots have shown to have great photostability as compared to other fluorescent materials, such as polystyrene nanospheres, which photo-bleach in a half an hour of constant light exposure.[2–5]

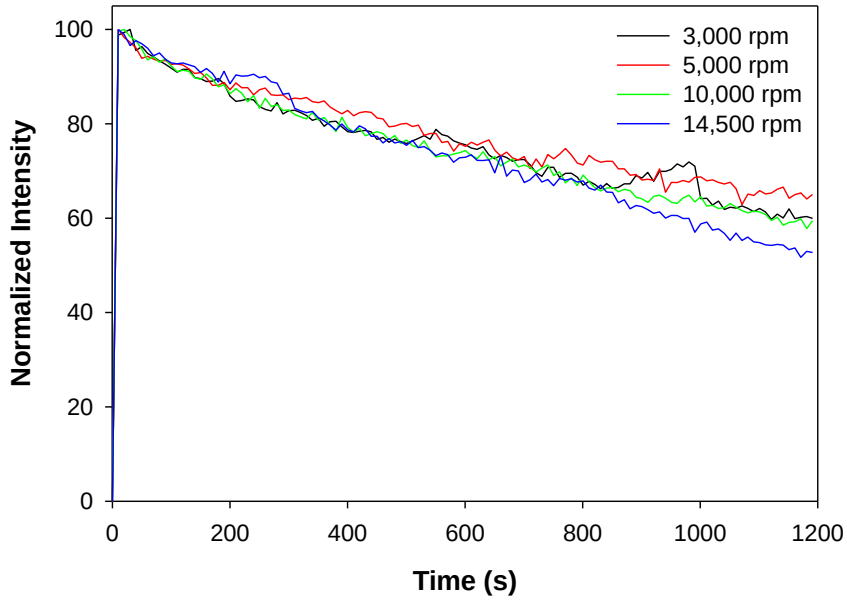


**Figure 2.13** Normalized time dependent steady-state emission intensity recorded for carbon nanodots at various centrifugation speeds. The excitation wavelength was 532 nm and the power 247mW.

### Time-Resolved Intensity Decay Characterization

Time resolved experiments were carried out to determine the fluorescence lifetime of carbon nanodots. These experiments revealed multi-exponential luminescence intensity decay for the carbon nanodots that required a 3-expontential fit. The averaged lifetime for all centrifugation fractions collected were determined, using equation 2.3, to be approximately 4 ns, when excited with a 474 nm NanoLED$^{TM}$ and the emission collected at 530 nm. The decay, fitting and residual traces for all four fractions can be seen in Figure 2.14 and Table 2.2 summarizes the fitting data, showing the multi-exponential lifetime results. The lifetime results were very similar for the four fractions, which only serve to confirm that centrifugation is not able to size-separate carbon nanodots, as first thought.

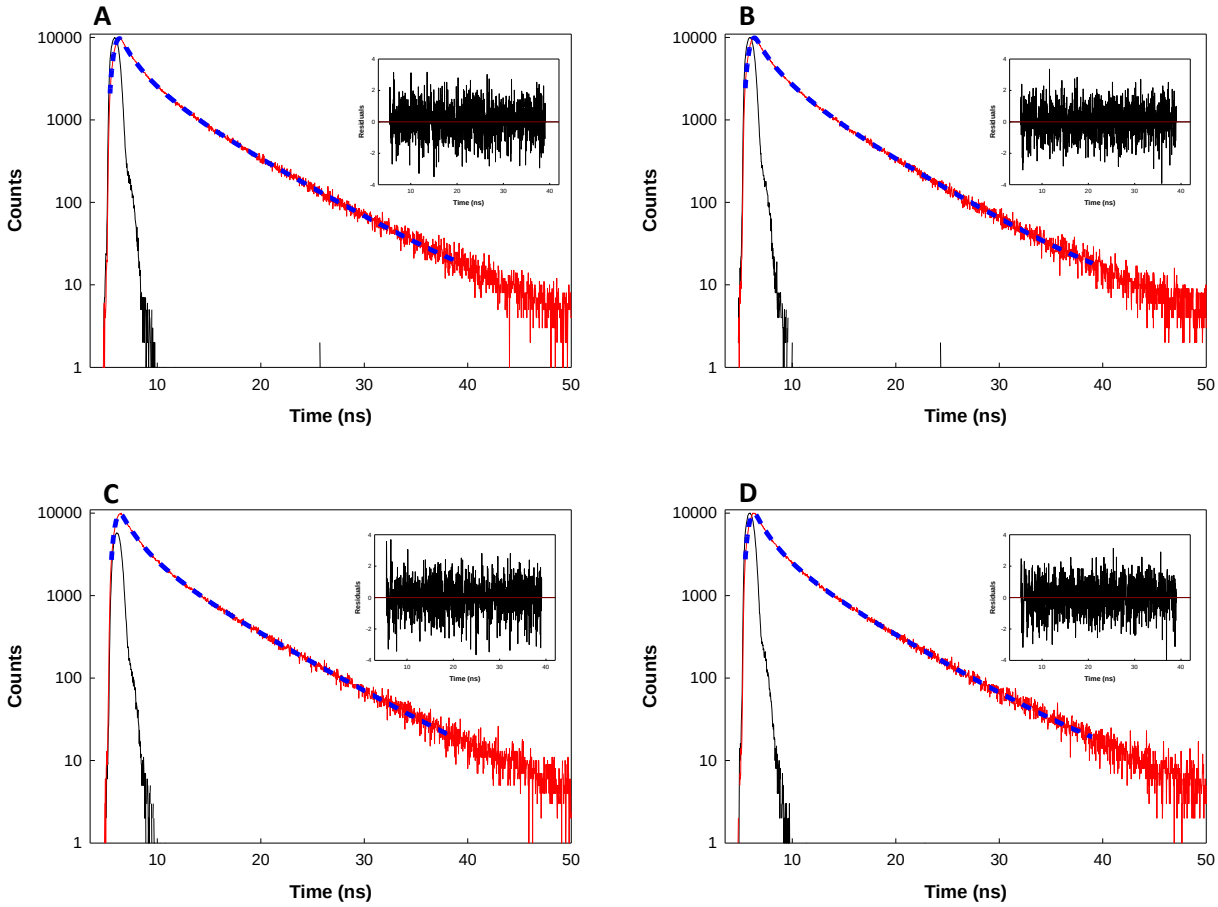


**Figure 2.13** Fluorescence lifetime intensity decays of carbon nanodots centrifuged at A) 3,000 RPM, B) 5,000 RPM, C) 10,000 RPM and D) 14,500 RPM and all fitted to a 3-exponential intensity decay. The $\lambda_{ex}$= 474 nm and the $\lambda_{em}$= 530 nm. (Black line- instrumental response function (IRF), Red line- fluorescence intensity decay, Blue line- 3 exponential decay). **Inset** Weighted residual graph.

**Table 2.3** Average fluorescence lifetimes of carbon nanodots at different centrifugation speeds calculated from equation 2.3.

| Sample (rpm) | $\lambda_{ex}$ (nm) | $\lambda_{em}$ (nm) | $\tau_1$ (ns) | $f_1$ (%) | $\tau_2$ (ns) | $f_2$ (%) | $\tau_3$ (ns) | $f_3$ (%) | $\tau_{avg}$ (ns) | $\chi^2$ |
|---|---|---|---|---|---|---|---|---|---|---|
| 3000 | 474 | 530 | 0.71 ± 0.02 | 13 | 2.12 ± 0.11 | 33 | 6.10 ± 0.04 | 54 | 4.10 | 1.09 |
| 5000 | 474 | 530 | 0.64 ± 0.02 | 12 | 2.17 ± 0.09 | 33 | 5.85 ± 0.04 | 55 | 4.02 | 1.01 |
| 10 000 | 474 | 530 | 0.74 ± 0.02 | 13 | 2.15 ± 0.11 | 33 | 6.20 ± 0.04 | 54 | 4.14 | 1.12 |
| 14 500 | 474 | 530 | 0.59 ± 0.02 | 11 | 1.92 ± 0.08 | 33 | 5.96 ± 0.02 | 56 | 4.03 | 1.03 |

It was hypothesized that since the emission properties were dependent on excitation wavelength, the same would also be true for the fluorescence lifetimes at different excitation and/or emission wavelengths. Therefore, several more time-resolved experiments were conducted to see if the lifetimes were also affected by changing either excitation or emission wavelengths. The data was compiled using the 10,000 RPM fraction of carbon nanodots and by keeping either the excitation wavelength constant (474 nm) or keeping the emission wavelength constant (530 nm). Tables 2.3 and 2.4 show a summary of the results of those experiments. We show that there are slight alterations in the average lifetime of carbon nanodots when the emission and excitation wavelengths are changed.

**Table 2.4** Average lifetimes of carbon nanodot centrifuged at 10,000 RPM at various emission wavelengths calculated from equation 2.3.

| $\lambda_{ex}$ (nm) | $\lambda_{em}$ (nm) | $\tau_1$ (ns) | $f_1$ (%) | $\tau_2$ (ns) | $f_2$ (%) | $\tau_3$ (ns) | $f_3$ (%) | $\tau_{avg}$ (ns) | $\chi^2$ |
|---|---|---|---|---|---|---|---|---|---|
| 474 | 500 | 0.48 ± 0.01 | 12 | 1.89 ± 0.07 | 33 | 5.78 ± 0.03 | 55 | 3.86 | 0.981 |
| 474 | 530 | 0.74 ± 0.02 | 13 | 2.15 ± 0.11 | 33 | 6.20 ± 0.04 | 54 | 4.14 | 1.12 |
| 474 | 650 | 1.48 ± 0.04 | 24 | 5.46 ± 0.04 | 36 | 0.18 ± 0.006 | 40 | 2.39 | 1.20 |

**Table 2.5** Average lifetimes of carbon nanodot centrifuged at 10,000 RPM at various excitation wavelengths calculated from equation 2.3.

| $\lambda_{ex}$ (nm) | $\lambda_{em}$ (nm) | $\tau_1$ (ns) | $f_1$ (%) | $\tau_2$ (ns) | $f_2$ (%) | $\tau_3$ (ns) | $f_3$ (%) | $\tau_{avg}$ (ns) | $\chi^2$ |
|---|---|---|---|---|---|---|---|---|---|
| 311 | 530 | 0.49 ± 0.01 | 16 | 1.77 ± 0.04 | 41 | 6.21 ± 0.03 | 43 | 3.47 | 1.04 |
| 351 | 530 | 0.61 ± 0.01 | 25 | 2.03 ± 0.11 | 43 | 6.67 ± 0.08 | 32 | 3.16 | 1.19 |
| 474 | 530 | 0.74 ± 0.02 | 13 | 2.15 ± 0.11 | 33 | 6.20 ± 0.04 | 54 | 4.14 | 1.12 |

To further gain understanding of the photophysics of carbon nanodots, the time-resolved data for the 10,000 RPM fraction ($\lambda_{ex}$= 474 nm and $\lambda_{em}$= 530 nm) was analyzed by using the maximum entropy method. This analysis was completed by another lab member, Dr. Jan Karolin. Figure 2.15 shows the result of this analysis. Although the time-resolved data can be adequately described by a three-exponential decay function (k=3 in equation 2.1), with lifetimes 600 ps, 2 ns and 6 ns, respectively (Table 2.2), it is evident from the life-time distribution that the photophysics is far more complex, and is constructed by a broad range of decay times, tailing out to 25 ns. Each emissive center on the carbon nanodots could have its own unique fluorescence intensity decay time, consequently resulting in a multi-exponential decay and broad distribution of lifetimes. Therefore, the suggestion that the carbon nanodots emission is affected by diverse emissive sites is further supported by the multiple lifetimes decay and the broad distribution of lifetimes recorded for these carbon nanodots.[5,6]

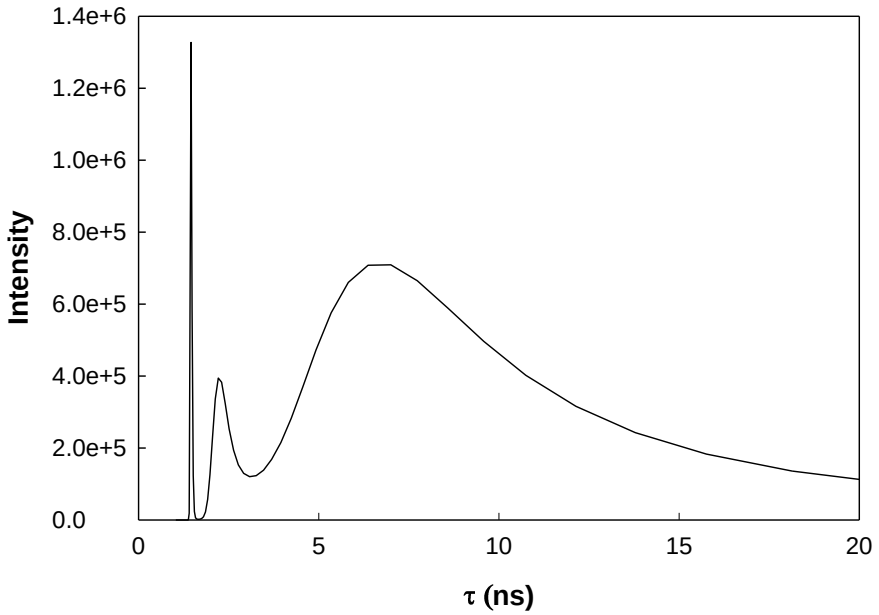


**Figure 2.14** Maximum Entropy lifetime distribution for a 10,000 RPM fraction of carbon nanodots.

## 2.4 Conclusions

Fluorescent carbon nanodots were successfully synthesized by two combustion methods, utilizing the oxidation of candle soot, and their respective photophysical properties characterized. The first synthetic procedure, following the procedures developed by Ray, *et al.*, was found to be difficult to replicate due to the lack of complete experimental details, along with the multi-step neutralization procedure and size separation steps.[13] As a result of these experimental inconsistencies, a secondary method was developed to simplify and improve the experimental procedures. The second method only modified the neutralization and size separation steps to shorten the overall experimental time, however, the new size separation steps were only able to separate out the large, un-reacted particles. This is noted by the nearly identical luminescence properties seen for each of the centrifugation fractions in Figures 2.7-2.10. Since centrifugation was unable to separate small sized nanodots, columns (exclusion limit 5000 molecular weight) were utilized and showed to have the ability to separate out different emissive fractions of carbon nanodots (Figure 2.11).

Analyzing the photophysical properties, showed that the candle carbon nanodots synthesized, by the second combustion method, displayed the common characteristics reported in literature.[2–5] Candle carbon nanodots showed a broad absorption, excitation wavelength-dependent emission, and good photostability.[2–5] However, the nanodots' relative fluorescence quantum yields were low, ~ 2%. Also, the carbon nanodots show multi-exponential fluorescence intensity decay and broad distribution of lifetime decays through time-resolve measurements and maximum

entropy analysis. The source of luminescence of carbon nanodots is not completely understood, but it speculated to depend on the synthetic route used.[2–4,6,42,87] The most probable mechanism for the luminescence of candle-based carbon nanodots could be diverse emissive center within the particles based on the experimental condition used (low temperatures), excitation-wavelength dependence, broad emission bands, complex fluorescence intensity decays and broad lifetime distributions.

Carbon nanodots were successfully synthesized from oxidizing candle soot, but the overall experimental procedures (synthesis, neutralization, and size separation) were time-consuming, requiring over 12 hours to complete all three steps, and produced weakly fluorescent particles ($\Phi_F$ = ~2%). Therefore, a new combustion synthetic method, utilizing ultra-pure methane gas, was developed, and will be discussed in Chapter 3.

# Chapter 3: Synthesis and Photophysical Characterization of Methane-Based Carbon Nanodots

## 3.1 Introduction

In this chapter, the development of a new combustion pathway aimed at improving the long synthetic procedures and low quantum yields described in Chapter 2 will be discussed. The photophysical properties of the resulting methane-based carbon nanodots were investigated to gain a better understanding of their luminescence origin. The synthetic method presented in this chapter involved the synthesis of the nanodots within a burning methane flame, instead of oxidizing candle soot (Chapter 2). Small carbon-based particles can be formed within a flame, before they can aggregate into soot, therefore, by using a vacuum, the carbon nanodots can be collected directly into the solvent. This synthetic method significantly reduced the synthesis time from the required 12+ hours using candle soot to 4 hours. The methane-based carbon nanodots showed similar luminescence properties to the carbon nanodots previously reported in literature and in chapter 2.[2–4,87] The photophysical properties were investigated to help gain a better understanding of the origin of the luminescence of methane-based carbon nanodots.

## 3.2 Experimental Details

### *3.4.1 Synthesis of Methane-Based Carbon Nanodots*

***Synthetic Set-Up.*** The experimental set-up for the synthesis of methane-based carbon nanodots is shown in Figure 3.1. Briefly, an ultra-pure methane gas cylinder (Airgas,

Radnor, PA) was connected to a standard bunsen burner through a black viton tubing (Cole-Parmer, Vernon Hills, IL). A long stem funnel was clamped above the bunsen burner and the flame was contained within the funnel. The stem of the funnel was connected to the top of the stopper of an impinger glassware (VWR, Radnor, PA) through black viton tubing. The top of the impinger stopper led into the impinger bottle, where the solvent was held. The side of the impinger stopper was connected to the vacuum in the hood via black viton tubing.

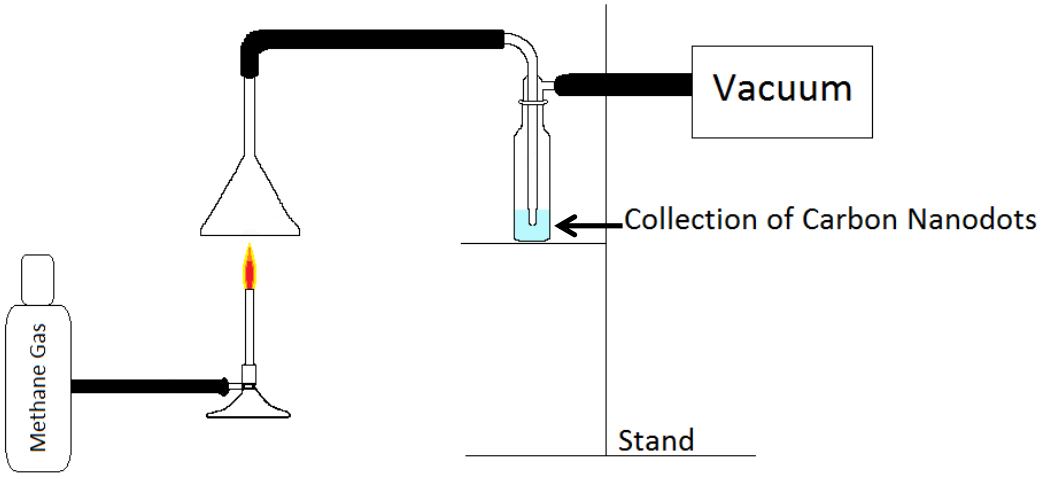


**Figure 3.1** Block diagram of the experimental methane-based carbon nanodot synthesis.

***Synthesis.*** Ultra-pure methane gas was flowed into the bunsen burner, where a sooting flame was lit. The carbon nanodots are formed within the flame and subsequently pulled through into the 5 mL of solvent in the impinger bottle using a vacuum. The vacuum was set to cause gently bubbling of the solvent to ensure that the carbon nanodots were pulled from the flame into the solvent. The duration of the synthesis of carbon nanodots was either 2 or 4 hours and four solvents were used: water, ethanol, methanol, and hexane to collect the carbon nanodots. For ethanol,

methanol, and hexane, an ice bath around the impinger bottom, was used to prevent the solvent from evaporating, a consequence of the vacuum pressure. Figure 3.2A and B show the experimental set-up for the different solvents used for the collection of the carbon nanodots.

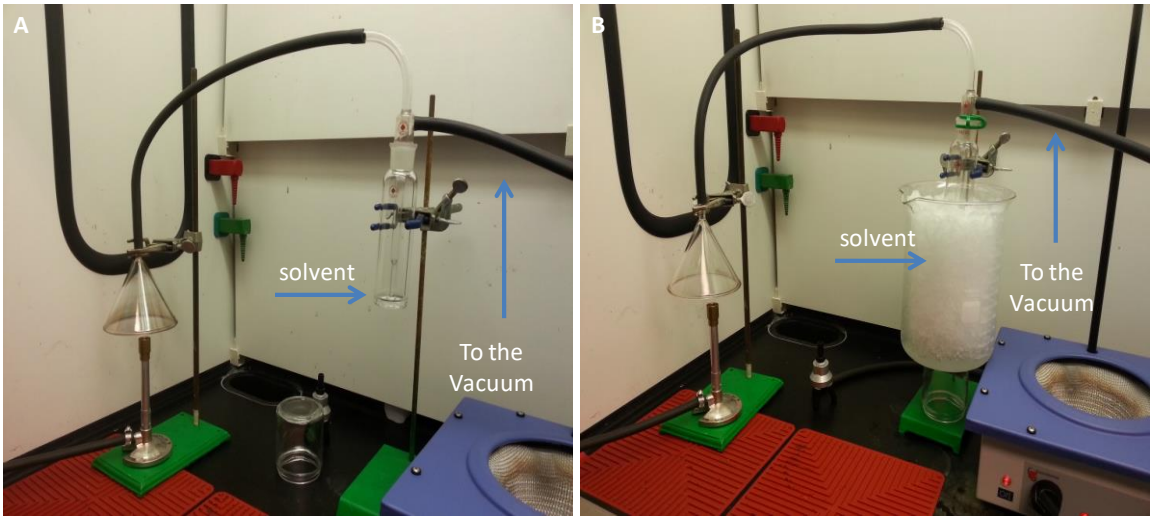


**Figure 3.2** (A) Experimental set-up used for carbon nanodots collected in water. (B) Experimental set-up used for carbon nanodots collected in ethanol, methanol, or hexane.

### *3.4.2 Photophysical Characterization of Methane-Based Carbon Nanodots*

***Absorption Measurements.*** Absorption measurements were collected on a Cary 50 UV-Vis spectrophotometer (Agilent Technologies, Santa Clara) equipped with a full spectrum xenon pulse lamp (190-1100 nm). Samples and solvent blanks (water, ethanol, methanol) were measured in a 1-cm quartz or glass cuvette with a scan rate of 300 nm/min**.**

***Steady-State Fluorescence.*** Steady-state fluorescence measurements were taken on a FluoroMax-4 or FluoroMax-4P spectrofluorometer (Horiba Scientific, Edison, NJ). The experimental data was collected using the FluorEssence software with samples

measured in a 1-cm glass or quartz cuvette. All spectra were corrected for the lamp's profile by setting the software to divide the signal of the sample by the reference signal ($S_1/R_1$). Both the emission and 3D emission spectra were collected as previously described in Chapter 2.

***Steady-State Phosphorescence.*** Phosphorescence measurements were carried out on FluoroMax-4P spectrofluorometer (Horiba Scientific, Edison, NJ). The instrument light source was a pulsed xenon lamp. The experiments were carried out utilizing the FluorEssence software in phosphorescence mode with samples in a 1-cm glass or quartz cuvette. The experimental parameters are summarized in Table 3.1 while Figure 1.8 depicts the typical data acquisition process used for the phosphorescence measurements. Flash delay is the delay after the lamp pulse (~50 μs), sample window opens after the flash delay and where the sample is counted and measured, time per flash is cycle length per flash, and flash count sets the number of lamp pulse that contribute to each data point.

**Table 3.1** Experimental parameters for phosphorescence measurements.

| | |
|---|---|
| Flash Delay | 0.05 ms |
| Sample Window | 0.20 ms |
| Time per Flash | 61 ms |
| Flash Count | 100 |

***Fluorescence Anisotropy.*** Steady-state anisotropy experiments were carried out on a FluoroMax-4 or FluoroMax-4P spectrofluorometer (Horiba Scientific, Edison, NJ). Experimental data was collected using the FluorEssence software in anisotropy mode with samples measured in a 1-cm glass or quartz cuvette. Carbon nanodots were mixed with glycerol to slow down any rotational motion. The carbon nanodot-

glycerol solutions were mixed for one hour and then analyzed. Summary of the typical experimental parameters are listed in Table 3.2.

**Table 3.2** Typical experimental parameter for steady-state anisotropy measurements.

| | |
|---|---|
| $\lambda_{ex}$ | 400 nm |
| $\lambda_{em}$ | 420-700 nm |
| Excitation Slit | 5 nm |
| Emission Slit | 5 nm |

Time-resolved anisotropy measurements were taken on a FluoroCube system (Horiba Scientific, Edison, NJ). Carbon nanodots samples were excited using either 400 or 474 nm NanoLED$^{TM}$ (Horiba Scientific, Edison, NJ) and the emission wavelengths (500 and 550 nm) were selected with a monochromator, after passing through a polarizer that was position in either the vertical, horizontal, or magic angle direction, and subsequently the signal was detected on a TBX-04 timing module (Horiba Scientific, Edison, NJ). Decay spectra were collected using the DataStation V 2.7.2 software and the decay curves were fitted using the DAS 6 Analysis software.

***Time-Resolved Fluorescence.*** Time-resolved fluorescence decays were obtained using the time-correlated single photon counting technique on a FluoroCube system (Horiba Scientific, Edison, NJ). An instrument response function (IRF) was collected as previously described in Chapter 2. The IRF and carbon nanodots samples were excited using NanoLEDs centered at 334 and 400 nm (Horiba Scientific, Edison, NJ) and the emission wavelengths (400, 450, 500, 550, and 600 nm) were selected with a monochromator after passing through a polarizer at the magic angle (54.75°), and subsequently the signal was detected on a TBX-04 timing module (Horiba Scientific,

Edison, NJ). The IRF times of 900 and 300ps were calculated by using the full width, half maximum (FWHM) of the IRF decay at the NanoLEDs 334 and 400 nm, respectively. The decay traces were collected and fitted on the DataStation V 2.7.2 software and DAS 6 Analysis software, using previously described parameters (Table 2.1).

***Elemental Analysis.*** Elemental analysis was carried out by Atlantic Microlab, Inc. (Norcross, GA). Carbon nanodots samples were dried in an oven at 40°C for one week. The dried samples (5-10 mg) were stored in and submitted for analysis in glass vials. However, it appeared that the samples were un-combustible based on the low, inconsistent results obtained.

***Dynamic Light Scattering.*** Dynamic light scattering data was collected on a Zetasizer Nano ZS (Malvern, Worcestershire, UK) equipped with a 633-nm laser source with help from Dr. Daniel's lab group. Carbon nanodots samples were analyzed in 1-cm plastic cuvette at room temperature. Pure samples (no centrifugation) and centrifuged samples of carbon nanodots were both analyzed.

***Fourier Transform Infrared (FT-IR).*** FT-IR experiments were carried out on Spectrum Two IR spectrometer (Perkin Elmer, Waltham, MA) using Spectrum 10 Spectroscopy software. Dried carbon nanodots sample were analyzed.

***Quantum Yields.*** Relative quantum yields were calculated using equation 2.1, described in Chapter 2. Three standard reference fluorophores were used to determine the quantum yields at various wavelengths. The reference fluorophores used were quinine sulfate (0.1M $H_2SO_4$, $\lambda_{ex}$= 350 nm), fluorescein di-sodium salt (0.1M NaOH, $\lambda_{ex}$= 496 nm), rhodamine 101 (Ethanol, $\lambda_{ex}$= 450-460 nm). The optical

densities of the references and the carbon nanodots were matched at the excitation wavelength (350, 496 or 450 nm). The steady-state emission spectra were integrated using SigmaPlot 11.0 software.

## 3.3 Results and Discussion

Carbon nanodots synthesized from methane gas were collected in four solvents: water, ethanol, methanol, and hexane. Duration of the synthesis was either 2 or 4 hours with a noticeable color change from clear to yellow under white light along with a blue emission under UV-light, as shown in Figure 3.3. The carbon nanodots will be referred to as water, ethanol, methanol, or hexane dots to help distinguish between the various carbon nanodots developed within this chapter and future chapters.

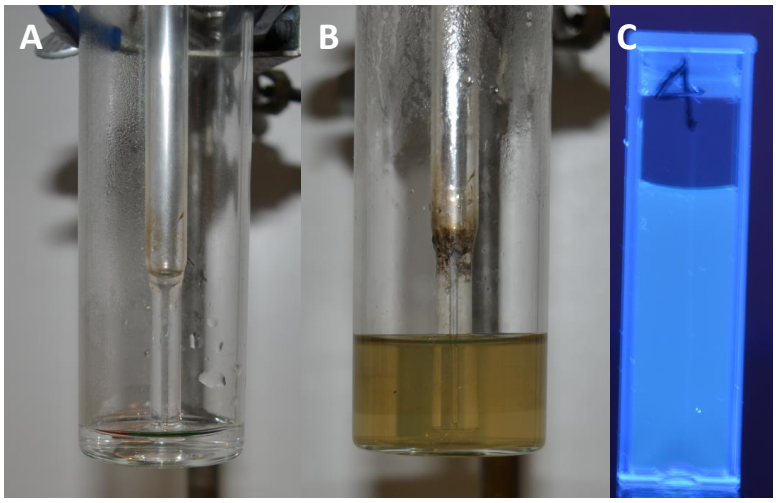


**Figure 3.3** A) Before synthesis of water dots. B) After 4-hour synthesis. C) Water dots after 4-hour synthesis under UV light.

### Absorption Characterization

The absorption spectra of carbon nanodots in water, ethanol and methanol are shown in Figure 3.4. Carbon nanodots collected in hexane are discussed later in this

chapter. For 2 and 4-hour duration times, the absorption spectra show a high UV absorbance tailing off into the visible region. This broad absorbance spectrum is a common characteristic of carbon nanodots.[2–5]

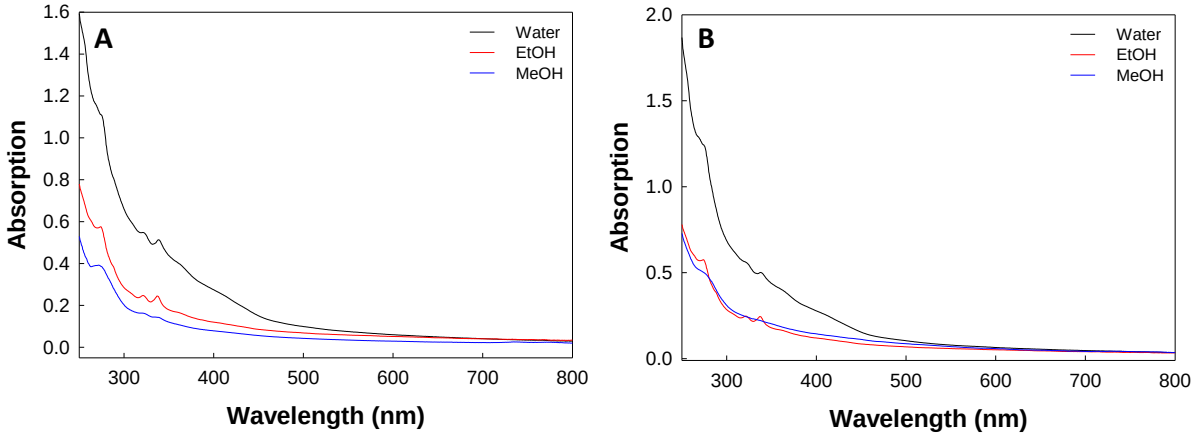


**Figure 3.4** Absorption spectra of methane-based carbon nanodots in various solvents synthesized for A) 4 and B) 2 hours.

Examining the nanodots in the three solvents, it was typically observed that water dots have a higher absorbance value whereas, ethanol and methanol dots are about the same, but noticeably lower than water dots. When comparing the two duration times for each solvent, it can be seen that there was no significant differences in the water dots absorbance spectra (Figure 3.5A), while ethanol and methanol show noticeable differences in their spectra (Figure 3.5B and C).

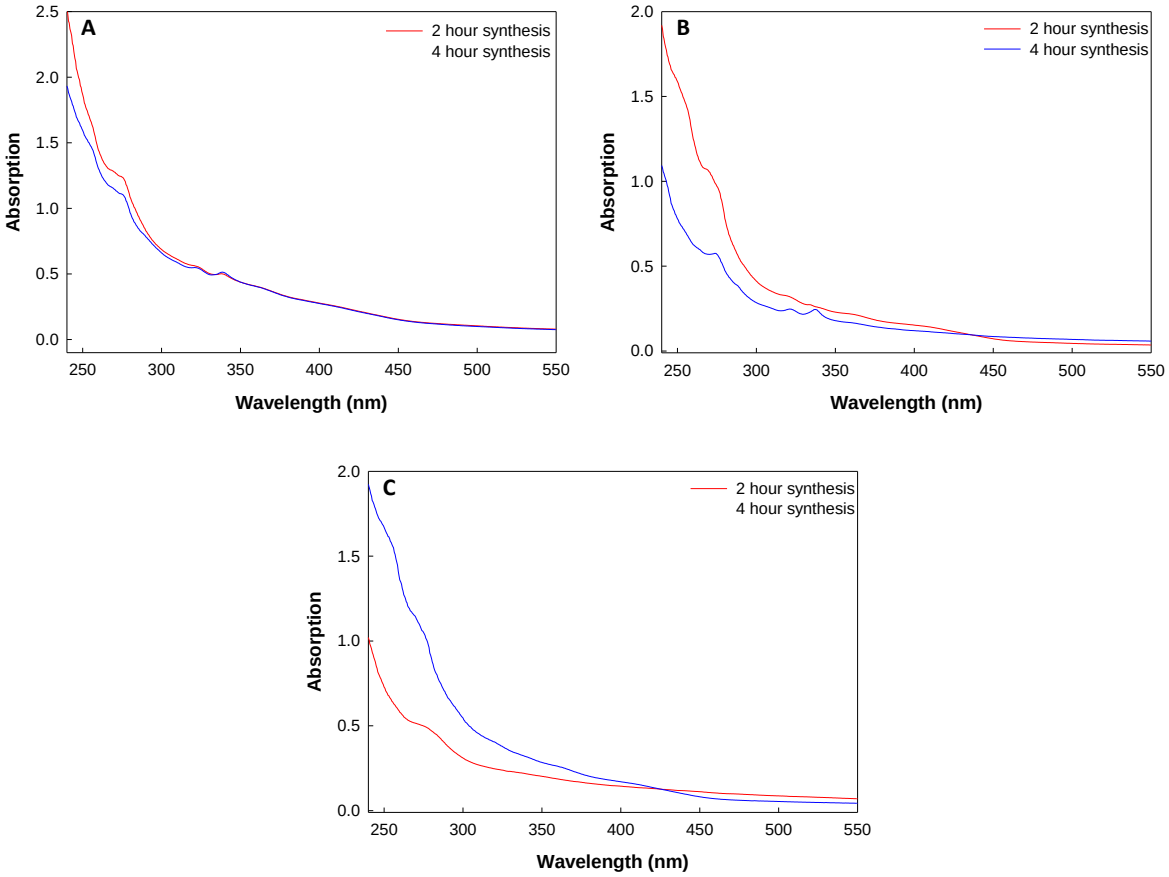


**Figure 3.5** Absorption spectra of methane-based carbon nanodots synthesized for 2 and 4 hours in (A) water, (B) ethanol and (C) methanol.

These differences could be attributed to the concentration of carbon nanodots in solution over the duration time. This can be seen in Figure 3.6 of the carbon nanodots solutions under white light. The water dots synthesized for 2 or 4 hours look nearly identical under white light whereas, ethanol dots a clear color difference can be seen.

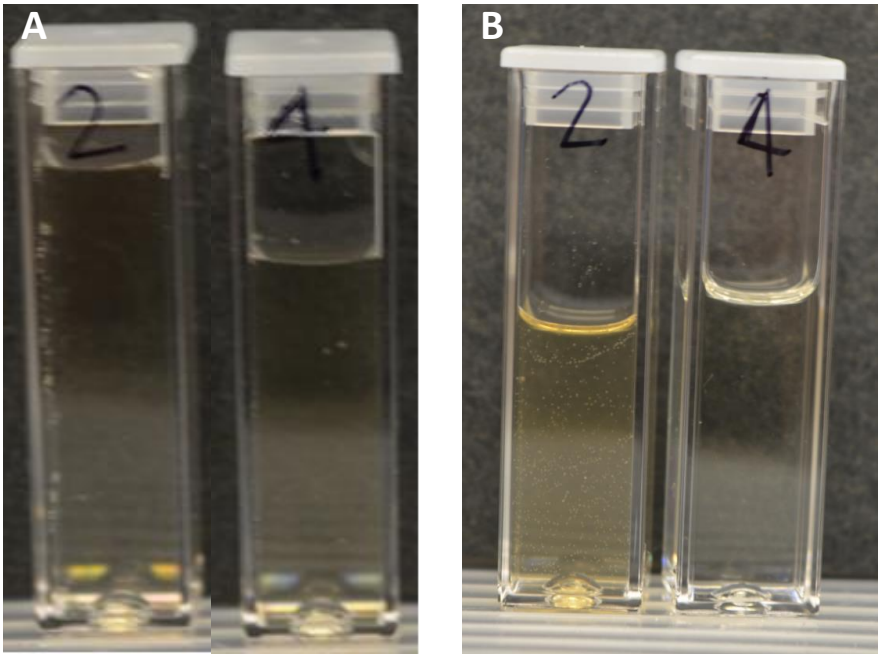


**Figure 3.6** A) Water dots B) ethanol dots under white light**.**

The absorption spectra of the carbon nanodots were compared to Rayleigh light scatter due to the relatively small sizes observed from DLS measures, which are discussed later in this chapter. Figure 3.7 shows the normalized comparison of methane-based carbon nanodots to Rayleigh scatter. It was observed that methane-based carbon nanodots have a great deal of Rayleigh scattering, which can be explained by the size of nanodots. Rayleigh scatter occurs from particles that are the same size as the wavelength of incident light and methane-based carbon nanodots appear to be a few hundred nanometers or smaller in size based on DLS measurements.

Overall, the absorption spectra revealed that carbon nanodots synthesized from methane gas have a broad absorbance that can be influenced by the length of the collection time and the nanodots absorbance spectra are dominated by scattered light.

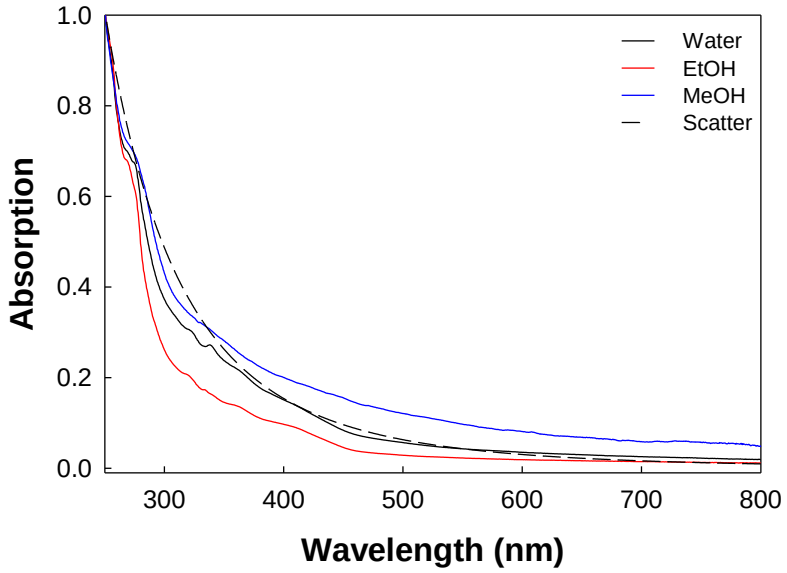


**Figure 3.7** Normalized absorption spectra of carbon nanodots in water, ethanol, and methanol (2hrs) and Rayleigh scattering ($\lambda^{-4}$ trace). Data normalized from Figure 3.5, indicating a notable amount of scattered light present in the samples.

## Fluorescence Characterization

### *Water Dots*

Water dots emission properties were studied to evaluate the effect of synthesis length and solvent on this property. Figures 3.8 and 3.9 illustrate the emission spectra for water dots in either a contour or standard emission plots. First, looking at Figure 3.8 (contour plots), it can be seen that the intensity of emission increased at the longer the synthesis time. The plot for the 4-hour synthesis shows an emission peak between 350-400 nm, highlighted by the white dashed circle, which is not clearly seen in the 2-hour synthesis. However, the overall structure of the contour plots suggested that these differences are most likely due to concentration carbon nanodots in solution and not the emergence of new and/or different particles collected at longer synthesis times.

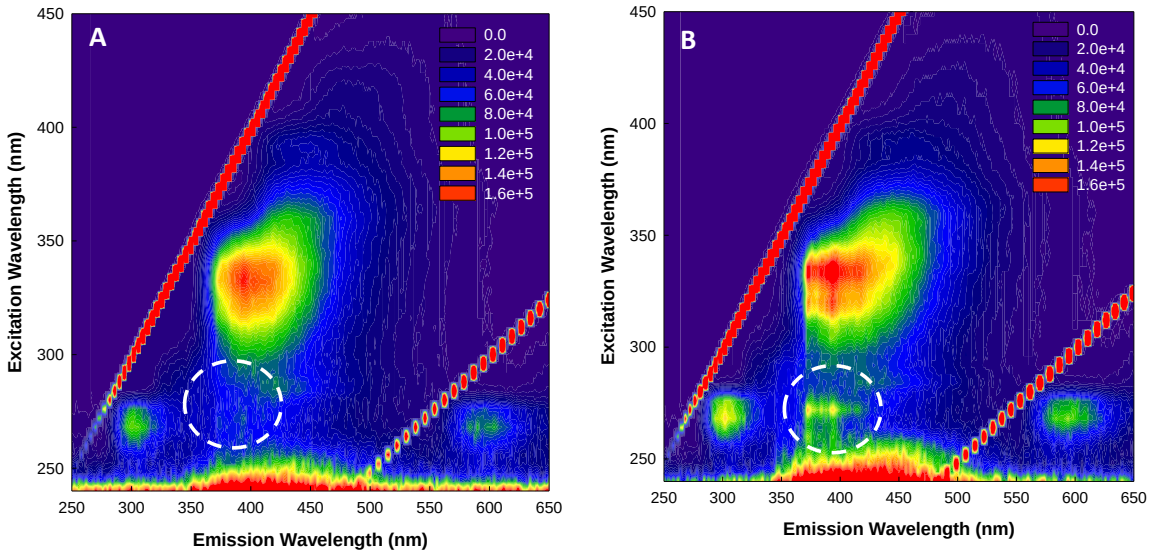


**Figure 3.8** Contour plot of methane-based carbon nanodots in water synthesized for A) 2 and B) 4 hours. The red intensity bands observed are the zero and first order overtone bands.

Next, examining the normalized emission plots shown in Figure 3.9, the excitation wavelength dependent emission is present in these carbon nanodots, which is a unique property of the nanodots. Also, there is a decrease in the emission intensity as the excitation wavelength increases. Again, when comparing the two synthetic times, there is a similar emission structure seen between the two syntheses, which helps to further support the hypothesis that similar particles are synthesized at both duration times.

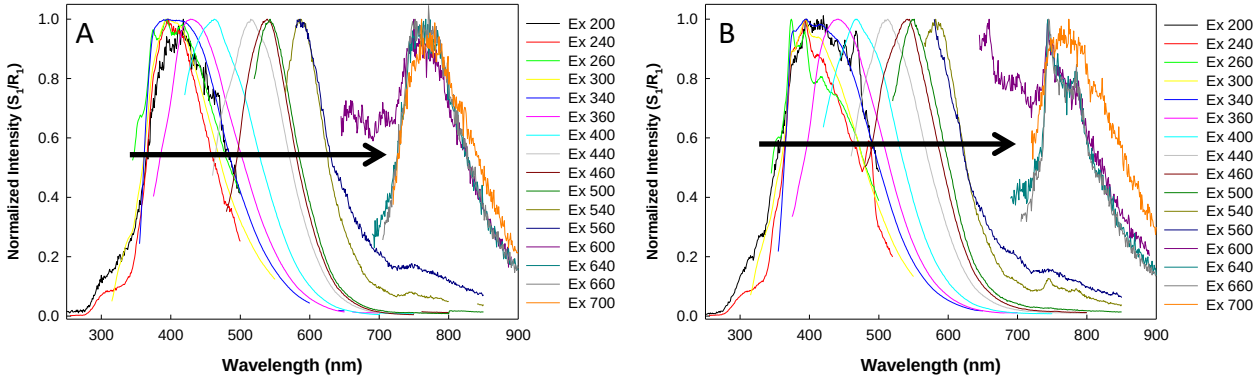


**Figure 3.9** Normalized emission spectra of carbon nanodots in water synthesized for A) 2 and B) 4 hours.

### *Ethanol and Methanol Dots*

Similar, but not identical, results are seen in the contour plots for ethanol and methanol dots along with some differences that are highlighted by the white dashed circles in Figures 3.10 and 3.11. For ethanol dots (Figure 3.10), there is an emergence of emission between 400-450 nm and 350-400 nm, when excited at 350 nm and 260nm, respectively, in the 4-hour synthesis. But, there is a decrease in the emission intensity at the longer duration time. This is thought due to the concentration of carbon nanodots collected over the time frames as shown in Figure 3.6B**.** The similar structure of the contour plots between the two syntheses suggests that comparable carbon nanodots are produced at each duration time.

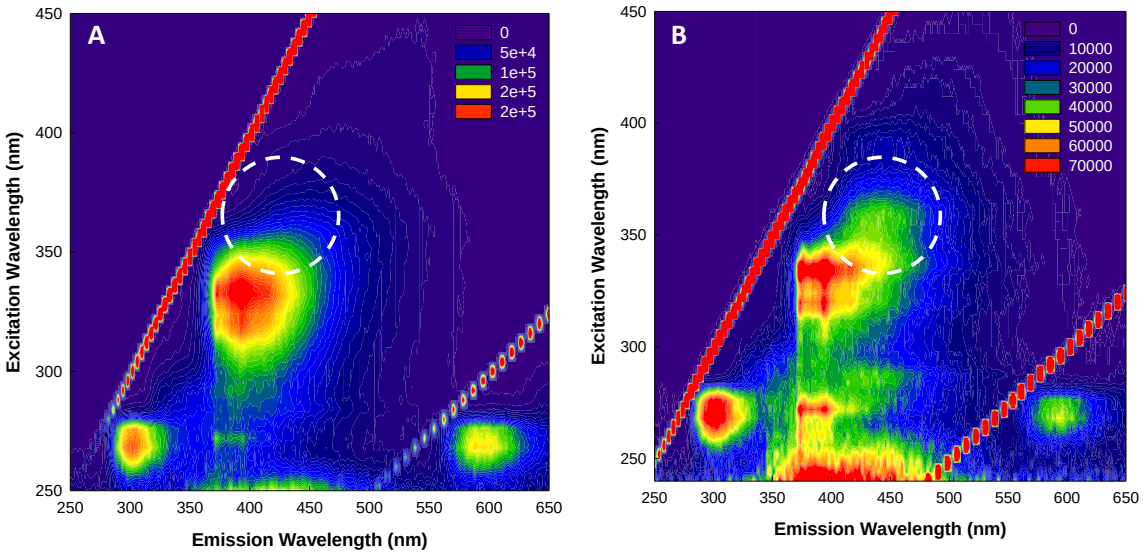


**Figure 3.10** Contour plot of methane-based carbon nanodots in ethanol synthesized for A) 2 and B) 4 hours.

For methanol dots, differences in the emission spectra can be seen in Figure 3.11 at around 300-350 nm emission. After a 4-hour synthesis, there is an apparent increase in the intensity and more emission structure seen within the highlighted

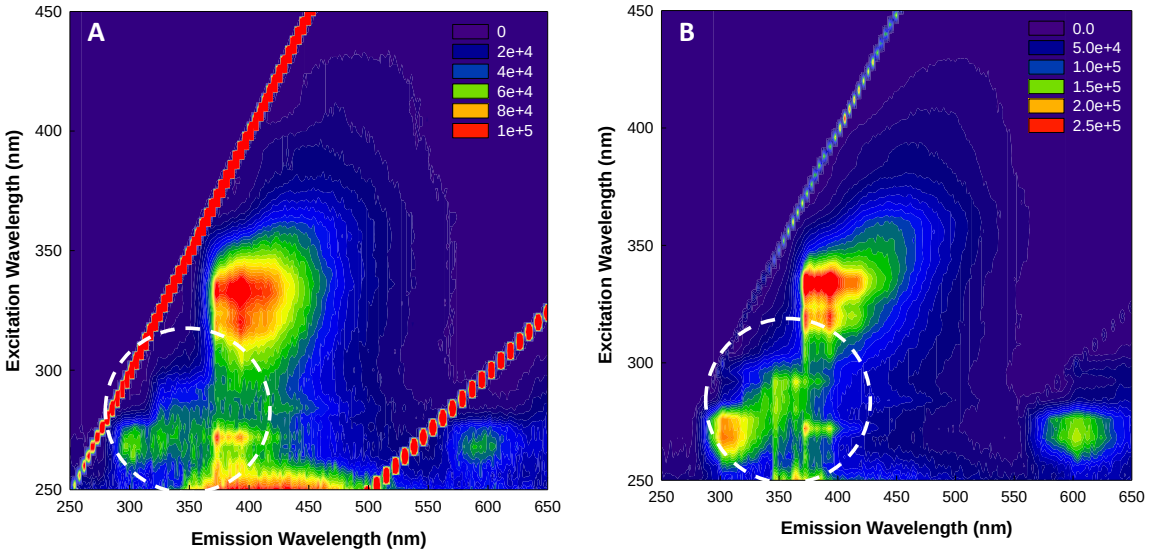


**Figure 3.11** Contour plot of methane-based carbon nanodots in methanol collected for A) 2 hours and B) 4 hours.

region. Similar to the water and ethanol dots, the entire emission structure over all wavelengths is comparable for both 2 and 4 hours' syntheses.

When analyzing the normalized emission spectra for ethanol and methanol dots, the excitation wavelength dependence is visible, as well as a decrease in emission intensity as the excitation wavelength is increased. These spectra are shown in Figures 3.12 and 3.13.

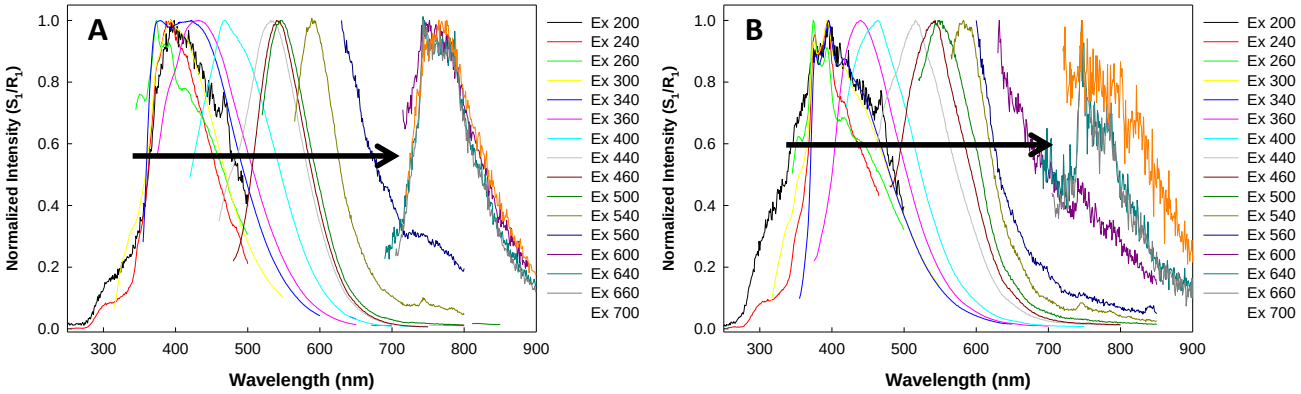


**Figure 3.12** Normalized emission spectra of methane-based carbon nanodots in ethanol synthesized for A) 2 and B) 4 hours.

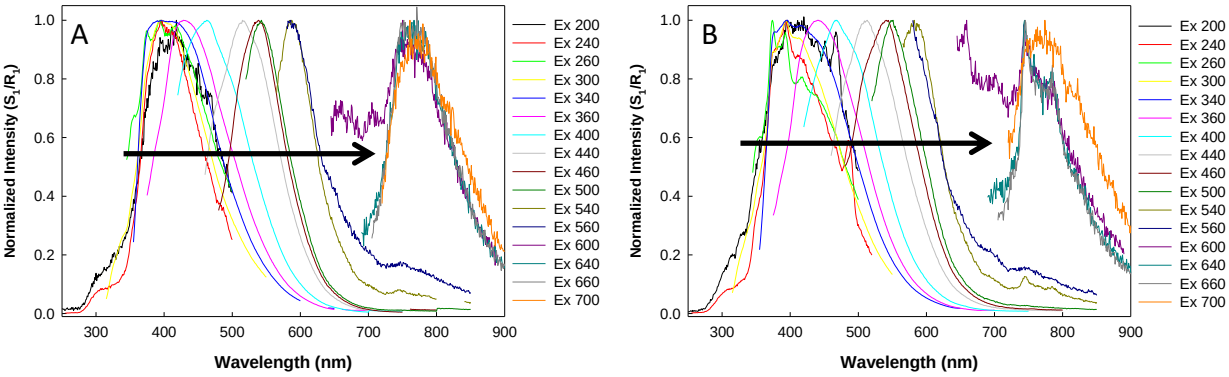


**Figure 3.13** Normalized emission spectra of methane-based carbon nanodots in methanol synthesized for A) 2 and B) 4 hours.

When comparing the three solvents emission spectra, they appear to look very analogous; however, there are slight differences in the emissive properties for the carbon nanodots. Water dots tend to have a broader emission spectrum whereas, ethanol and methanol appeared to have more vibronic structure present in their spectrum, which is illustrated in Figure 3.14**.** The presence of vibronic structure suggests that there are buried or core chromophores that are inaccessible to the solvent, which will be further explored in the next chapter. The solvent has been previously described to influence the emission properties of carbon nanodots, thus seeing slight differences in the emission spectra would be expected.[30,88–90] Along with vibronic differences, there is a slight hypsochromic shift in the maximum emission when one compares water dots to methanol dots which again can be attributed to how the nanodots are solvated in the three solvents. Overall, it appears that slightly

different structured carbon nanodots being synthesized in each solvent giving them their own unique spectra.

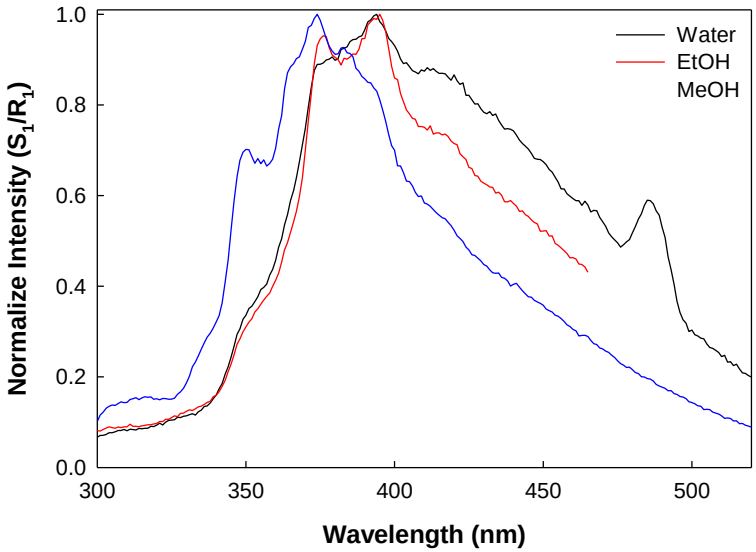


**Figure 3.14** Comparison of normalized emission spectra of methane-based carbon nanodots in various solvents after 4-hour synthesis. $\lambda_{ex}$ = 240 nm and $\lambda_{em}$ = 260-520 nm.

### *Hexane Dots*

The three previous solvents are polar solvents, so to study the effects of a non-polar solvent would have on the emission properties of carbon nanodots, an experiment using of hexane as the collection solvent was completed. It can be observed that in the presences of hexane, there is clearly more vibronic structure (Figure 3.15 A and B). There is also a bathochromic shift in the emission spectrum as compared to the water dots, when both dots are synthesized for 2 hours (Figure 3.15 C). These differences between water and hexane dots reveal that there are *completely different* carbon nanodots are collected in the two solvents. As stated in the earlier section, the solvent used to collect the nanodots can influence the emission properties, therefore photophysical different carbon nanodots are collected in hexane than in

water. These results further support the notion that by changing the solvent, the type and/or the emissive properties of carbon nanodots can be influenced.[30,88–90]

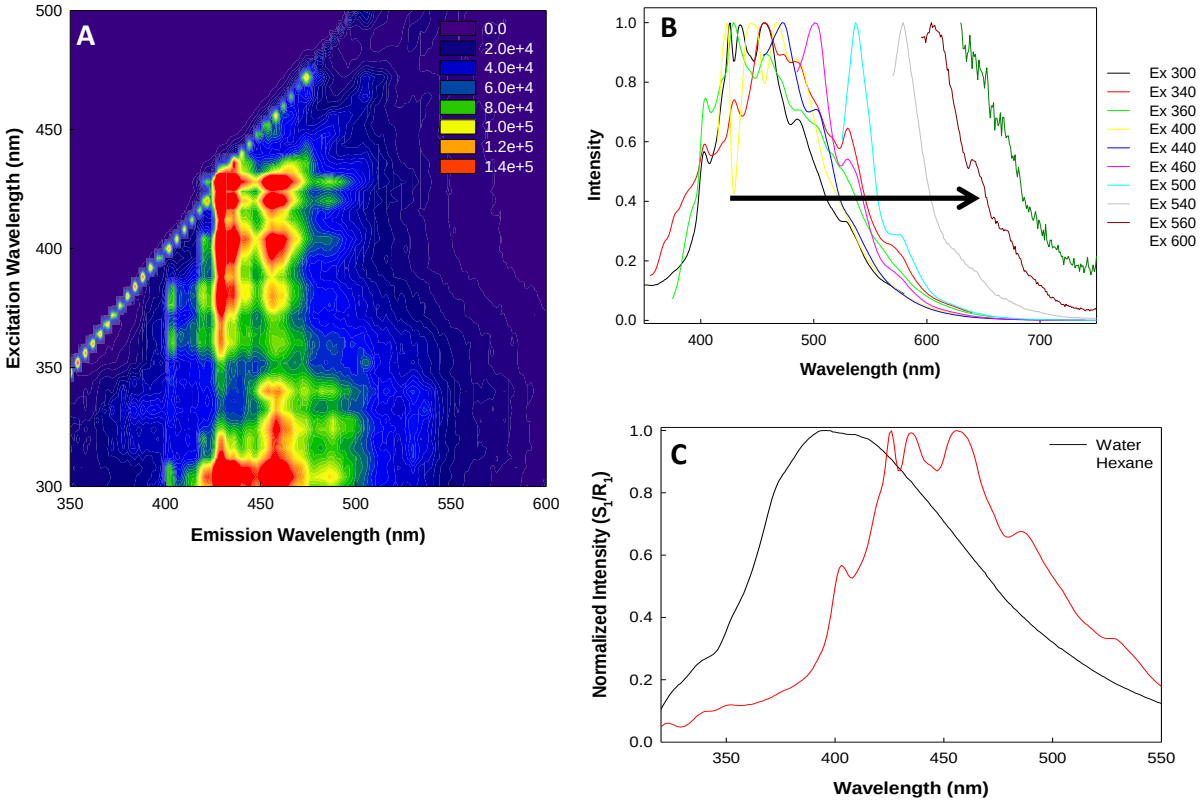


**Figure 3.15** A) Contour plot and B) normalized emission of carbon nanodots collected in hexane for 2 hours. C) Comparison of water and hexane dots when excited at 300 nm.

## Infrared Spectroscopy (IR) Characterization

Infrared spectroscopy was used to analyze the functional groups present in methane-based carbon nanodots. The results of this analysis revealed the presence of multiple functional groups in carbon nanodots. Carbon nanodots appear to have aromatic alkenes, alkenes, alcohols, alkanes, amines, and nitro groups based on the peaks observed in Figure 3.16. The presence of many different functional groups can lead to various electronic transitions, i.e., $\pi \rightarrow \pi^*$ for the alkene groups or $n \rightarrow \pi^*$ for

possible alcohol (O-H) groups.[50] Therefore, the presence of surface traps or multiple emissive centers on the carbon nanodots surface are possible.[2–5,13,37,88,91,92]

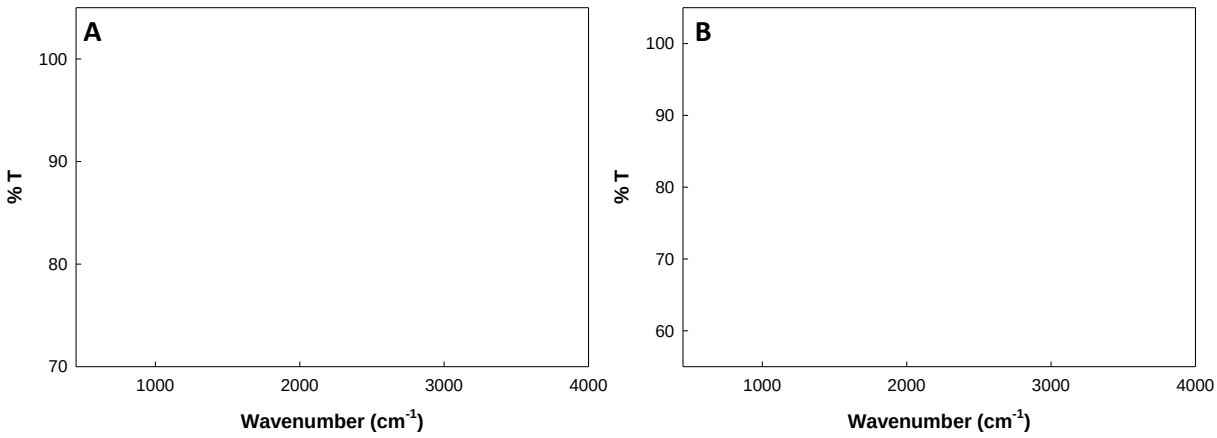


**Figure 3.16** Infrared spectra of methane-based carbon nanodots in A) water and B) ethanol synthesized for 4 hours.

### Origin of Methane-Based Carbon Nanodots' Fluorescence

Methane-based carbon nanodots display similar properties as the candle-based carbon nanodots, as the synthetic process is relatively similar for both. It is likely that the emission would be due to the same mechanism of several different emitter centers on the carbon nanodots. Methane-based carbon nanodots display the common characteristics of this mechanism and the multi-exponential time-resolved data further supports the multiple emissive centers mechanism. However, it is possible that methane-based carbon nanodots luminescence could be due to a core structure and surface traps based on the FT-IR results and vibronic structure observed in the emission spectra. It has recently been speculated that carbon nanodots could have a combination of both the multiple emissive center and the core/surface trap mechanisms.[5,6,42] The core structure, i.e. carbogenic core, is formed at high

temperatures (> 230°C) whereas, the emissive centers form at low temperatures.[5,6,42] Methane-based carbon nanodots are collected directly from the flame, which reaches temperature of >300°C, therefore, a carbogenic core could start to form, along with the emissive centers.[5,6,42] Data supporting the presence of a core structure and dual fluorescence mechanism is presented in Chapter 4.

**Fluorescence Quantum Yields Determination**

The relative fluorescence quantum yields were determined by using three known fluorophores: quinine sulfate, fluorescein di-sodium salt, and rhodamine 101. Methanol dots were only compared to quinine sulfate and those quantum yields were found to be 15-17%. For water dots, the quantum yields were determined to be 10-15% and 20-25% for 2 and 4-hour synthesis time, respectively when compare to quinine sulfate. When compared to fluorescein, the quantum yields of water dots dropped to 7-11% or 4-7% for 2 and 4-hour synthesis, which could due to the weaker emission of the nanodots at longer wavelengths. Water dots were also compared to rhodamine 101 and resulted in quantum yields of 5-8% or 4-6% for 2 and 4-hour syntheses, respectively. Ethanol dots were also compared to quinine sulfate, fluorescein, and rhodamine 101. The quantum yields for the quinine sulfate comparison were determined to be 27% and 20% for 2 and 4-hour syntheses. The quantum yields, when compared to fluorescein and rhodamine 101, drop to 5-8% and 4-5%, correspondingly. Table 3.5 summarizes the quantum yield data.

**Table 3.3** Relative approximate quantum yield calculations of carbon nanodots in various solvents at different excitation wavelengths.

| Sample | Average Φ (%) | Average Φ (%) | Average Φ (%) |
|---|---|---|---|
| | $\lambda_{EX}$= 350 nm | $\lambda_{EX}$= 496 nm | $\lambda_{EX}$= 450 nm |
| Water (4hr) | 11.30 ± 0.15 | 7.46 ± 0.54 | 6.03 ± 0.21 |
| Water (4hrs) | 14.87 ± 2.05 | 3.99 ± 1.28 | 4.37 ± 0.69 |
| Water (2hrs) | 24.07 ± 0.70 | 11.15 ± 0.98 | 8.99 ± 0.35 |
| Water (2hrs) | 20.37 ± 1.06 | 7.78 ± 0.29 | 4.64 ± 0.02 |
| Ethanol (4hrs) | 19.95 ± 2.35 | 5.80 ± 0.98 | 5.15 ± 0.51 |
| Ethanol (2hrs) | 27.19 ± 0.99 | 7.97 ± 0.33 | 4.16 ± 0.08 |
| Methanol (2hrs) | 15.98 ± 0.15 | N/A | N/A |

*Each average quantum yield calculation is from triplicate measurements within same batch of nanodots. Each excitation wavelength corresponds to a specific reference list in the experimental details.

By using three different references, ideally, the relative quantum yields of different emissive centers could be determined. All methane-based carbon nanodots showed weak absorption and emission in the longer ranges of the visible region, which explains why the quantum yields are low with both the fluorescein and rhodamine 101 reference standards. Also, methane-based carbon nanodots were shown to have large amounts of scatter present in their absorption spectra, which could lead to an underestimation of the quantum yields. The quantum yields are calculated by matching the optical densities of the standard and the nanodots.[49] Therefore, having higher amounts of scatter in the solution would make it appear as if there was a higher concentration of nanodots than there actually were in solution. Methanol dots were only compared to quinine sulfate due to the inability to match optical density of the carbon nanodots to the other references. Water and ethanol dots

were concentrated enough that the optical densities could be match to all three references.

**Phosphorescence Characterization**

The phosphorescence of methane-based carbon nanodots was studied to see if there was any triplet state emission. Long-lived triplet states can be quenched readily by molecular oxygen[49–51,77], so to alleviate this, carbon nanodot samples were mixed with glycerol (1:1 ratio) to slow down the molecular diffusion of quenchers in the solution. Two excitation wavelengths were chosen at 240 and 400 nm because carbon nanodots show maximum emission at 240 nm excitation and at 400 nm excitation, the emission is considerably lower. The phosphorescence spectrum was collected in a gated manner (~50 μs after lamp pulse), as outline in table 3.1. Figures 3.16-3.18 show the normalized emission and gated spectra for water, ethanol, and methanol dots in glycerol.

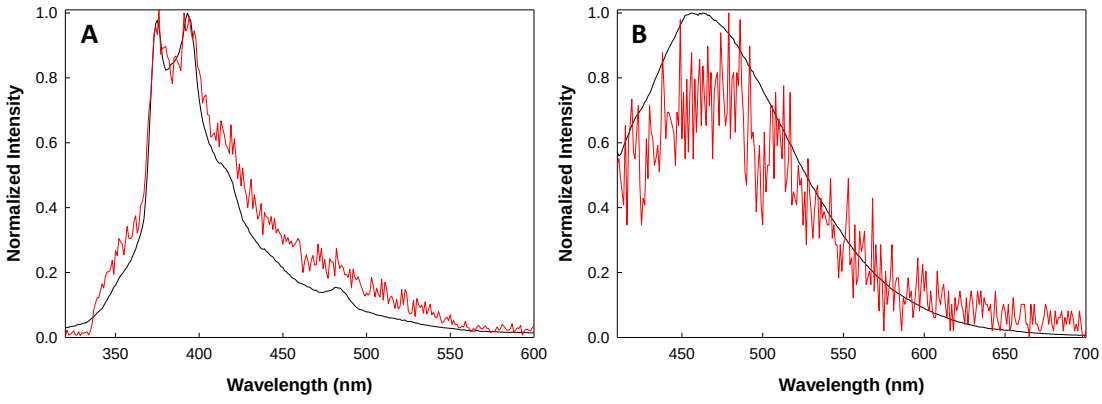


**Figure 3.17** Normalized fluorescence (black) and gated emission (red) of methane-based carbon nanodots in water (4hrs) excited at A) 240nm and B) 400 nm.

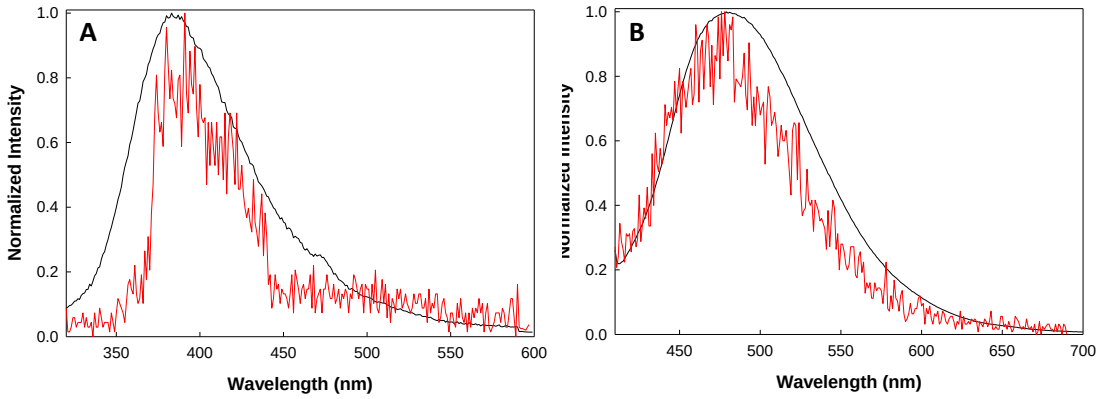


**Figure 3.18** Normalized fluorescence (black) and gated emission (red) of methane-based carbon nanodots in ethanol (2hrs) excited at A) 240nm and B) 400 nm.

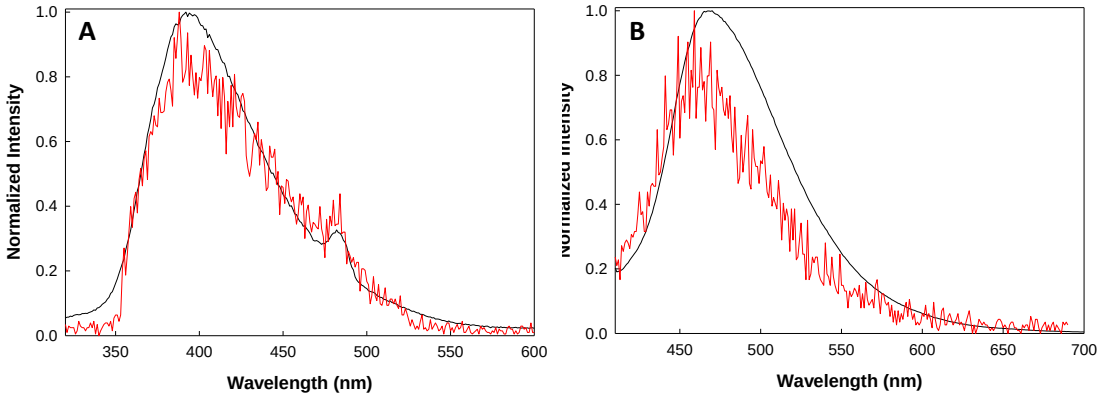


**Figure 3.19** Normalized fluorescence (black) and gated emission (red) of methane-based carbon nanodots in methanol (2hrs) excited at A) 240nm and B) 400 nm.

It is notable that the fluorescence and gated spectra look nearly identical. As described in chapter 1, the phosphorescence spectrum is collected after a gated delay so that no fluorescence signal is recorded and also the phosphorescence signal is usually red-shifted from the fluorescence signal. As shown in Figures 3.17-3.19, there appears to be no significant red-shift in the gated spectra. The similar appearance of the fluorescence and gated spectra could be due delayed fluorescence. This would mean that the carbon nanodots can intersystem cross into the triplet state, but then back-intersystem cross to the singlet state, where delayed emission occurs from the $S_1$ state (similar to fluorescence). This process of intersystem and back-intersystem

crossing requires a long-time scale for the emission to occur, which is why it is captured in the phosphorescence (gated) mode of the spectrofluorometer.

**Anisotropy Characterization**

Anisotropy measurements were used to estimate the diameter of the carbon nanodots synthesized. Steady-state and time-resolved techniques were used to obtain the necessary data to calculate the particle sizes of carbon nanodots. Equation 3.1 was used for size calculations where $\tau_r$ is the rotational correlation time, $D_r$ is the diffusion coefficient, T is the temperature in Kelvin, k is the Boltzmann constant, V is the volume ($V=4/3\pi r^3$) and η is the viscosity of the sample.[49]

$$\tau_r = \frac{1}{6D_r} = \frac{V\eta}{kT} \qquad \textbf{(3.1)}$$

From this calculation, the diameter of the methane-based carbon nanodots were determined to be approximately 1 nm or less. Table 3.6 lists the sizes of water and ethanol dots that were calculated from equation 3.1 at different excitation wavelengths used for time-resolved measurements of anisotropy. While it is believed that carbon nanodots are on the nanometer scale, having the sizes determined to be approximately 1 nm or less was not expected. Therefore, the sizes of carbon nanodots were further analyzed through dynamic light scattering.

**Table 3.4** Time-resolved anisotropy diameter size determination for water and ethanol dots in glycerol.

| Sample | $\lambda_{ex}$ (nm) | $\lambda_{em}$ (nm) | $\tau_R$ (ns) | Size (nm) |
|---|---|---|---|---|
| Water Dots | 400 | 500 | 2.4 | 1.66 |
| Water Dots | 474 | 500 | 8.2 | 1.16 |
| Ethanol Dots | 400 | 500 | 4.7 | 0.97 |
| Ethanol Dots | 474 | 500 | 8.9 | 1.19 |

**Dynamic Light Scattering (DLS)**

Dynamic light scattering measurements revealed a large distribution of sizes of carbon nanodots. Carbon nanodot samples were studied before centrifugation and after 14,500 RPM centrifugation, to determine if centrifugation could remove the excessively large carbon nanodots from the sample. Figure 3.19 shows the DLS results before and after centrifugation for water and ethanol dots.

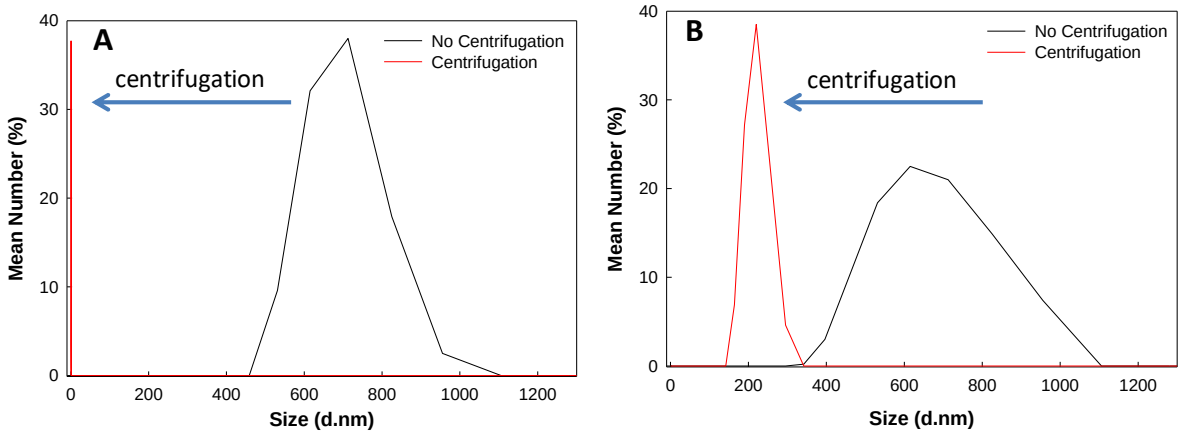


**Figure 3.20** Dynamic light scattering of carbon nanodots in A) water and B) ethanol before and after centrifugation at 14,500 RPM.

DLS revealed that after synthesis, there is a distribution of sizes particles from 1 nm to >1000 nm but using centrifugation, the smaller particles can be somewhat separated and their sizes become visible after the large particles are removed. When the DLS sizes are compared to the anisotropy sizes, it is clear that anisotropy seems to underestimate the total size of carbon nanodots in solution.

## Time-Resolved Intensity Decay Characterization

The time-resolved experiments illustrate that, like candle-based carbon nanodots, methane-based carbon nanodots show multi-exponential fluorescence intensity decays. The multi-exponential fits were determined based on the chi squared ($\chi^2$) minimization values. Water dots required a 3-exponential fit whereas, ethanol and methanol only needed a 2-exponential fit to minimize the $\chi^2$ of the intensity decays. The average lifetimes for water, ethanol and methanol dots was determined to be 7.72, 5.42, and 6.70 ns, respectively, when excited at 334 nm and the emission collected at 400 nm. The decay, fitting and residual traces for all three samples are depicted in Figure 3.17.

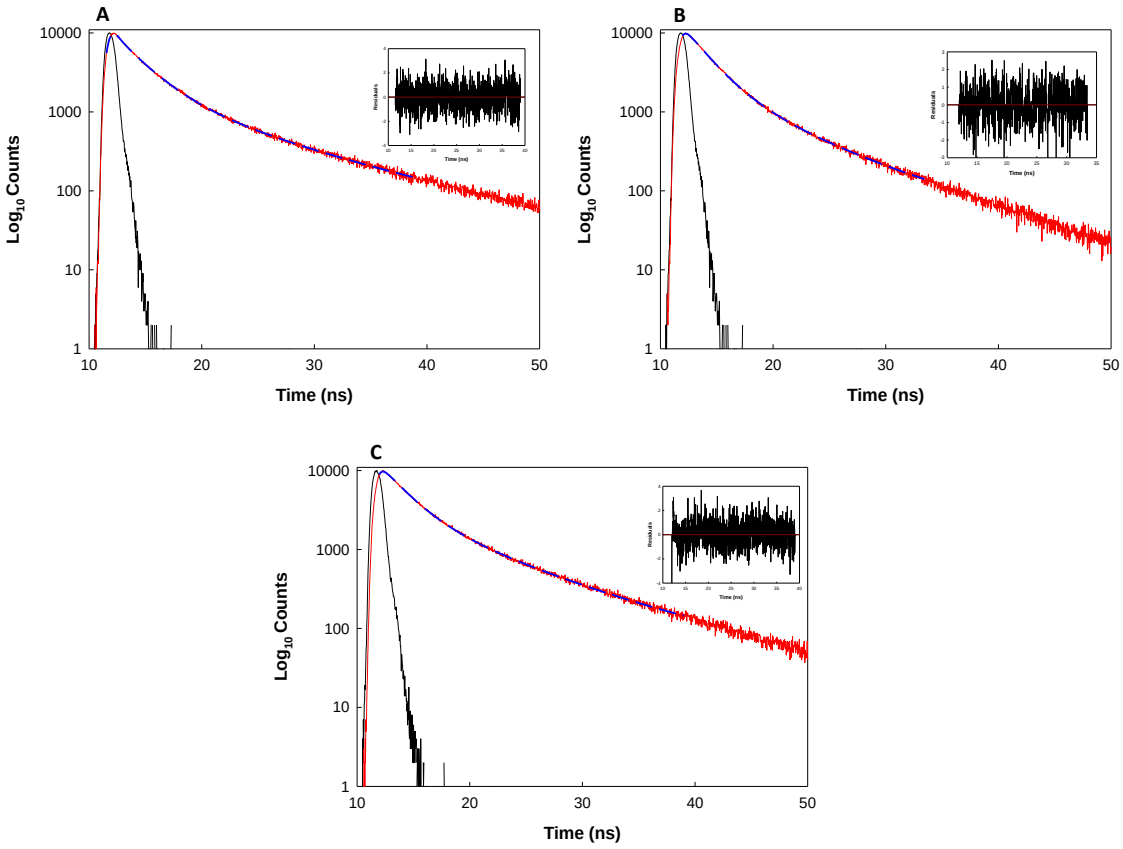


**Figure 3.21** Fluorescence intensity decay of methane-based carbon nanodots in A) water fitted to a 3-exponential decay, B) ethanol fitted to a 2-exponential decay, and C) methanol fitted to a 2-exponential decay. The excitation wavelength was 334 nm and the emission was collected at 400 nm. (Black line- instrumental response function, Red line - fluorescence decay). **Inset** Weighted residual graph.

The differences in the lifetimes between the three solvents supports the previous hypothesis that the solvent influences the photophysical properties of carbon nanodots.[30,88–90] The consequence of changing the emission wavelengths were also studied for water and ethanol dots and shown in Tables 3.7 and 3.8 for excitation at 400 nm. There are small changes in the average lifetime as the emission wavelength is changed.

**Table 3.5** Average fluorescence lifetimes of water dots synthesized for 2 hours.

| $\lambda_{ex}$ (nm) | $\lambda_{em}$ (nm) | $\tau_1$ (ns) | $f_1$ (%) | $\tau_2$ (ns) | $f_2$ (%) | $\tau_3$ (ns) | $f_3$ (%) | $\chi^2$ | $\tau_{avg}$ (ns) |
|---|---|---|---|---|---|---|---|---|---|
| 400 | 450 | 1.89 | 24.46 | 5.43 | 48.84 | 0.156 | 26.69 | 1.15 | 4.84 |
| 400 | 500 | 1.80 | 21.03 | 5.24 | 39.82 | 0.154 | 39.15 | 1.27 | 4.60 |
| 400 | 550 | 1.47 | 17.71 | 4.85 | 52.08 | 0.14 | 30.21 | 1.28 | 4.46 |
| 400 | 600 | 0.52 | 10.94 | 4.38 | 69.98 | 0.086 | 19.08 | 0.96 | 4.29 |

**Table 3.6** Average fluorescence lifetimes of ethanol dots synthesized for 2 hours.

| $\lambda_{ex}$ (nm) | $\lambda_{em}$ (nm) | $\tau_1$ (ns) | $f_1$ (%) | $\tau_2$ (ns) | $f_2$ (%) | $\tau_3$ (ns) | $f_3$ (%) | $\chi^2$ | $\tau_{avg}$ (ns) |
|---|---|---|---|---|---|---|---|---|---|
| 400 | 450 | 1.67 | 22.84 | 4.55 | 53.74 | 0.171 | 23.42 | 1.16 | 4.10 |
| 400 | 500 | 1.62 | 15.38 | 4.78 | 53.11 | 0.156 | 31.51 | 1.01 | 4.43 |
| 400 | 550 | 1.61 | 11.66 | 4.74 | 64.91 | 0.154 | 23.42 | 1.06 | 4.52 |
| 400 | 600 | 1.89 | 14.55 | 5.70 | 61.25 | 0.169 | 24.2 | 0.98 | 5.37 |

As previously discussed in the fluorescence section, the mechanism of emission is most likely due to a combination of a core structure and various emissive centers present on the carbon nanodots.[6,87] It could be reasoned that each center would have its own unique decay time, therefore, the multi-exponential lifetime decays observed for methane-based carbon nanodots helps to support this hypothesis.

## 3.4 Conclusions

Carbon nanodots were effectively synthesized from methane gas and the fluorescence quantum yields were improved from less than 2% for candle-based carbon nanodots up to 30% for methane-based carbon nanodots. The synthesis time for carbon nanodots was significantly reduced (≤ 4 hours) by collecting the nanodots in the solvent as they formed in the flame, instead of breaking down soot. This new combustion synthesis also influenced the optical properties.

The methane-based carbon nanodots photophysical properties are similar to the candle-based carbon nanodots and to that reported in literature.[2–5] The methane-based carbon nanodots contained a broad absorption, excitation wavelength dependent emission, multi-exponential fluorescence lifetime decays and increased fluorescence quantum yields of up to 30%. It was concluded that the solvent influenced the properties of the methane-based carbon nanodots as seen when comparing hexane dots to water dots in Figure 3.15C. Dynamic light scattering revealed a broad distribution of sizes in solution and that centrifugation could be used, to some extent, to separate large and small sized particles.

The origin of fluorescence for methane-based carbon nanodots seem most likely due to various emissive centers however, it can be hypothesized that since the methane carbon nanodots are collected directly from the flame (>300°C), that a carbogenic core structure would be formed along with diverse emitting centers.[5,6,42] This possible dual fluorescence mechanism due to a core structure and diverse emissive centers will be further discussed in Chapter 4.

# Chapter 4: Probing the Structural Properties of Carbon Nanodots through Stern-Volmer Analysis

## 4.1 Introduction

This chapter describes the analysis of methane-based carbon nanodots through quenching to gain a further understanding of their structural and luminescence properties. Within this chapter, three different quenchers were investigated at various concentrations using steady-state and time-resolved spectroscopies. Both types of spectroscopy analysis, along with temperature studies, were used to differentiate between dynamic and static quenching mechanisms. The Stern-Volmer plots generated were used to determine the effectiveness of the quenchers and accessibility of the chromophore to the quenchers.[49,93]

Fluorescence quenching experiments were carried out using two methods and different concentrations of quenchers. The first method, *multiple cuvette method*, was utilized to analyze the quenching of methane-based carbon nanodots. However, this method showed some inconsistency in the emission spectra when analyzing different nanodots samples that could be due to either dilution effects or the variation between the cuvettes used.

The second method, *single cuvette method*, was used to carry out a more controlled analysis, which could prevent dilution effects from influencing the carbon nanodots spectra. Also, the quenching of carbon nanodots was studied over multiple excitation and emission wavelengths (3D Quenching) to analyze the effects of quenchers on the overall emission of carbon nanodots. The results of the quenching

experiments in this chapter were used to elucidate surface charges, structural characteristics, and the possible origin of fluorescence of the methane-based carbon nanodots.

## 4.2 Experimental Details

### *4.2.1 Fluorescence Quenchers and Carbon Nanodots*

***Multiple Cuvette Quencher Concentrations.*** Fresh stock solutions (0.1 M) of sodium bromide (NaBr, Sigma Aldrich, St. Louis, MO), cesium chloride (CsCl, Sigma Aldrich, St. Louis, MO) and acrylamide (Sigma Aldrich, St. Louis, MO) were prepared in water then diluted to obtain 75, 50, 25, 10 and 1 mM concentrations. Each concentration of quencher (1.5 mL) was combined with 1.5 mL of carbon nanodots in disposable, plastic cuvettes (Perfector Scientific, Inc. Atascadero, CA) and analyzed. Table 4.1 shows the samples that were prepared and analyzed.

**Table 4.1** Sample used for multiple cuvette experiments in disposable, plastic cuvettes. $V_{CD}$ and $V_{Q\ is}$ the volume of carbon nanodots and quencher in cuvette**,** respectively.

| Cuvette # | $V_{CD}$ (mL) | $V_Q$ (mL) | Concentration (mM) |
|---|---|---|---|
| 1 | 3 | 0 | 0 |
| 2 | 1.5 | 1.5 | 1 |
| 3 | 1.5 | 1.5 | 10 |
| 4 | 1.5 | 1.5 | 25 |
| 5 | 1.5 | 1.5 | 50 |
| 6 | 1.5 | 1.5 | 75 |
| 7 | 1.5 | 1.5 | 100 |

***Single Cuvette Quencher Concentrations.*** Fresh stock solutions at 0.1 and 0.8 M of each quencher (NaBr, CsCl, and acrylamide) were prepared in water and stored until needed of analysis.

***3D Quencher Concentrations.*** Fresh stock solution of NaBr, CsCl, and acrylamide at either 0.8 M or 2.9 M were prepared and stored until use for analysis.

***Carbon Nanodots.*** Methane-based carbon nanodots collected in water, ethanol and methanol were prepared as previously described (3.2.1). The carbon nanodot solutions were used immediately after synthesis with no prior treatment necessary.

### *4.2.2 Multiple Cuvette Experiments*

***Steady-State Fluorescence.*** Steady-state fluorescence measurements were collected on a FluoroMax-4 spectrofluorometer using the FluorEssence software (Horiba Scientific, Edison, NJ). Samples were measured in multiple 1-cm disposable, plastic cuvettes (Table 4.1) with excitation wavelength of 320 nm and emission wavelength range of 330-600 nm. Stern-Volmer plots ($I_0/I$ vs [Q]) were created using either the lambda max or the area under the curve (AUC) values over the entire wavelength range (330-600 nm).

### *4.2.3 Singlet Cuvette Experiments*

***Steady-State Fluorescence.*** Steady-state fluorescence measurements were collected on a FluoroMax-4 spectrofluorometer using the FluorEssence software (Horiba Scientific, Edison, NJ). These experiments were carried out in a single glass or quartz cuvette with various concentrations of quencher, as outlined in Table 4.2, where the columns represent the volume of quench for each addition ($V_Q$), total volume of quencher added to the cuvette ($V_{total\ Q}$), moles of quencher added ($Moles_Q$), total

volume of the cuvette ($V_{cuvette}$) and concentration of quencher in the cuvette ($[Q]_{cuvette}$). After each addition of quencher, the cuvette was inverted 10 times to completely mix the sample. The excitation wavelength of 334 nm and emission wavelength range of 343-600 nm was selected to match the time-resolved excitation source. Stern-Volmer analysis was carried as previously described (4.2.2).

**Table 4.2** Steady-state samples for single cuvette method experiments in quartz or glass cuvette.

| Addition | $V_{Q\ added}$ (uL) | $V_{total\ Q\ added}$ (uL) | $Moles_{Q\ added}$ | $V_{cuvette}$ (mL) | $[Q]_{in\ cuvette}$ (mM) |
|---|---|---|---|---|---|
| 0 | 0.000 | 0.000 | 0.000000 | 2.000 | 0.000 |
| 1 | 5.000 | 5.000 | 0.000004 | 2.005 | 1.995 |
| 2 | 5.000 | 10.000 | 0.000008 | 2.010 | 3.980 |
| 3 | 5.000 | 15.000 | 0.000012 | 2.015 | 5.955 |
| 4 | 5.000 | 20.000 | 0.000016 | 2.020 | 7.921 |
| 5 | 10.000 | 30.000 | 0.000024 | 2.030 | 11.823 |
| 6 | 10.000 | 40.000 | 0.000032 | 2.040 | 15.686 |
| 7 | 10.000 | 50.000 | 0.000040 | 2.050 | 19.512 |
| 8 | 10.000 | 60.000 | 0.000048 | 2.060 | 23.301 |
| 9 | 10.000 | 70.000 | 0.000056 | 2.070 | 27.053 |
| 10 | 10.000 | 80.000 | 0.000064 | 2.080 | 30.769 |

***Time-Resolved Fluorescence.*** Time-resolved fluorescence decays were obtained using the FluoroCube system (Horiba Scientific, Edison, NJ). An instrument response function (IRF) was taken as previously detailed. The IRF and carbon nanodot samples were excited using NanoLEDs™ centered at 334 (Horiba Scientific, Edison, NJ) and the emission wavelength of 400 and 500 nm were selected as described in earlier chapters. Table 4.3 lists the samples and quencher concentration used to study the fluorescence quenching of water, ethanol, and methanol dots. All decay traces were collected and fitted as described in Chapter 2.

**Table 4.3** Time-resolved samples used for single cuvette method experiments in quartz or glass cuvette.

| Addition | $V_{Q\ added}$ (uL) | $V_{total\ Q\ added}$ (uL) | $Moles_{Q\ added}$ | $V_{cuvette}$ (mL) | $[Q]_{in\ cuvette}$ (mM) |
|---|---|---|---|---|---|
| 0 | 0.000 | 0.000 | 0.000000 | 1.000 | 0.000 |
| 1 | 3.000 | 3.000 | 0.000002 | 1.003 | 2.393 |
| 2 | 10.000 | 13.000 | 0.000010 | 1.013 | 10.267 |
| 3 | 12.000 | 25.000 | 0.000020 | 1.025 | 19.512 |
| 4 | 14.000 | 39.000 | 0.000031 | 1.039 | 30.029 |

***Temperature Steady-State and Time-Resolved***. Fluorescence quenching of water dots were analyzed at 10 and 40°C using NaBr, CsCl, and acrylamide quenchers. Both steady-state and time-resolved measurements were collected at 10 and 40°C using the instrument and solution parameters as described in the previously subsections (*Steady-state* and *time-resolved fluorescence)*. At each temperature, the cuvette was allowed to equilibrate for 15 minutes. Stern-Volmer plots were created from either lambda max or average lifetime data for steady-state and time-resolved measurements, respectively.

#### *4.2.4 3D Quenching*

***Steady-State Fluorescence.*** Steady-state fluorescence measurements were collected on a FluoroMax-4 spectrofluorometer using the FluorEssence software in 3D mode (Horiba Scientific, Edison, NJ). These experiments were carried out in a single cuvette with various additions of quencher (Table 4.4). Samples were measured in a single 1-cm quartz or glass cuvette with an excitation range of 350-450 nm and an emission range of 280-650 nm with each sample inverted 10 times to mix the sample thoroughly.

**Table 4.4** Emission samples used for 3D quenching experiments in quartz or glass cuvette.

| Addition | $V_{Q\ added}$ (uL) | $V_{total\ Q\ added}$ (uL) | $Moles_{Q\ added}$ | $V_{cuvette}$ (mL) | $[Q]_{in\ cuvette}$ (mM) |
|---|---|---|---|---|---|
| 0 | 0 | 0 | 0 | 3 | 0 |
| 1 | 3 | 3 | 0.0000087 | 3.003 | 2.90 |
| 2 | 5 | 8 | 0.0000232 | 3.008 | 7.71 |
| 3 | 5 | 13 | 0.0000377 | 3.013 | 12.51 |
| 4 | 9 | 22 | 0.0000638 | 3.022 | 21.11 |
| 5 | 10 | 32 | 0.0000928 | 3.032 | 30.61 |

## 4.3 Results and Discussion

### *4.3.1 Fluorescence Quenching of Methane-Based Carbon Nanodots utilizing the Multiple Cuvette Method*

The fluorescence quenching mechanisms was first studied using various concentrations of the quencher (Table 4.1). Figure 4.1 shows the emission spectra for water dots as a function of increasing quencher concentrations.

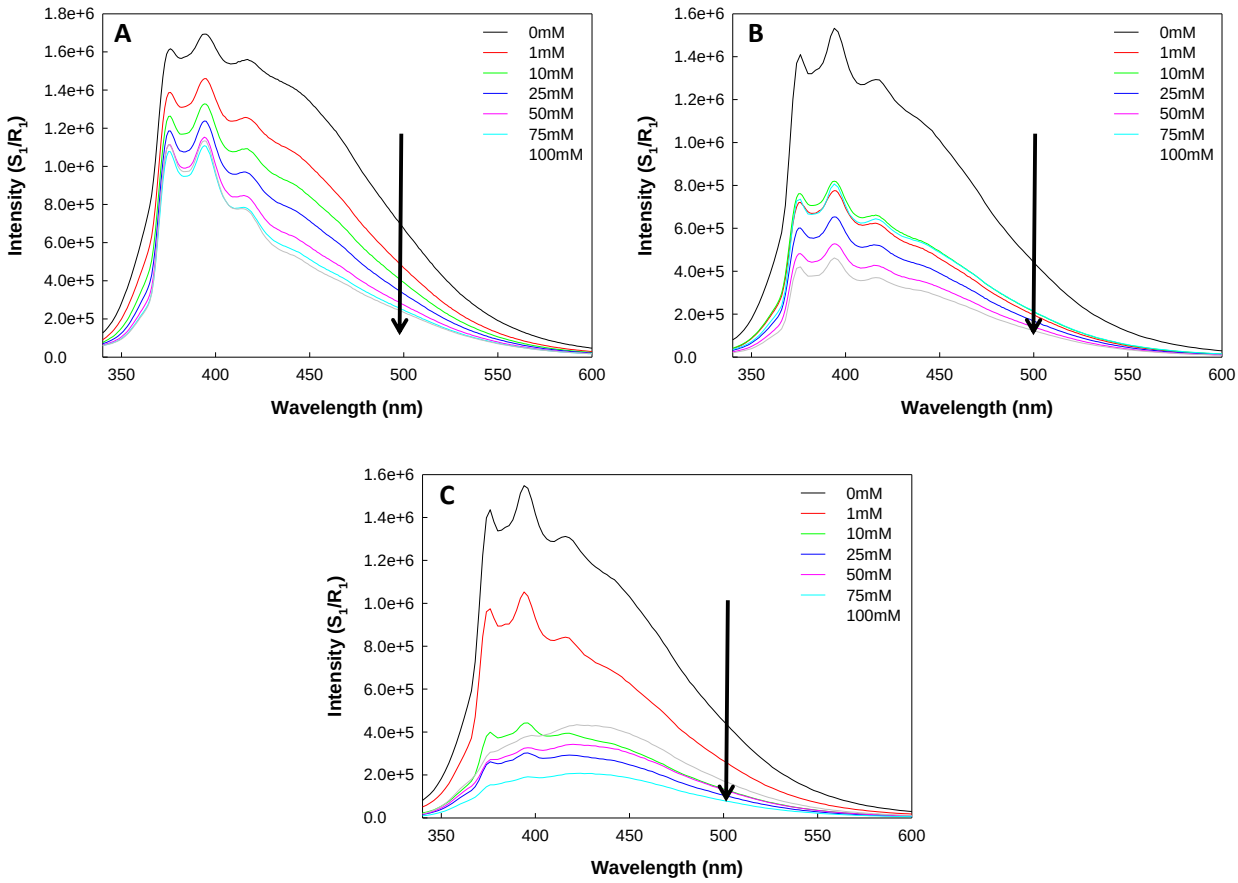


**Figure 4.1** Water dots synthesized for 4 hours quenched with A) NaBr B) CsCl and C) Acrylamide. The concentration of each quencher is noted in the figure.

It can be observed from Figure 4.1, that all three quenchers are effective at decreasing the emission of water dots. However, there are some inconsistencies worth noting. As the quencher concentration increases, the emission intensity should continuously decrease, however Figure 4.1 B and C shows that for CsCl and acrylamide, that this is not the case. For a few of the higher concentrations for CsCl and acrylamide, the emission intensity appeared to increase, instead of decrease, as seen with NaBr. This issue was seen over multiple trials with the same quenchers and different synthesized carbon nanodots samples. There are two potential reasons for this observation. First, the use of different cuvettes for each experimental condition

(quencher concentration) could have introduced experimental error into each spectrum. Additionally, dilution effects could also be responsible for the inconsistency noted since there is significant decrease observed after the first addition of quencher for CsCl and acrylamide. Therefore, a new single cuvette method was developed to help reduce error within the quenching experiments.

### *4.3.2 Fluorescence Quenching of Methane-Based Carbon Nanodots utilizing the Single Cuvette Method*

In order to prevent inconsistencies observed in the previous experiments, a new experimental protocol, utilizing a single cuvette with less than 5% change in total volume in the cuvette, was developed. The same three quenchers were investigated to analyze the surface charges of the methane-based carbon nanodots. It is thought that a negatively-charged chromophore, on the surface of the nanodots, would be more efficiently quenched by a positively-charged quencher, whereas, a positive-charged chromophore would be efficiently quenched with a negatively-charged quencher.[49,57] A neutral quencher would affect the fluorescence of both the negatively- and positively-charged chromophores on the surface, but it could also diffuse by the surface and possibly quench a buried chromophore that is not readily accessible to the other two quenchers.[49,50,57] The experimental parameters (quencher concentrations) used for each analysis are outline in Tables 4.2-4.4.

## Steady-State Fluorescence Quenching Analysis

Water, ethanol, and methanol dots were analyzed to see how the various charged quenchers affected their fluorescence properties. The excitation wavelength (334 nm) used for these measurements was matched to the NanoLED™ used for time-resolved experiments to ensure a direct comparison between steady-state and time-resolved data could be made. Figure 4.2 shows emission spectra of water dots in the presence of various quenchers at different concentrations.

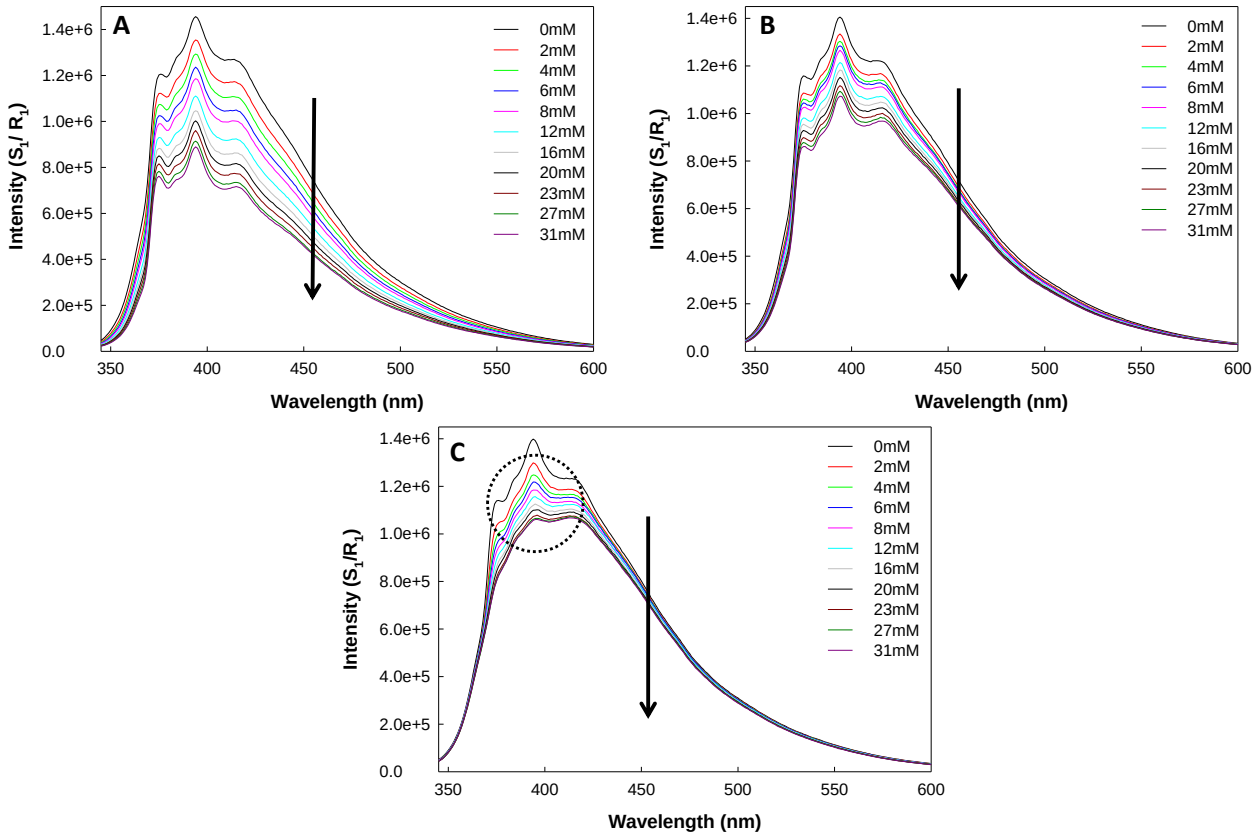


**Figure 4.2** Water dots synthesized for 2 hours quenched with A) NaBr, B) CsCl and C) Acrylamide. The quencher concentrations are noted in the figure.

When comparing the different quenchers, the emission spectra revealed that the NaBr appeared to quench the emission at 334 nm more efficiently than CsCl or acrylamide. Also, it important to note that acrylamide appeared to quench the vibronic structure of the emission spectra at 334 nm, which is highlighted by the black dashed circle. The loss of vibronic structure for only acrylamide shows that the neutral quencher is able to diffuse into the nanodots and quench a buried chromophore center, that is not accessible to the other quenchers or solvent. It is important to note that the loss of the vibronic structure could also be due to exciplex formation, i.e., an excited-state complex being formed between the quencher and nanodots. Exciplex formation is typically described by the appearance of a broad, structure-less emission spectrum, coupled with a bathochromic shift in the spectrum.[50,51] It is worth noting that we observe loss of the vibronic structure but, no spectral shifts are observed. The quenching of the vibronic structure with acrylamide revealed that methane-based nanodots, have buried fluorescence core, which supports the hypothesis of origin of luminescence of these nanodots could be from a core structure. From the emission spectra, it could be concluded that the surface of carbon nanodots contain both positively and negatively-charged chromophores and a buried core chromophore that is inaccessible to NaBr or CsCl, but is accessible to acrylamide. These quenching results support the thought that luminescence of carbon nanodots is due to a dual mechanism of a buried core structure and multiple emissive center on surface of nanodots. The same quenching trends seen with water dots were also visualized with ethanol dots, as shown in Figures 4.3.

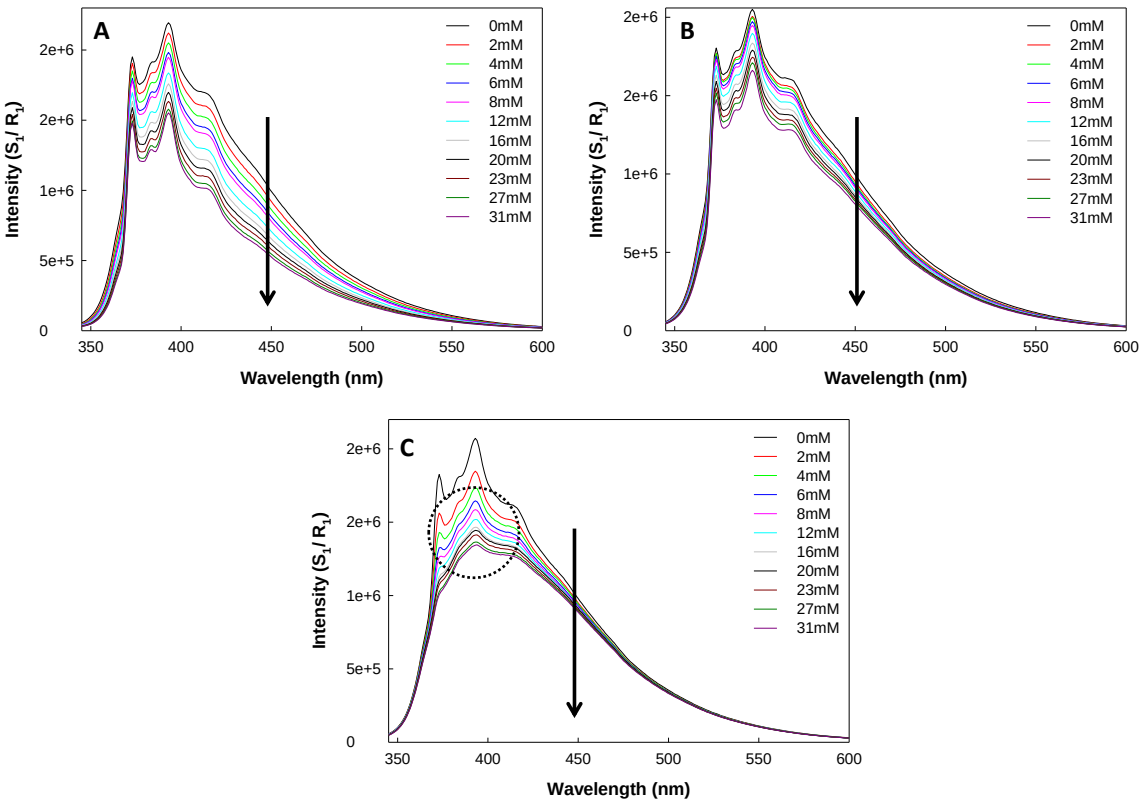


**Figure 4.3** Ethanol dots synthesized for 2 hours quenched with A) NaBr, B) CsCl and C) Acrylamide.

However, methanol dots showed a slightly different trend. As shown in Figure 4.4, acrylamide appears to have the greatest quenching effect when compared to NaBr and CsCl and the quenching of vibronic structure is still seen only with acrylamide. As noted in chapter 3, the solvent can affect the type of carbon nanodots synthesized, so the differences seen with the quenching of methanol dots may possibly be attributed to the different properties among these dots.

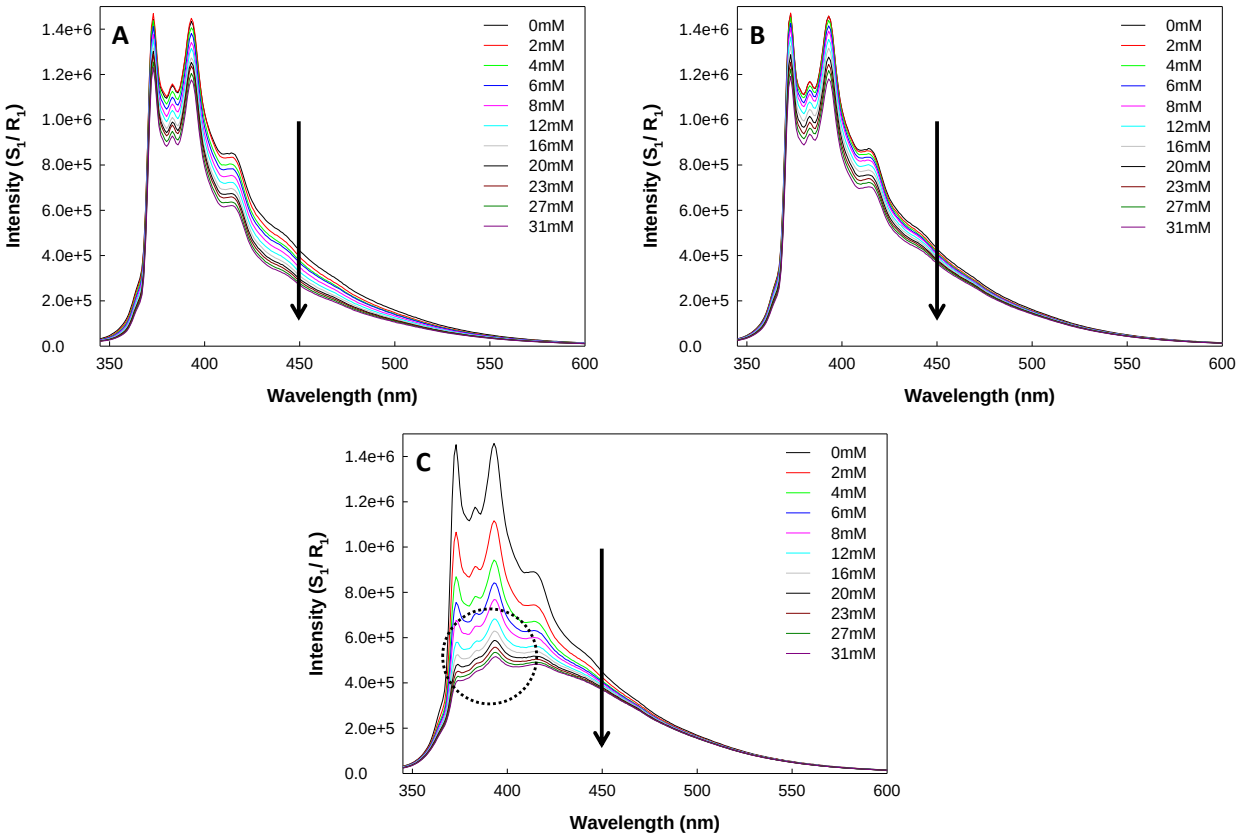


**Figure 4.4** Methanol dots synthesized for 2 hours quenched with A) NaBr, B) CsCl and C) Acrylamide.

To evaluate the effectiveness of each quencher, Stern-Volmer plots ($I_0$/I vs [Q]) were created for water, ethanol, and methanol dots. Using SigmaPlot 11.0, each quencher was fitted to a linear or 1-population line. Recalling equations 1.4 and 1.5, the slope of the linear fitted line is the Stern-Volmer constant ($K_{SV}$). This constant is

related to the quenching biomolecular rate constant, $k_q$ and the radiative lifetime, which is used to determine how effective a quencher is at quenching the emission of a fluorophore.[49,93] Figure 4.5 shows the Stern-Volmer plots for water, ethanol and methanol dots.

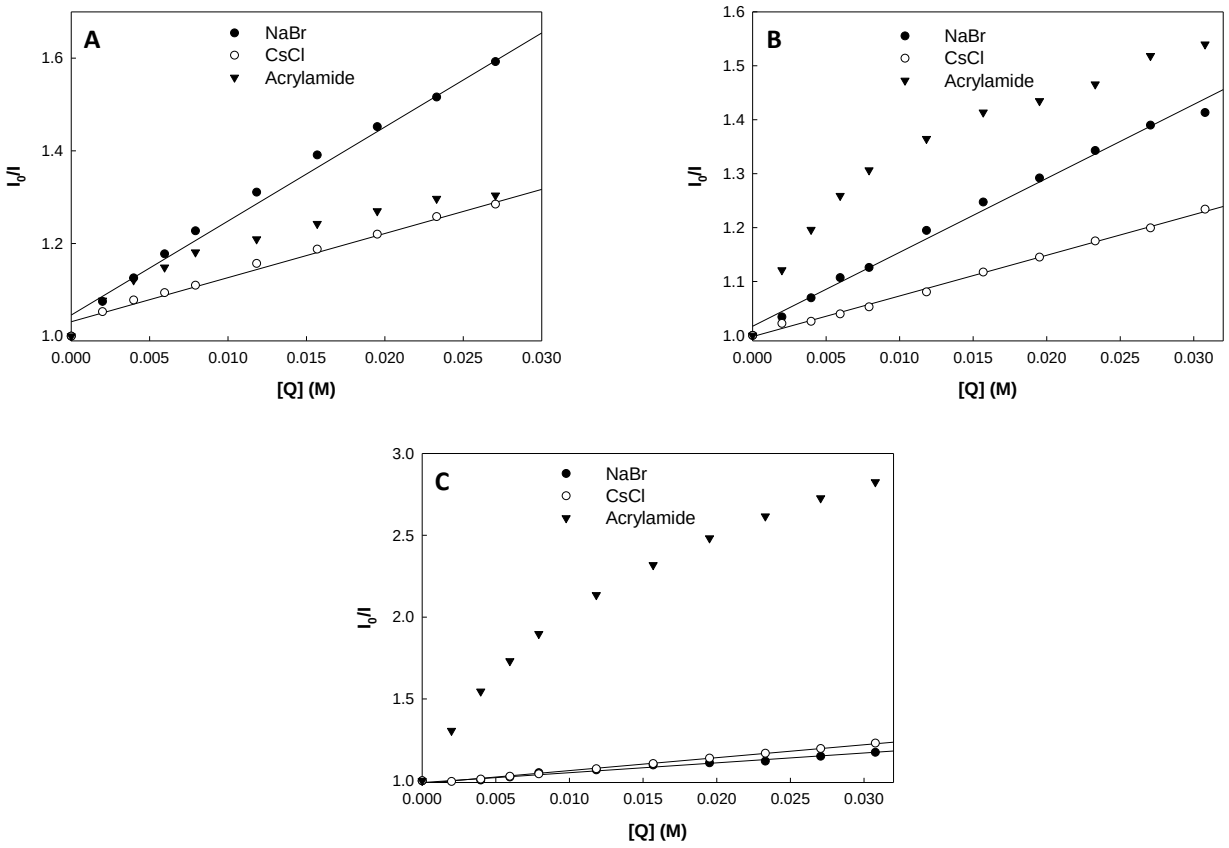


**Figure 4.5** Steady-state Stern-Volmer plots of A) water dots, B) ethanol dots and C) methanol dots synthesized for 2 hours.

Only NaBr and CsCl appeared to be a linear fit whereas, acrylamide, for all three dots, showed a deviation towards the x-axis, i.e., a positive inflection. This deviation is typical if there are two-populations of chromophores, one that is accessible to the quencher and one not accessible, similar to the fluorescence quenching of complex protein structures.[49,57] The presence of two-populations of

chromophores for acrylamide were supported by the quenching of the vibronic structure along with the quenching of the overall emission spectra of methane-based nanodots. The resulting $k_q$ values for water, ethanol and methanol dots are listed in Table 4.5. These $k_q$ values are smaller than diffusion limited values (i.e., approaching $1x10^{10}$ $M^{-1}s^{-1}$), meaning that these quenchers have a low quenching efficiency with methane-based carbon nanodots.[49,93] It is worth noting that some of the $k_q$ values are approaching the diffusion limited values (methanol dots quenched with NaBr and acrylamide). These values indicate that the chromophores being quenched are accessible to the quenchers. When the $k_q$ values of the nanodots are compared to another fluorophore, for example indole, quenched also with acrylamide, the values are not too different (8.25 for the nanodots compared to 7.1 for indole).[50] Therefore, some the $k_q$ values for the nanodots are similar to a freely accessible fluorophore in solution, whereas other values are not and those values may be indicative of a inaccessible chromophore. The steady-state quenching experiments cannot definitively reveal the mechanism of quenching. Both dynamic and static quenching mechanisms can result in linear Stern-Volmer plots, therefore time-resolved and temperature experiments were carried out.

**Table 4.5** Bimolecular rate constant for various quenchers used with carbon nanodots.

| | **$k_q$ Values ($10^9$ $M^{-1}$ $s^{-1}$)** | | |
|---|---|---|---|
| **Solvent/Quencher** | **NaBr** | **CsCl** | **Acrylamide** |
| **Water** | 3.07 | 1.44 | 1.38 |
| **Ethanol** | 2.15 | 1.18 | 2.41 |
| **Methanol** | 8.92 | 1.17 | 8.25 |

**Time-Resolved Fluorescence Quenching Analysis**

To determine which quenching mechanism each quencher follows, time-resolved intensity decays were studied for all three quenchers at room temperature. As stated in Chapter 1, dynamic quenching shortens the fluorescence lifetime of a fluorophore, whereas static quenching has no effect on the lifetime.[49,57] Subsequently, by monitoring the fluorescence lifetimes of carbon nanodots in the presence of various concentrations of quenchers, dynamic or static quenching mechanism can be determined. Figures 4.6-4.8 show the lifetime decays of water, ethanol, and methanol dots in the presence of NaBr, CsCl, and acrylamide quenchers. Only a few concentrations were used for lifetime analysis to reduce analysis time due to the weak signal at the selected emission wavelengths.

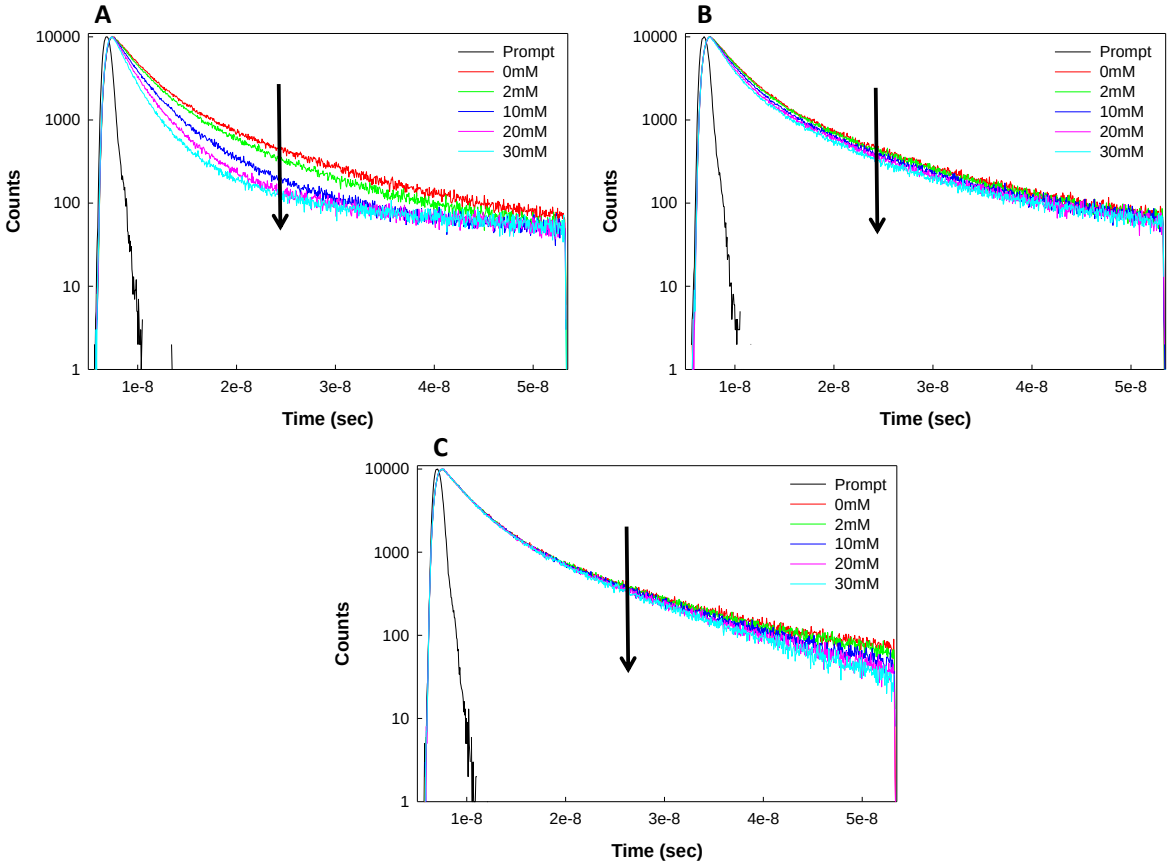


**Figure 4.6** Intensity decays ($\lambda_{em}$ =400 nm) of water dots synthesized for 2 hours quenched with A) NaBr, B) CsCl and C) Acrylamide.

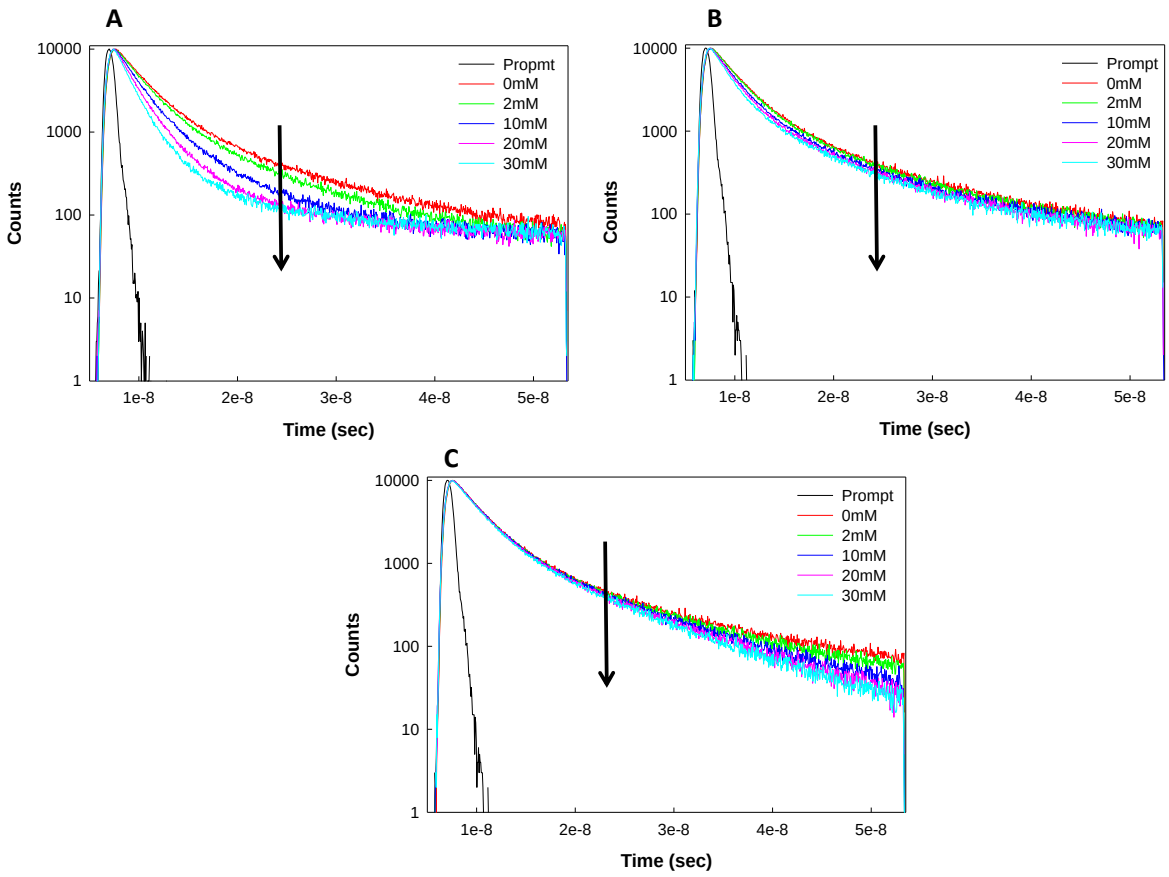


**Figure 4.7** Intensity decays ($\lambda_{em}$ =400 nm) of ethanol dots synthesized for 2 hours quenched with A) NaBr, B) CsCl and C) Acrylamide.

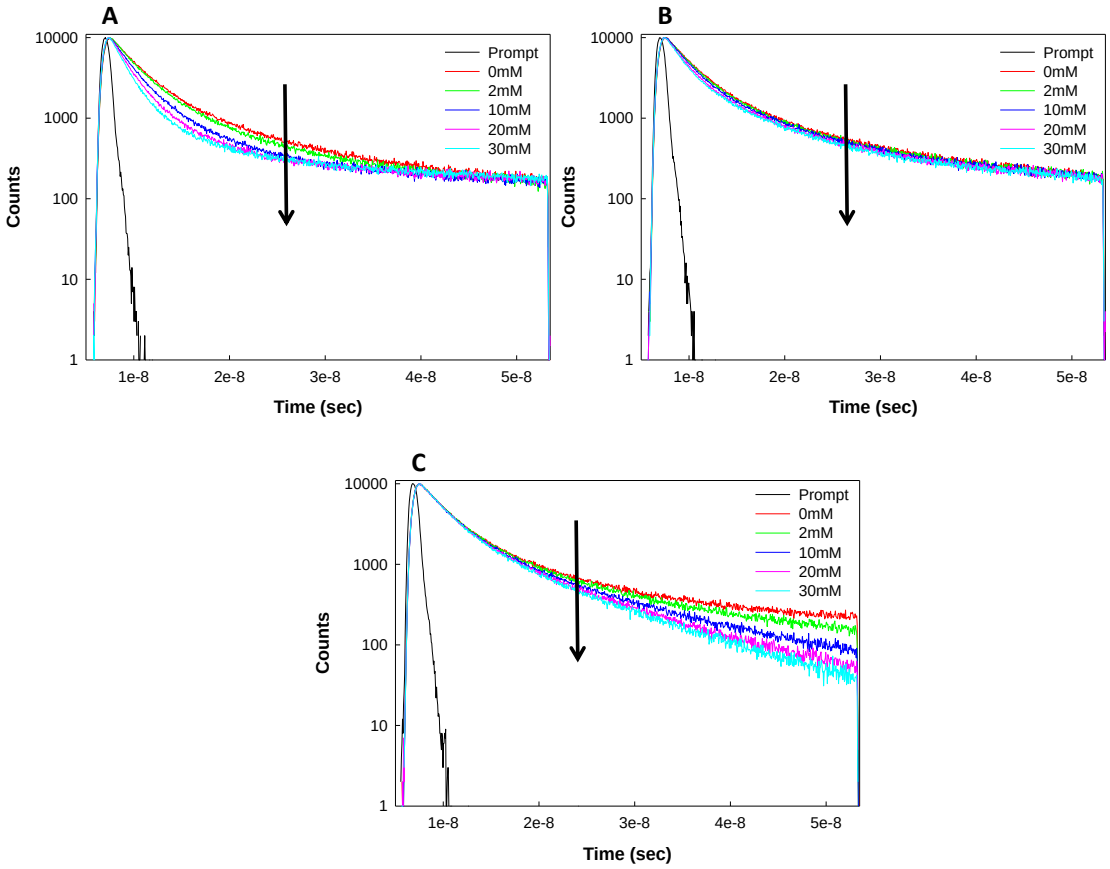


**Figure 4.8** Intensity decays ($\lambda_{em}$ =400 nm) of methanol dots synthesized for 2 hours quenched with A) NaBr, B) CsCl and C) Acrylamide.

For water, ethanol, and methanol dots, when NaBr was used as the quencher, a change in the lifetime decay can be observed. NaBr appeared to affect water and ethanol dots more than methanol dots based extent of quenching observed for the decay spectra at the various concentrations (Figures 4.6-4.8 A). It was difficult to determine if CsCl affected the lifetime for water, ethanol, and methanol. Therefore, the average lifetime at each concentration were calculated (equation 2.3) and showed that there was a slight decrease in the average lifetimes (Table 4.6) of methane-based nanodots, when CsCl was utilized.

**Table 4.6** Average lifetimes ($\lambda_{em}$ =400 nm) for carbon nanodots quenched with CsCl.

| | 0 mM | 2 mM | 10 mM | 20 mM | 30 mM |
|---|---|---|---|---|---|
| **Water (ns)** | 6.57 | 6.43 | 6.08 | 5.94 | 5.54 |
| **Ethanol (ns)** | 6.28 | 6.03 | 6.14 | 5.80 | 5.51 |
| **Methanol (ns)** | 6.75 | 6.56 | 6.66 | 6.21 | 6.12 |

When analyzing acrylamide's quenching spectra, there appeared to be no effect on the average lifetime, but there appeared to be an effect on the longer lifetimes, as shown in Figure 4.6-4.8 C. This suggests that acrylamide is able to quench the longer-lived chromophores on carbon nanodots i.e. the core structure, whereas NaBr and CsCl are not able to do this.[49,50] This can be related to the quenching of vibronic structure seen in the steady-state plots by acrylamide. The vibronic structure is most likely coming from a buried chromophore that is not accessible to the solvent or quenchers and therefore, appears to longer lifetime than the chromophores that are readily accessible. The buried core can be only quenched by a neutral quencher that is able to diffuse deeper into the structure of nanodots. The charged quenchers will interact with the charged surfaces of the nanodots and therefore, will not diffuse as much to the core structure, like the neutral quencher. The quenching of long-lived buried chromophores can be observed for all three methane-based nanodots studied, however, methanol dots appeared to have the largest quenching seen. When analyzing the average lifetimes for acrylamide, there was not a significant difference in the average lifetimes, which is the reason the Stern-Volmer plots (Figure 4.9) for acrylamide appeared, basically as a flat line. However, NaBr and CsCl Stern-Volmer plots have linear fits, which revealed that the quenching

mechanism for these two quenchers is dynamic, whereas acrylamide appeared to be a static mechanism.

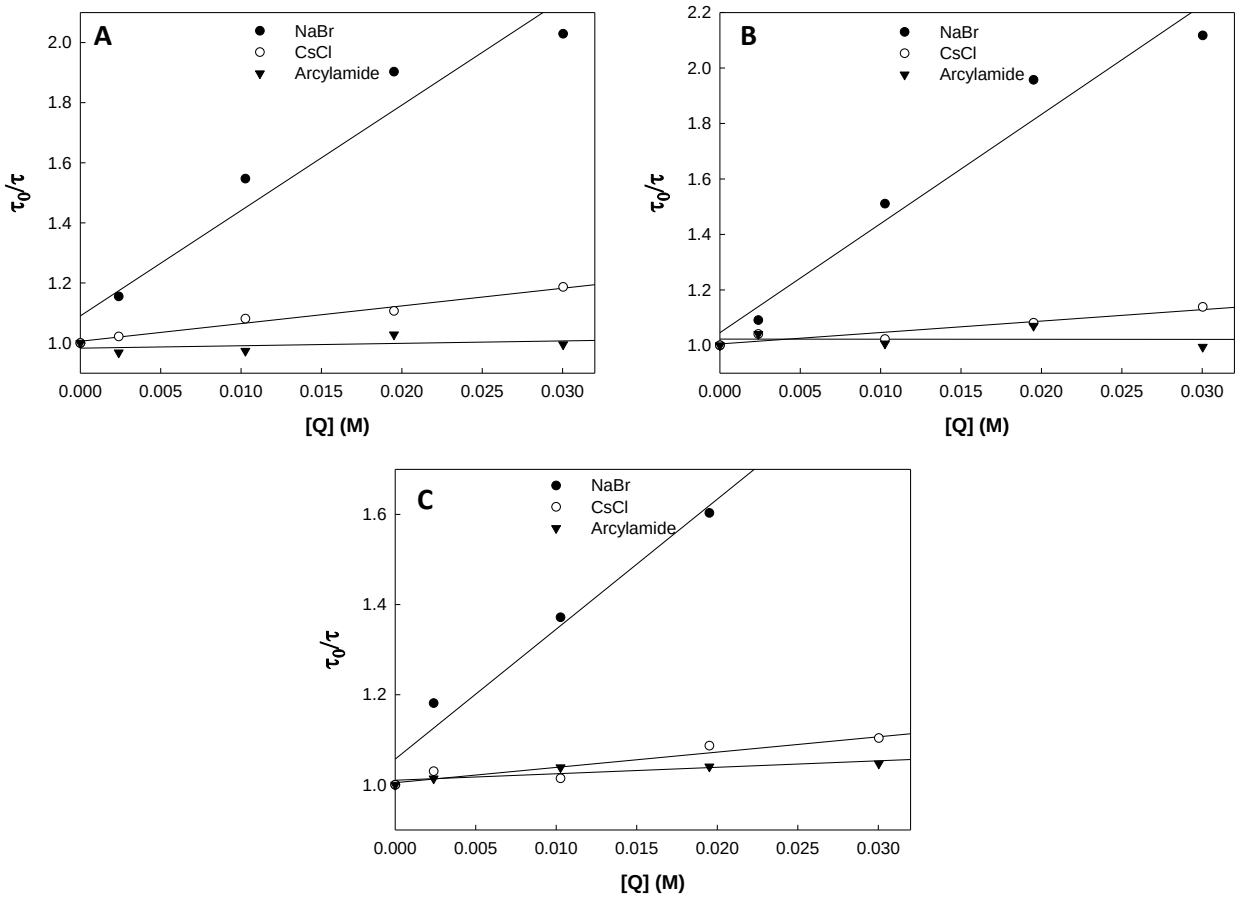


**Figure 4.9** Time-resolved Stern-Volmer plots of A) water dots, B) ethanol dots and C) methanol dots for 2 hours.

**Temperature Fluorescence Quenching Analysis**

In order to further confirm the quenching mechanism for acrylamide, steady-state and time-resolved experiments were analyzed at 10 and 40°C. At higher temperatures, there is faster diffusion of the molecules in solution and therefore an increased amount of dynamic quenching is expected. However, at higher temperatures, statically formed complexes formed are more likely to dissociate, leading to a decrease in static quenching amount.[49–52,57] The effects of temperature are observed in the change of the steepness of the slope of the Stern-Volmer plots, with dynamic quenching resulting in a steeper slope (higher $K_{SV}$ value) and static quenching resulting in a flatter slope (lower $K_{SV}$ value).[49–52,57] The temperature dependent time-resolved data did not show any significant differences in the average lifetime at either 10 or 40°C for nanodots quenched with acrylamide (Data not shown). The Stern-Volmer plots for the time-resolved data at both temperatures appeared as flat lines, similar to plots shown Figure 4.9. However, the steady-state data revealed inconsistent quenching of the nanodots' fluorescence at higher temperatures, as shown in Figure 4.10.

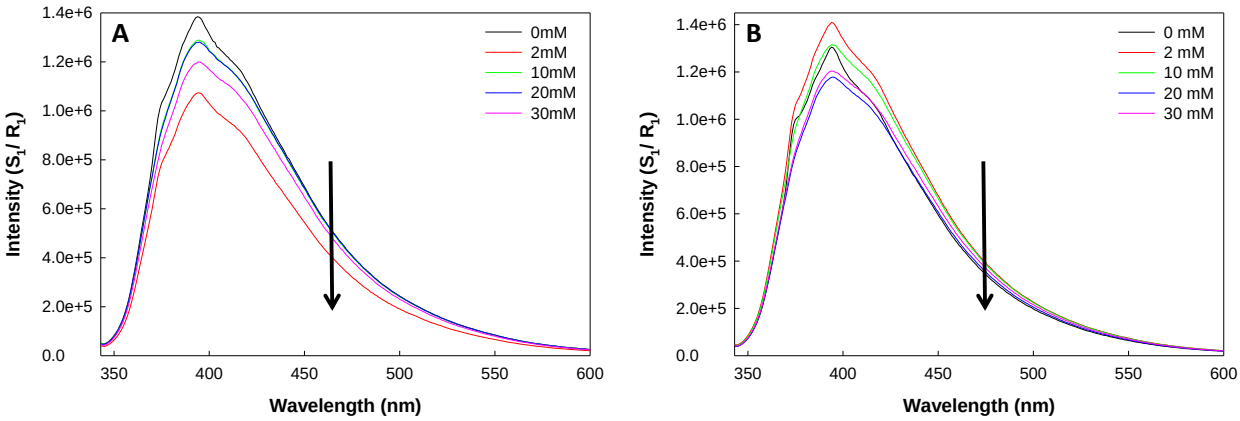


**Figure 4.10** Steady-state temperature quenching experiments of water dots quenched with acrylamide at A) 10°C and B) 40°C.

At room temperature, there appeared to be a systematic quenching of the nanodots' fluorescence (Figures 4.2-4.4), but at the higher temperature (40°C), there were inconsistent changes observed in the spectra. As seen in Figure 4.10, as the quencher concentration increased, the fluorescence intensity, in some cases, unexpectedly increased as well. These experiments were replicated several times and each time these unexpected quenching results were obtained. To determine if the inconsistencies were due to the acrylamide, temperature experiments were conducted with NaBr and CsCl. As shown previously, NaBr and CsCl quench fluorescence in a dynamic manner, therefore at higher temperatures, an increased $k_q$ value was expected. Using the other two quenchers, the same issues were observed for water dots at 40°C. At the higher temperature (40°C), the systematic quenching could not be replicated, therefore Stern-Volmer plots were not generated, but at the lower temperature (10°C) the systematic quenching was observed. Figure 4.11 shows the steady-state quenching of water dots at 10 and 40°C using the NaBr quencher. These unexpected results led to the study of carbon nanodots, without quencher, at various

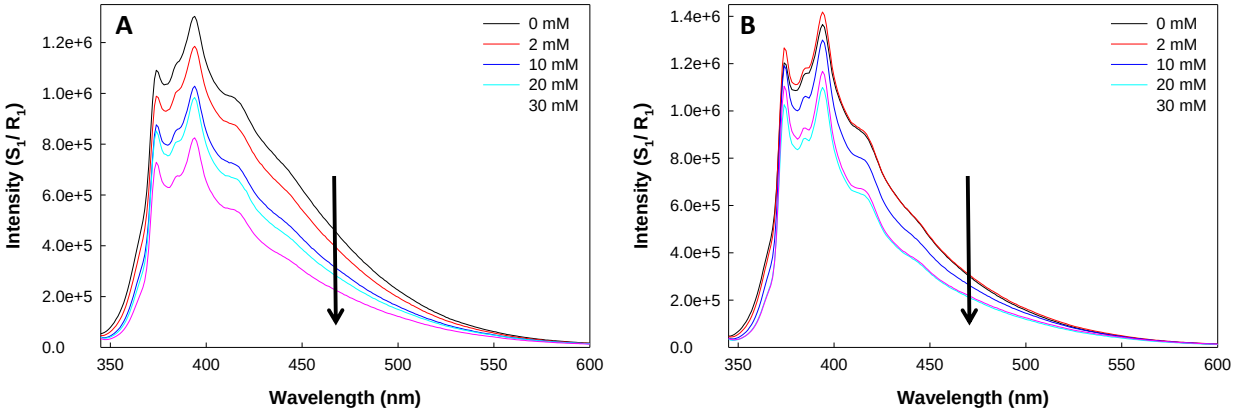


**Figure 4.11** Temperature quenching experiments of water dots quenched with NaBr at A) 10°C and B) 40°C.

temperatures. The temperature studies just described led to the discovery of temperature dependent emission of carbon nanodots, which will be discussed in the next chapter.

### *4.3.3 3D Fluorescence Quenching of Methane-Based Carbon Nanodots*

Only one wavelength was analyzed for fluorescence quenching in the previous sections, but carbon nanodots have an excitation wavelength dependent emission that is most likely due to a dual mechanism of a core structure and multiple emissive centers. It can be reasoned that each surface chromophore would react differently to the presence of the quenchers and to understand the effect of the quenchers on the multiple chromophores, quenching experiments were carried out over multiple excitation and emission wavelengths (3D quenching).

Figures 4.12 and 4.13 illustrate the results of 3D quenching experiments for water dots quenched with NaBr and CsCl at various concentrations. The extent of quenching is most notable with NaBr, which can be accredited to the efficiency of the quenchers (Table 4.5), i.e. quenching with halides scales as $Z^4$, where Z is the atomic number.[49,50]

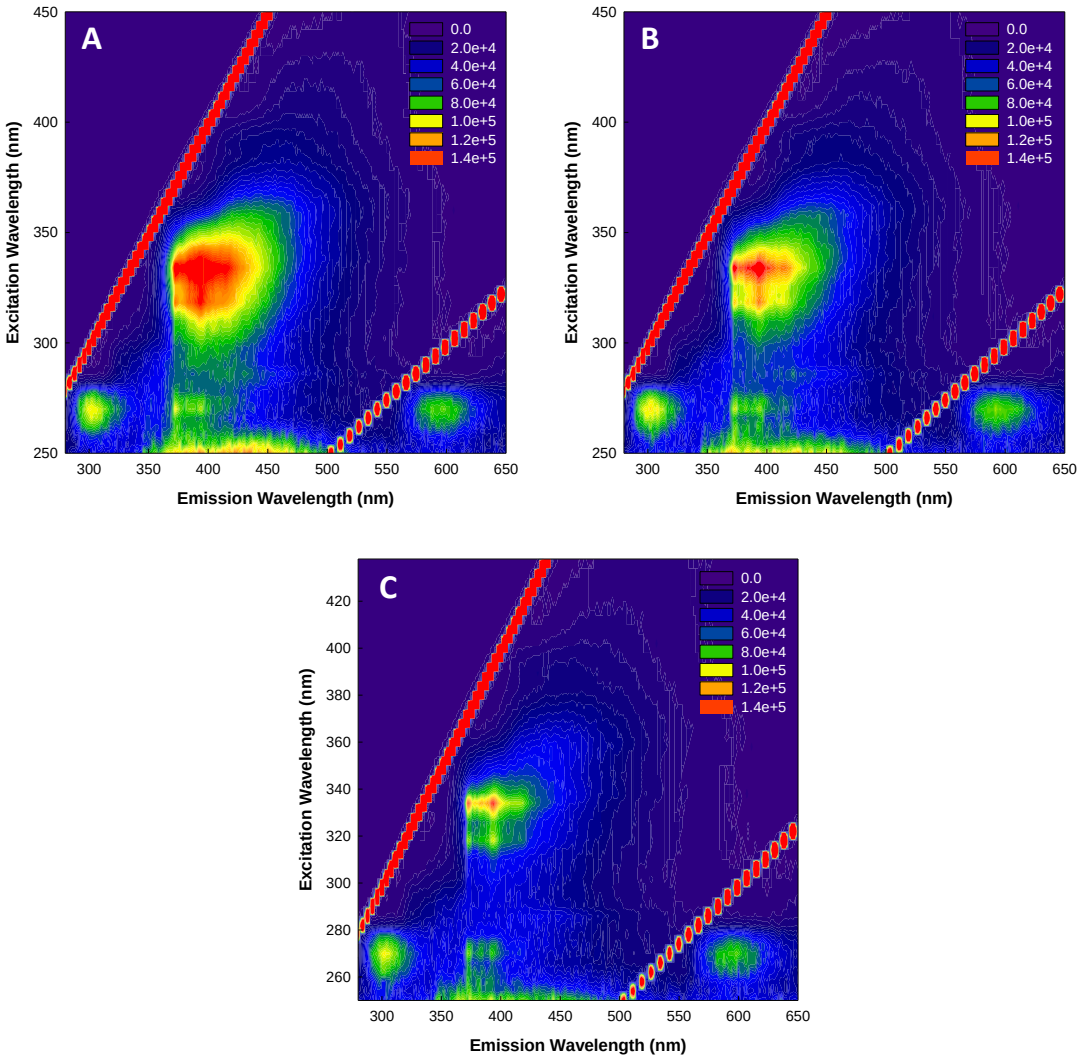


**Figure 4.12** Contour plots of water dots emission spectra quenched with NaBr at A) 0 mM B) 7 mM C) 30 mM.

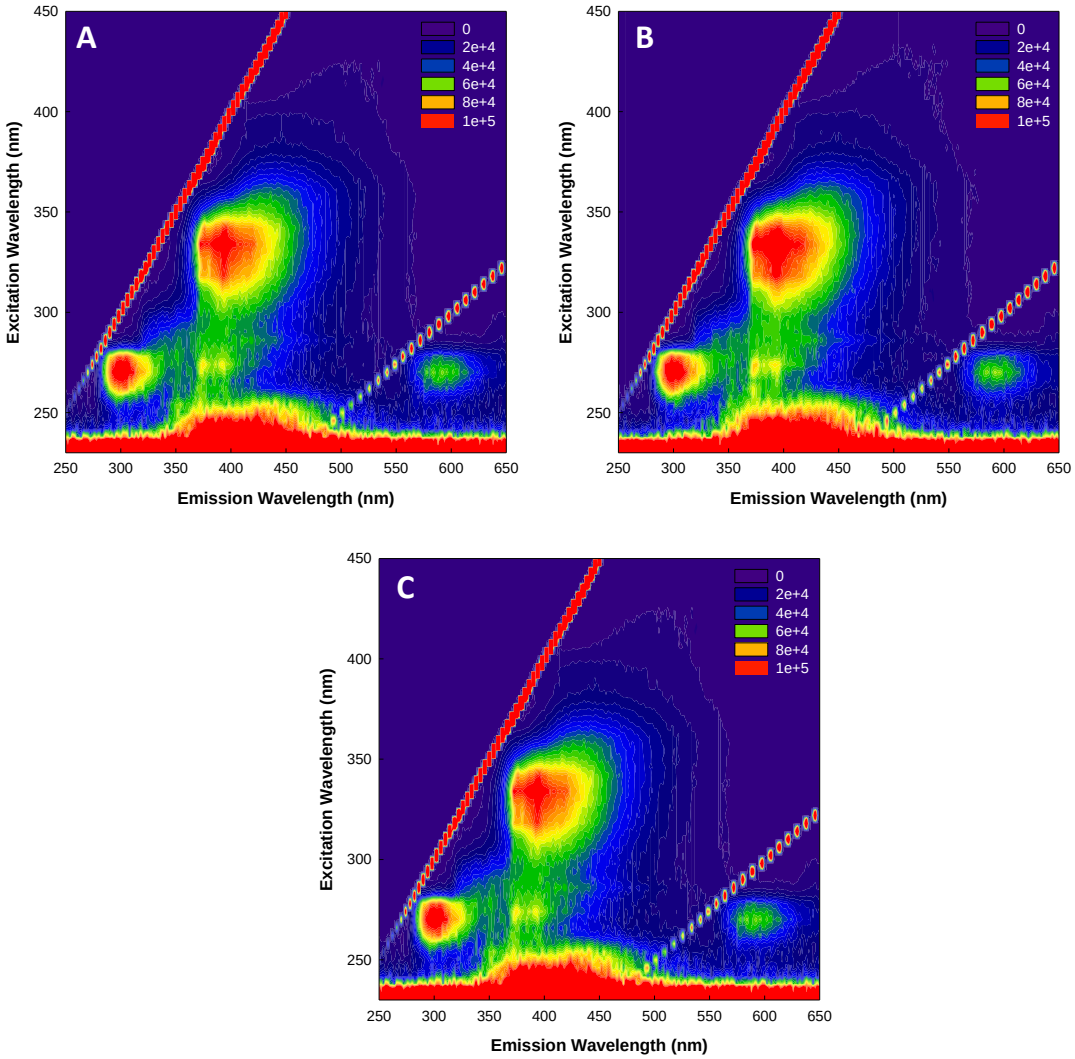


**Figure 4.13** Contour plots of water dots emission spectra quenched with CsCl at A) 0 mM B) 7 mM C) 30 mM.

Fluorescence quenching was observed over multiple excitation and emission wavelengths with a notable amount occurring between 350 and 450 nm emission wavelengths. Knowing that quenching occurs at multiple excitation and emission wavelengths, the $k_q$ values could be determined for each wavelength and could help give a better understanding of influence the quenchers have on the various surface chromophores.

## 4.4 Conclusions

From the Stern-Volmer analysis, it can be reasoned that the fluorescence quenching of the methane-based carbon nanodots is complex but, can be used to further elucidated the structural and luminescence properties of the nanodots. The results of the quenching experiments loosely conclude that the nanodots contain pores, which are likely to contain various charged and buried chromophores. The complex FT-IR spectrum (Chapter 3) further supports the presence of charged chromophores, which showed several functional groups that could be responsible for the presence of the charged chromophores within the nanodots. Together, these results support the thought that the fluorescence mechanism of methane-based carbon nanodots is due to multiple emissive centers and a core structure.

By utilizing multiple techniques, the mechanism of quenching of the three quenchers, NaBr, CsCl and acrylamide, were analyzed. Based on the degree of quenching in the steady-state and time-resolved spectra, it is believed that $Br^-$ and $Cs^+$ quench the charged chromophores in a predominately dynamic manner. However, the neutral quencher, acrylamide, is reasoned to quench the fluorescence of the nanodots in a static manner. The static quenching mechanism is believed to be due to the formation of an exciplex, which is supported by the loss of the vibronic structure in the emission spectra. Given that acrylamide is neutral, it is thought that acrylamide would be able to quench any buried chromophores within the nanodots, whereas the $Br^-$ and $Cs^+$ would not. This could be the reason for the non-linear Stern-Volmer plot for acrylamide, which is not unlike the results observed for the fluorescence quenching of chromophores within complex protein structures.[49] The quenching

results gave details into the structural and luminescence properties of carbon nanodots and led to the discovery of a unique temperature dependent emission property of methane carbon nanodots, which will be discussed in Chapter 5.

# Chapter 5: Temperature Dependent Emission of Carbon Nanodots

## 5.1 Introduction

Previous temperature studies of carbon nanodots have reported a decrease in the fluorescence intensity as a function of increased temperatures.[8,92,94–96] This trend is expected based on the increasing probability of collisional quenching at higher temperatures[49,50] however, for methane-based carbon nanodots the inverse of this trend was reproducibly observed. While completing quenching temperature experiments in Chapter 4, the emission intensity of carbon nanodots increased as a function of increased temperatures. This unique observation led to the investigation of this temperature dependent emission property of methane-based carbon nanodots.

The source of this temperature dependent emission is thought to originate from Thermally Activated Delayed Fluorescence (TADF), which is also commonly found in another allotrope of carbon, namely the fullerenes.[50,97–102] The mechanism of TADF takes place by way of a triplet manifold in which, the excited singlet state, $S_1$, intersystem crosses (ISC) to an excited triplet state, $T_n$, and then back intersystem crosses to the $S_1$ state, where then fluorescence occurs[46,50,97–102] Figure 5.1 depicts a simplified Jablonski diagram showing the mechanism of TADF, which is due to the ISC and then back ISC between the $S_1$ and $T_1$ states. TADF is a rare phenomenon that is usually observed to be a much weaker signal than the fluorescence signal of a typical fluorophore.[50,97–102] The goal of this chapter was to develop a basic

characterization and understanding of the temperature dependent emission property of the methane-based carbon nanodots.

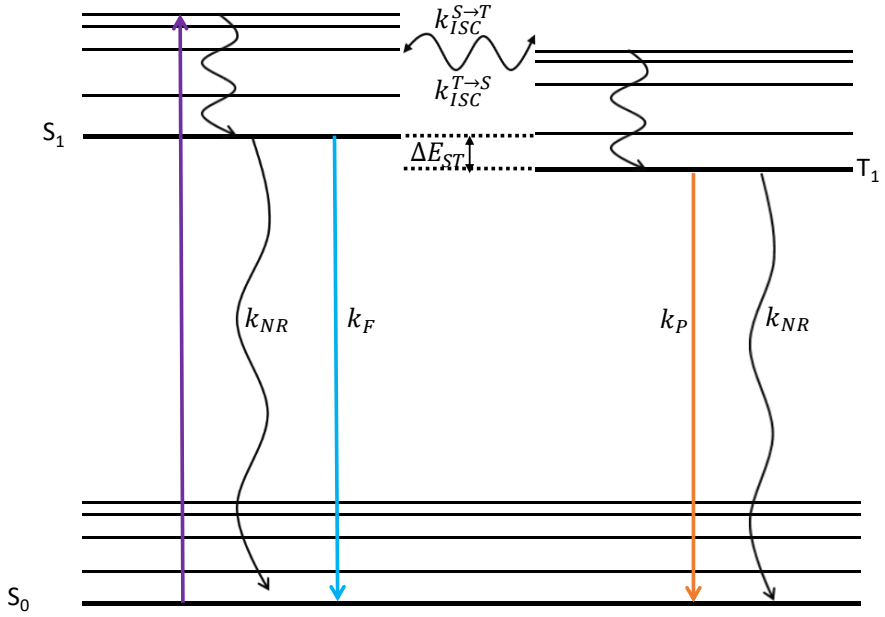


**Figure 5.1** Simplified Jablonski diagram highlighting the mechanism of TADF through intersystem crossing from $S_1 \rightarrow T_1$ ($k_{ISC}^{S\rightarrow T}$) and $T_1 \rightarrow S_1$ ($k_{ISC}^{T\rightarrow S}$). Where $k_{NR}$, $k_F$, $k_P$, $S_1$, $T_1$ represent non-radiative, fluorescence and phosphorescence rate constants, singlet, and triplet states, respectively and $\Delta E_{ST}$ is the energy gap between the singlet and triplet states.

## 5.2 Experimental Details

### *5.2.1 Temperature Steady-State Measurements*

***Steady-State Fluorescence.*** Steady-state fluorescence measurements were used to study the effects of different temperatures on the emission of carbon nanodots. These measurements were collected on a FluoroMax-4P spectrofluorometer equipped with a temperature-peltier controller, using the FluorEssence software (Horiba Scientific, Edison, NJ). Samples were analyzed in a 1-cm quartz or glass cuvette at six

temperatures: 10, 20, 30, 40, 50, 60 °C. The cuvette was equilibrated for 15 minutes at the selected temperature to ensure that the samples reached equilibrium. Samples were also purged with nitrogen gas ($N_2$), to remove oxygen from solution that could result in fluorescence quenching. Emission spectra were collected at two excitation wavelengths, 240 and 400 nm, with all spectra corrected for the lamp by dividing the signal of the sample by the reference signal ($S_1/R_1$). The $\lambda_{ex}$ at 240 nm had $\lambda_{em}$ range of 250-700 nm and the $\lambda_{ex}$ at 400 nm had $\lambda_{em}$ range of 410-700 nm. Water, ethanol, and methanol dots were subsequently analyzed at all temperatures and wavelengths.

***Steady-State Delayed Fluorescence***. Delayed fluorescence measurements were completed to determine if the delayed emission of carbon nanodots was influenced by temperature in the same manner as the fluorescence. These measurements were carried out in FluoroMax-4P spectrofluorometer equipped with a temperature controller using the FluorEssence software in phosphorescence (gated manner) mode (Horiba Scientific, Edison, NJ). Sample were investigated in a 1-cm quartz or glass cuvette at 10, 20, 30, 40, 50, 60 °C with a 15-minute equilibrium time to allow the samples to reach the selected temperatures. Samples were $N_2$ purged and/or mixed with glycerol to prevent any quenching due to oxygen. The same carbon nanodot samples, excitation wavelengths, and emission wavelengths were examined as described in *Steady-State Fluorescence* section above.

***Steady-State 3D Fluorescence.*** Steady-state 3D fluorescence measurements were used to determine if there were more wavelengths that displayed this temperature dependent emission property. These measurements were collected on a FluoroMax-4P spectrofluorometer equipped with a temperature-peltier controller using the

FluorEssence software, in 3D mode, (Horiba Scientific, Edison, NJ) at six temperatures: 10, 20, 30, 40, 50, 60 °C. The samples were measured in 1-cm quartz or glass cuvette and equilibrated for 15 minutes at each temperature. Emission spectra were collected at an excitation range of 230-600 nm and an emission range of 250-650 nm.

***Temperature Cycling of Fluorescence.*** Cycling experiments were used to determine if the emission of the carbon nanodots was reversible after heating and cooling multiple times. The reversibility could be used to determine if the changes observed are due to a photophysical effect, i.e. increase of the density of states between the singlet and triplet excited-sates, as compared to any photochemical processes. These measurements were studied on a FluoroMax-4P spectrofluorometer equipped with a temperature controller using the FluorEssence software (Horiba Scientific, Edison, NJ). Samples were cycled in a 1-cm quartz or glass cuvette at three temperatures: 10, 30, and 60°C. First, samples were cooled to 10°C, allowed to equilibrate for 15 minutes and an emission spectra take at two excitation wavelengths, 240 and 400 nm. This same process was repeated for 30 and 60°C, with one cycle consisting of a 10, 30 and 60°C spectra for each excitation wavelength. After reaching 60°C, the sample sat untouched for 5 minutes to allow for equilibration after excitation. The sample was then re-analyzed at the two excitation wavelengths for 60°C. This re-analysis was considered the start of a second cycle and the process of heat/cooling the sample to either 10,30 or 60°C, as described previously, is repeated for a total of six cycles. The $\lambda_{ex}$ at 240 nm had $\lambda_{em}$ range of 250-700 nm and the $\lambda_{ex}$ at 400 nm. The samples were

additionally purged with nitrogen gas ($N_2$), to remove oxygen from solution that could possibly result in fluorescence quenching of the long lived-luminescence.

### *5.2.2 Temperature Time-Resolved Measurements*

Time-resolved fluorescence intensity decays were obtained to study how the excited-state lifetimes were effect at higher temperatures. The time-correlated single photon counting (TCSPC) technique on a FluoroCube system (Horiba Scientific, Edison, NJ) equipped with an Isotemp Digital-Control Water Bath (Thermo Fisher Scientific, Waltham, MA) was utilized to collect the intensity decay spectra. Samples were analyzed at 4, 10, 20, 30, 60 and 70 °C and allowed to equilibrate at each temperature for 20 minutes. The instrument response function (IRF) and carbon nanodot samples were excited using NanoLEDs$^{TM}$ centered at 400 nm (Horiba Scientific, Edison, NJ) and the emission wavelength of 460 nm was use to collect the intensity decay. The system's experimental parameters are previously described in chapter 3. Decay spectra were taken on the DataStation V 2.7.2 software and the fitting of the decays were completed using the DAS 6 Analysis software.

## 5.3 Results and Discussion

### *5.3.1 Temperature Dependent Steady-State Measurements*

**Fluorescence and Delayed Fluorescence Analysis of Methane-Based Nanodots**

In order to analyze effects of temperature on the emission spectra, water dots were exposed to six temperatures ranging from 10°C to 60°C. Also, two excitation wavelengths, 240 and 400 nm, were chosen to examine the effects of temperature at

the highest emission signal ($\lambda_{ex}$ = 240 nm) and at a weaker emission ($\lambda_{ex}$ = 400 nm). First, water dots, synthesized for 4 hours and purged with $N_2$, were analyzed at the various temperatures and excitation wavelengths and the resulting spectra are shown in Figure 5.2.

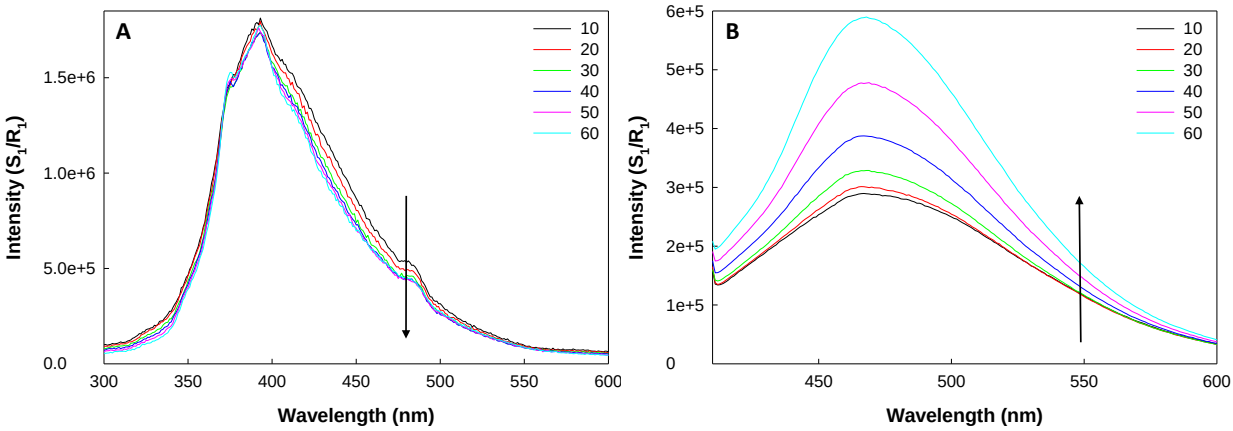


**Figure 5.2** Fluorescence spectra of water carbon nanodots, purged with $N_2$ gas, at various temperatures excited at A) 240nm and B) 400 nm.

As shown in the Figure 5.2A, there is a decrease in the emission signal when the temperature is increased from 10°C to 60°C at 240 nm as the excitation wavelength, however, the opposite trend was observed for 400 nm excitation wavelength. Figure 5.3 is an actual photograph of water dots cooled and heated to 5 and 85°C, respectively, excited with a 405-nm laser line with 420 nm long pass filter, showing the increase in the emission intensity at higher temperatures. The increase in the emission signal at higher temperatures is an uncommon phenomenon, but is seen in another allotrope of carbon, fullerenes.

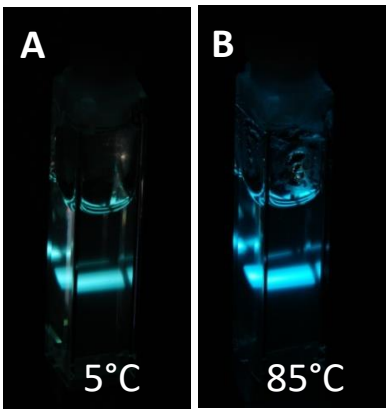


**Figure 5.3** Water dots excited with 405 nm laser line with 420 nm long pass emission filter at A) 5°C and B) 85°C.

In Chapter 3, it was shown that water dots displayed delayed emission (Figure 3.16) and in order to determine if TADF is a possible mechanism for the trends observed in Figure 5.2, temperature experiments of water dots, purged with $N_2$, were additionally carried out in phosphorescence mode of the spectrofluorometer to study the delayed emission spectra, i.e. in an off gated manner. Figure 5.4 shows the delayed emission spectra of water at various temperatures. As seen in the below figure, similar trends were observed for both excitation wavelengths as compared to the non-gated emission spectra collected. Ethanol and methanol dots were also studied to determine if the temperature dependent emission was present within those nanodots (Data not shown), which resulted in similar observations as to the water dots.

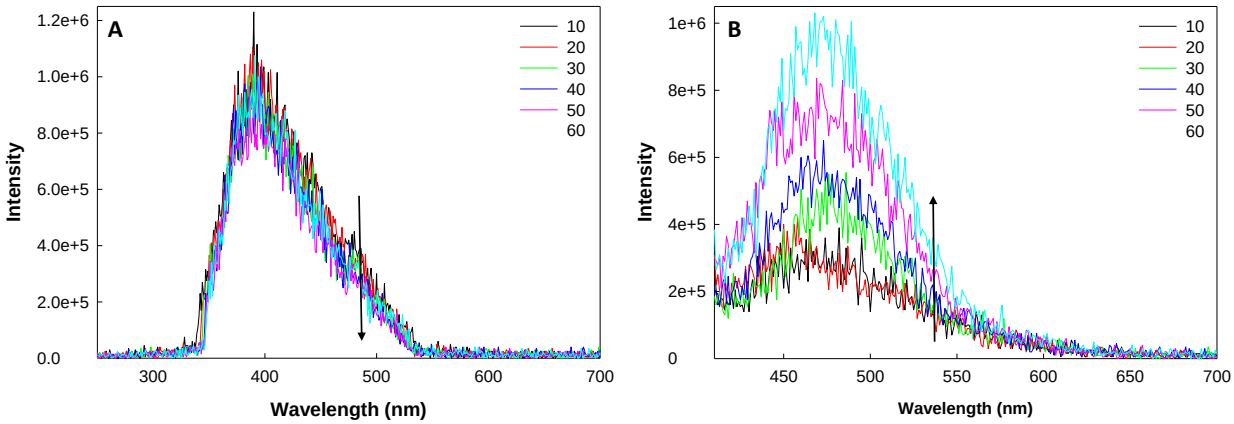


**Figure 5.4** Delayed fluorescence spectra of water carbon nanodots, purged with $N_2$ gas, at various temperatures, excited at (A) 240nm and (B) 400 nm. Spectra were collected in phosphorescence mode of fluorometer.

Observing the same temperature trends for the emission and delayed emission spectra is a strong indicator for TADF.[97,100,103] In order to have substantial TADF two condition must met: 1) high quantum yield of triplet formation, $\Phi_{T,}$ i.e. a high probability of intersystem crossing ($S_1 \rightarrow T_1$), and 2) high quantum yield of singlet formation, $\Phi_{S,}$ namely, a high probability of back intersystem crossing ($T_1 \rightarrow S1$).[97,100,102,104] These conditions imply that there is a small energy gap between $S_1$ and $T_1$ states ($\Delta E_{ST}$).[97,99–102,104] Therefore, determining the energy gap between the singlet and triplet states ($\Delta G_{ST}$) of carbon nanodots would provide stronger evidence that TADF is the reason these temperature dependent emission results are seen. There are several methods that have been used to analyze the TADF data of fullerenes, with the standard method involving the measurement of delayed fluorescence and phosphorescence intensities as function of temperature and using a plot of $\ln(I_{DF}/I_P)$ vs 1/T.[97,98,100,102] However, this standard method is not always viable due to difficulty or inability to measure phosphorescent spectra, thus an alternative method could be

employed.[97,98,100,102] Due to the lack of phosphorescent spectra of the carbon nanodots studied within this research, the alternative methods would have to be used to determine the $\Delta G_{ST,}$ however this method requires the quantum yield of the triplet state ($\Phi_T$). Therefore, further work must be carried out to determine the triplet state quantum yield and subsequently the $\Delta G_{ST.}$

**Temperature Cycling Analysis of Methane-Based Carbon Nanodots**

Temperature cycling experiments were carried out to study the reversibility of the emission of carbon nanodots after heating and cooling a sample multiple times. TADF occurs through cycling between the S and T excited-states, which requires a small energy gap between the two states (i.e. high density of states), therefore, it is believed that higher temperatures reduces this gap by increasing the density of excited-states.[46,100] Nanodots were subsequently heated from 10 to 30 to 60°C and then subsequently cooled from 60 to 30 to 10°C for a total of six cycles. Spectra of maximum intensity of emission versus the cycle number were plotted and shown in Figure 5.5. These experiments revealed that the carbon nanodots maximum emission intensity was reversible, for both excitation wavelengths, over six consecutive cycles of heating and cooling. This trend of reversibility after heating and cooling was also observed for a $C_{70}$/paraffin system and $C_{70}$/polymer systems, thus further supporting the TADF mechanism of methane-based nanodots, noting again that the carbon nanodots are simply another allotrope of carbon.[100] Therefore, carbon nanodots can be cycled multiple times without the loss of signal, allowing them to be potentially useful as temperature probes.

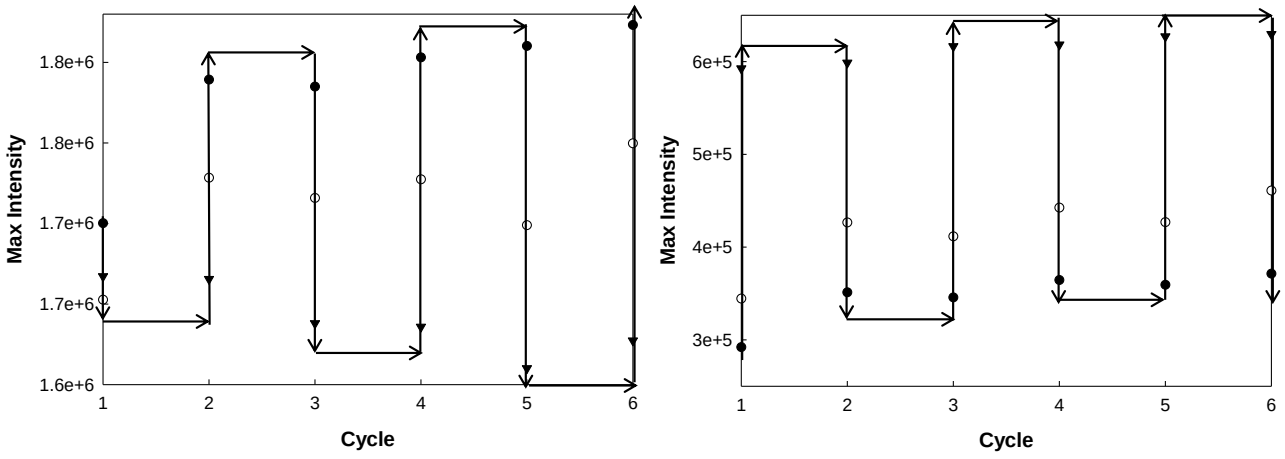


**Figure 5.5** Temperature cycling plots of water dots excited at A) 240 nm and B) 400 nm, with the max intensity at $\lambda_{max}$ at 390 nm and 470 nm, respectively. With ●, ○, and ▼ representing 10, 30, and 60°C respectively.

**Temperature Dependence of the 3D Fluorescence of Methane-Based Carbon Nanodots**

The previous results only examined the effect of temperature on the emission intensity at two wavelengths, therefore to determine if other wavelengths are temperature dependent, spectra of water dots were collected over multiple excitation and emission wavelengths. These experiments were carried out at the six temperatures and plotted as fluorescence contours plots shown in Figure 5.6.

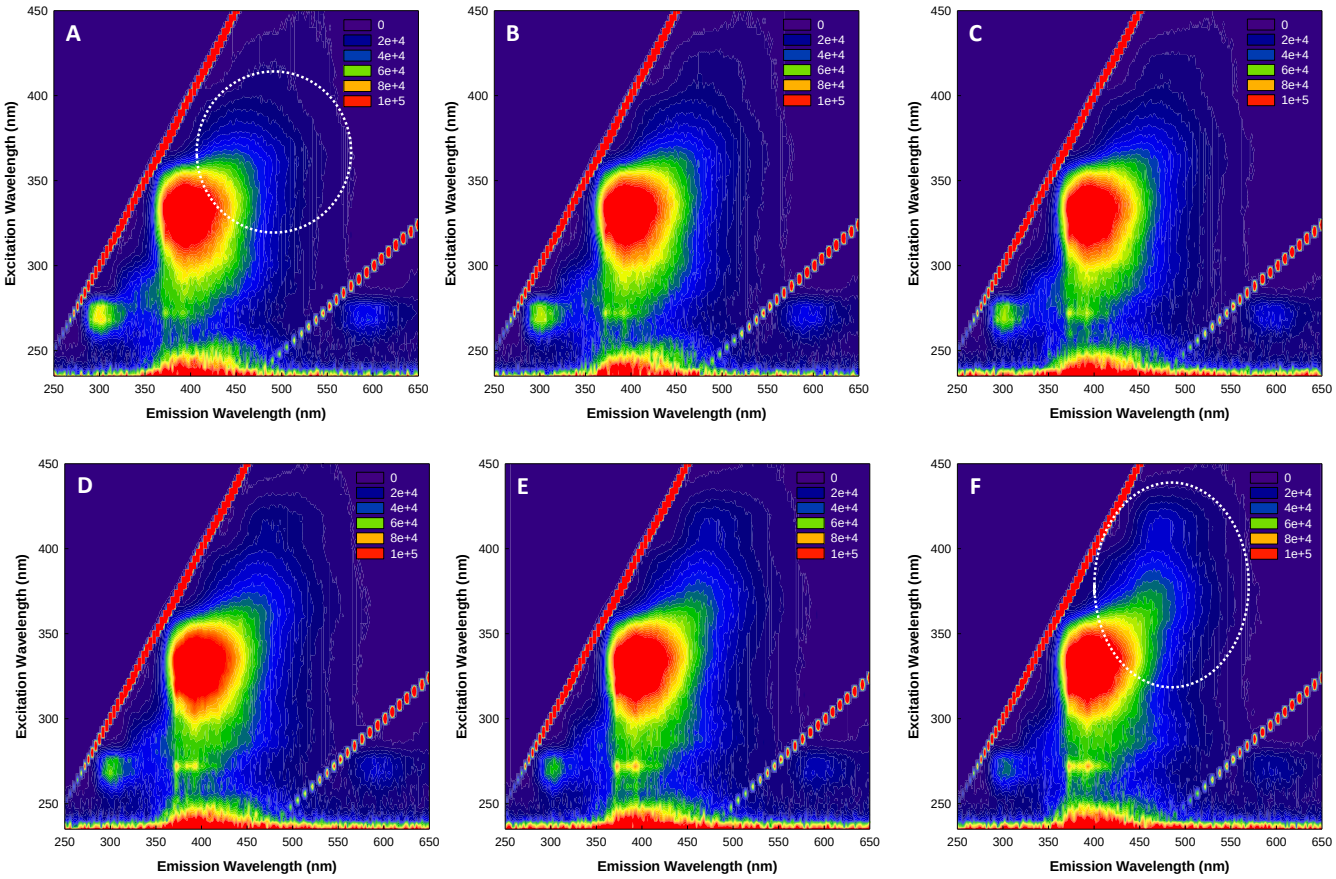


**Figure 5.6** Contour plots of temperature dependent emission experiments at A) 10, B) 20, C) 30, D) 40, E) 50, and F) 60°C. The white dashed circles highlight the increase in emission signal for excitation wavelengths greater than 350 nm.

These experiments revealed that the temperature dependent emission is not only observed at excitation wavelength 400 nm but at excitation wavelengths greater than 350 nm. When using the longer excitation wavelengths, it resulted in an increase of the emission signal at higher temperatures, which is highlighted by the white dashed circles seen on Figure 5.6A and F. The energy gap between excited-states tends to be larger for short wavelengths than for longer wavelengths.[6,48] For TADF to occur, the energy gap between the excited triplet and singlet states must be small, which could be why TADF is only observed for longer wavelengths. A similar

observation was seen for methanol dots when the emission spectra were analyzed over several excitation wavelengths (Data not shown).

### *5.3.2 Temperature Dependent Time-Resolved Measurements*

The fluorescence intensity decay of water dots was analyzed at various temperatures to gain an understanding of how the lifetimes were affected. Lifetime decay spectra were analyzed at 4, 10, 20, 30, 60, and 70°C with 400 nm NanoLED™ and the average lifetimes were calculated using equation 2.3[49], which is reproduce below as equation 5.1.

$$\bar{\tau} = \sum_i f_i \tau_i \qquad \textbf{(5.1)}$$

Where $f_i$ is the fractional contribution of each component to the steady-state intensity which is determined from equation 2.2. Figure 5.7 depicts the intensity decay spectra of water dots at various temperatures.

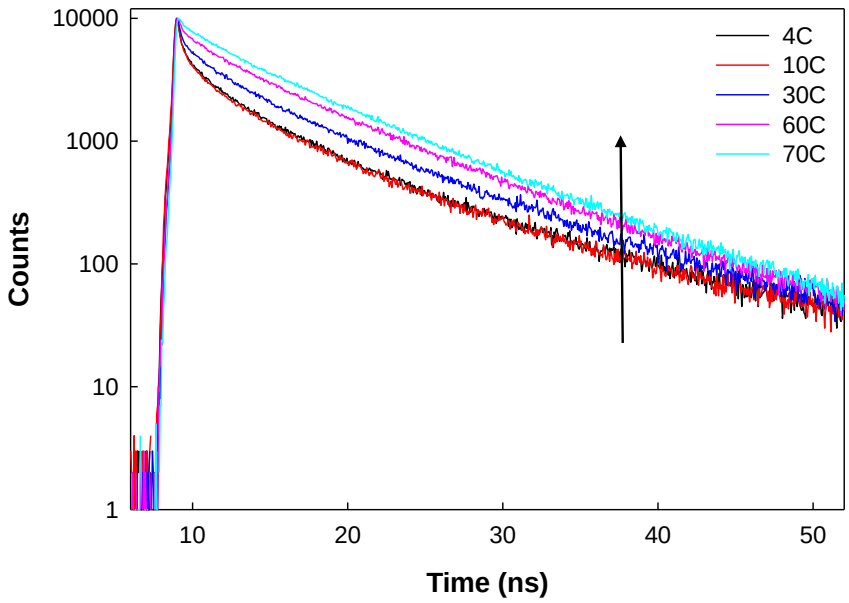


**Figure 5.7** Intensity decays ($\lambda_{em}$ =400 nm) of water dots synthesized for 2 hours at various temperatures.

These experiments revealed that the decay and subsequent average lifetimes for the water dots were influenced by increasing temperatures. The average lifetimes of the water dots at various temperatures were calculated (Table 5.1). The increase of the average lifetime of water dots at higher temperature is thought to be due to increase of fluorescence emission at higher temperatures. By exhibiting more fluorescence, the excited-singlet state of the water dots would be longer-lived and therefore resulting in longer average lifetimes.

**Table 5.1** Average lifetimes of water dots at various temperatures. Calculated form equation 5.1.

| **Temperature (°C)** | $\bar{\tau}$ **(ns)** |
|---|---|
| 4 | 7.53 |
| 10 | 7.44 |
| 30 | 7.81 |
| 60 | 7.88 |
| 70 | 7.95 |

## 5.4 Conclusions

Methane-based carbon nanodots were studied at six different temperatures, utilizing steady-state and time-resolved fluorescence techniques, to determine how the emission and intensity decay spectra were influenced by temperature. The temperature studies revealed an increase in the emission intensity and average lifetimes, at select excitation wavelengths, when the temperature was increased up to 70°C. Also, the cycling experiments showed that the emission intensities could be cycled and recovered over multiple heating and cooling cycles. Suggesting a

photophysical interpretation of the enhanced delayed fluorescence emission, not unlike what is observed for the fullerenes. These characteristics could make carbon nanodots potentially useful as temperature probes.

Methane-based carbon nanodots have been previously shown, in this research, to have delayed fluorescence (Chapter 3), therefore it is hypothesized that TADF is the mechanism for the temperature dependent emission phenomenon observed.[97,98,100–102] The results obtained from this research appear to support TADF as the reason for this temperature dependent emission, however, further work in determining the singlet-triplet energy gap ($\Delta G_{ST}$) and triplet quantum yield ($\Phi_T$) is needed in order to gain a full understanding of this property of carbon nanodots.

# Chapter 6: Bromination of Carbon Nanodots for Singlet Oxygen Generation

## 6.1 Introduction

The synthesis and modification of phosphorescent carbon nanodots for singlet oxygen generation will be discussed in this chapter. To achieve this, the synthetic set-up, described in Chapter 3, was adjusted to allow for the modification of methane-based carbon nanodots with halogens (bromide). Halogens are known to increase intersystem crossing to the triplet-state through spin orbital coupling (also known as the heavy atom effect), subsequently allowing for phosphorescence properties to be possible.[49–51,57,66,68,69] Phosphorescent carbon nanodots are thought to be able to generate singlet oxygen ($^1O_2$) by photosensitization, a method of electronic energy transfer from the triplet excited-state of carbon nanodots to the ground-state of molecular oxygen.[77–81,105,106] In order to study the photosensitization of $^1O_2$, Singlet Oxygen Sensor Green Reagent (SG) was employed to detect $^1O_2$, based on the increase of the fluorescence signal in the presence of $^1O_2$, as described in Chapter 1. This chapter is subsequently focused on the synthesis of brominated methane-based carbon nanodots, the characterization of their photophysical properties and their ability to generate singlet oxygen.

## 6.2 Experimental Details

### *6.2.1 Synthesis of Brominated Carbon Nanodots*

***Synthesis.*** The experimental synthetic set-up for methane-based carbon nanodots was previously detailed in Chapter 3 (Figure 3.1). For brominated carbon nanodots, only the solvent was changed from water, ethanol, or methanol to 5 M hydrobromic acid (HBr). Briefly, ultra-pure methane gas was flowed into a bunsen burner, where a sooting flame was produced. The nanodots are thought to be formed within the flame and were pulled into the impinger glassware and the collection solvent (5 mL of 5 M HBr) by a vacuum. The vacuum was set to cause gentle bubbling of the solvent to ensure that the carbon nanodots were pulled from the flame into the solvent. The duration of the synthesis of brominated carbon nanodots was for either 2 or 4 hours. After the completion of the synthesis, samples were refluxed in the HBr for 6 or 12 hours at 100-120°C. This step was carried out to determine if refluxing the samples could increase the chances of the bromination of the carbon nanodots, similar to the use of oxidization of candle soot with $HNO_{3,}$ to introduce oxygen and nitrogen onto the carbon nanodots as discussed in Chapter 2.

### *6.2.2 Photophysical Characterizations of Brominated Carbon Nanodots*

***Absorption Measurements.*** Absorption measurements were carried out on a Cary 50 UV-Vis spectrophotometer (Agilent Technologies, Santa Clara, CA) equipped with a full spectrum xenon pulse lamp (190-1100 nm). Samples and solvent blank (HBr) were measured in a 1-cm quartz or glass cuvette with a scan rate of 300 nm/min**.**

***Steady-State Fluorescence.*** Steady-state fluorescence measurements were carried out on a FluoroMax-4 or FluoroMax-4P spectrofluorometer (Horiba Scientific, Edison, NJ) utilizing the FluorEssence software. Samples were measured in a 1-cm glass or quartz cuvette. The excitation and emission monochromators were adjusted to obtain the appropriate wavelengths to collect emission data from an excitation wavelength range of 300 nm to 700 nm. The 3D emission spectra, plotted as contour plots, were collected using the 3D mode of the FluorEssence software with the excitation wavelengths ranging from 200 to 700 nm and the emission wavelengths ranging from 220 to 720 nm.

***Steady-State Phosphorescence.*** Phosphorescence measurements were carried out in FluoroMax-4P spectrofluorometer (Horiba Scientific, Edison, NJ). The instrument light source was a pulsed xenon arc lamp. The experiments were carried out utilizing the FluorEssence software in phosphorescence mode (gated signal collection) with samples in a 1-cm glass or quartz cuvette. The typical experimental parameters were previously described in Table 3.1. The excitation and emission monochromators were adjusted to obtain the desired wavelengths.

***Time-Resolved Fluorescence.*** Time-Resolved fluorescence intensity decays were obtained using the time-correlated single photon counting technique, in reverse start-stop mode, on a FluoroCube system (Horiba Scientific, Edison, NJ). An instrument response function (IRF) was taken using a dilute scattering solution of Ludox® AS-30 colloidal silica. The IRF and carbon nanodot samples were excited using a NanoLED centered at 351 nm (Horiba Scientific, Edison, NJ) and the emission wavelengths were selected with a monochromator, and subsequently the signal was

detected on a TBX-04 timing module (Horiba Scientific, Edison, NJ). The typical experimental parameters used were previously detailed in Chapter 2. Decay spectra were taken on the DataStation V 2.7.2 software and the fitting of the decays were completed using the DAS 6 Analysis software.

***Dynamic Light Scattering.*** Dynamic light scattering data was collected on a Zetasizer Nano ZS (Malvern, Worcestershire, UK) equipped with 633 nm laser source with the help of Dr. Daniel's lab group (Chemistry Department, UMBC). Carbon nanodots samples were ran in a 1-cm plastic cuvette at room temperature. Pure samples (no centrifugation) and centrifuged samples of carbon nanodots were both analyzed for their size distribution.

***Quantum Yields.*** Relative quantum yields were determined by comparing the integrated emission intensity, optical density, and refractive index of the carbon nanodots to a suitable reference in a 1-cm quartz cuvette at 20°C. The reference fluorophores used were quinine sulfate (0.1M $H_2SO_4$, $\lambda_{ex}$= 350 nm), fluorescein di-sodium salt (0.1M NaOH, $\lambda_{ex}$= 496 nm), rhodamine 101 (Ethanol, $\lambda_{ex}$= 450-460 nm). The optical densities of the references and the carbon nanodots were matched at the excitation wavelength (350, 496 or 450 nm). The steady-state emission spectra were integrated using SigmaPlot 11.0 software. Quantum yields were calculated using equation 2.1.

### *6.2.3 Singlet Oxygen Generation Experiments*

In order to study the $^1O_2$ generation of carbon nanodots, singlet oxygen sensor green reagent (SG, Thermo, Waltham, MA) was purchased and utilized. A stock solution of 5 mM SG was prepared and stored in a dark vial at -20°C until it was used. Experiments were carried out on the FluoroMax-4 spectrofluorometer (Horiba Scientific, Edison, NJ) utilizing the FluorEssence software. A black 1-cm cuvette with small 1-mm opening was used for measuring the spectra (Figure 6.1).

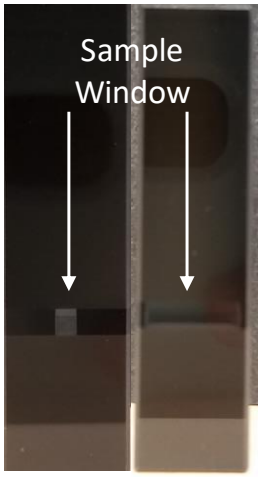


**Figure 6.1** Photograph of the black cuvette with 1-mm windows for excitation and emission collection used for singlet oxygen experiments.

To generate $^1O_2$, the sensitizer (S), in these experiments either methylene blue (MB) or carbon nanodots, must be in the triplet state ($^3S$) in order to interact with molecular oxygen ($^3O_2$) and produce $^1O_2$.[77–81,105,106] Therefore, the sensitizer was excited into its singlet-excited-state by a pump wavelength (630 nm for MB and 300 for nanodots), from where the sensitizer can intersystem cross into the triplet state.[77–81,105,106] The $^3S$ can interact with $^3O_2$ to generate $^1O_2$, which is subsequently detected by change in emission intensity of SG when excited at 470 nm. Experiments were

carried out to analyze the efficiency of SG and carbon nanodots in detecting and generating $^1O_2$.

***Methylene Blue Experiments*** A set of control experiments using methylene blue (MB), a well-known photosensitizer, were carried out to test SG as a detection method and to determine ideal experimental parameters needed. These experiments were completed with a pump wavelength for MB at 630 nm and excitation of SG at 470 nm for the detection of $^1O_2$. A typical control sample consisted of 3 µL of SG (5mM) and MB and 1.5 mL of 100 mM TRIS buffer, as suggested by the manufacturer.

The control experiments were carried out at different durations of the pump wavelength (630 nm) ranging from 1 to 6 minutes and the detection of $^1O_2$ was analyzed immediately after the pumping of MB and up to 5 minutes after the pump, in 1 minute increments. The typical parameters used for the control experiments are shown in Table 6.1.

**Table 6.1** Typical experimental parameters used for Methylene Blue control experiments. The pump of MB was varied from 1 to 6 minutes.

| | $\lambda_{ex}$ |
|---|---|
| Before pump | 470 |
| Pump of MB | 630 |
| Immediately After Pump | 470 |
| 1 Minute After Pump | 470 |
| 2 Minute After Pump | 470 |
| 3 Minute After Pump | 470 |
| 4 Minute After Pump | 470 |
| 5 Minute After Pump | 470 |

***Carbon Nanodot Experiments.*** Analyzing the ability of carbon nanodots to generate $^1O_2$ was carried out in a similar manner to the control experiments. These experiments

were completed with a pump wavelength for carbon nanodots at 300 nm and excitation of SG at 470 nm for the detection of $^1O_2$. The samples consisted of 2 µL of SG (5mM), 200 µL of carbon nanodots and 1 mL of 100 mM TRIS buffer. The same experimental parameters (Table 6.1) were used and analyzed for carbon nanodot samples. Water and HBr dots were analyzed and compared for their ability to produce $^1O_2$.

## 6.3 Results and Discussion

Brominated carbon nanodots were synthesized from methane gas and collected in 5 M hydrobromic acid (HBr) for either 2 or 4 hours. Following the synthesis, the nanodots solutions were further refluxed in the HBr solvent for 6 or 12 hours at up to 120°C in an effort to incorporate the bromide ions from the HBr onto the nanodots structure. The nanodots synthesized in this study are hereafter referred to as HBr dots to differentiate these brominated dots from the previously synthesized carbon nanodots.

### Absorption Characterization

The absorption spectra of brominated carbon nanodots synthesized for 2 and 4 hours, before the samples were refluxed, are shown in Figure 6.2 below. The spectra show a high absorbance in the UV region with tailing off into the visible regions. The spectra were similar to those of the water dots described in Chapter 3 and in literature described carbon nanodots.[2–5]

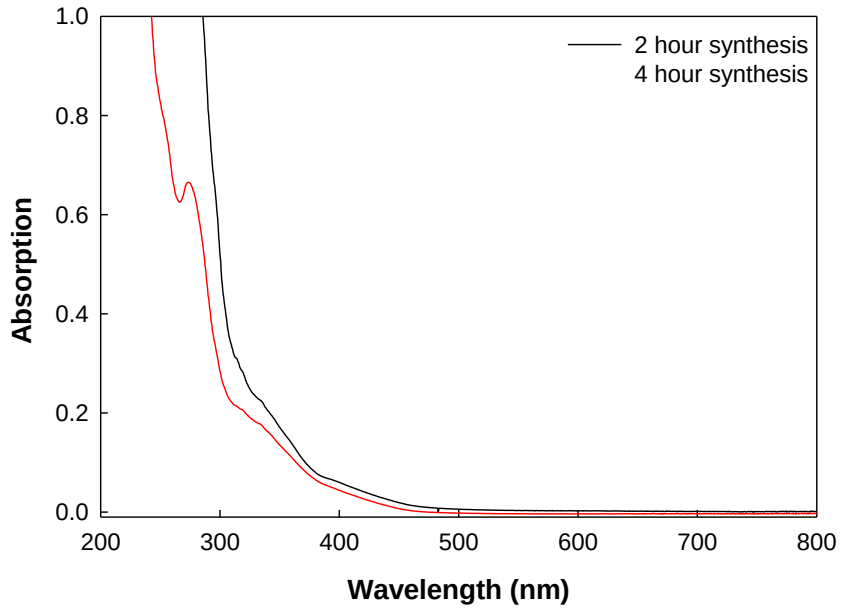


**Figure 6.2** Absorption spectra of HBr dots (before reflux) synthesized for 2 or 4 hours

When the HBr dots and water dots absorption spectra are compared (Figure 6.3), it can be seen that the water dots had a higher absorbance in the visible region than the HBr dots, however, this is simply likely due to concentration of nanodots collected in each sample. The difference could also be the result of carbon nanodots that have different optical properties based on the solvent. As shown in Chapter 3, that the solvent can influence the photophysical properties of the nanodots, therefore by using HBr as the solvent, we have speculated that it may be possible to obtain carbon nanodots with different properties.[30,31,88,89]

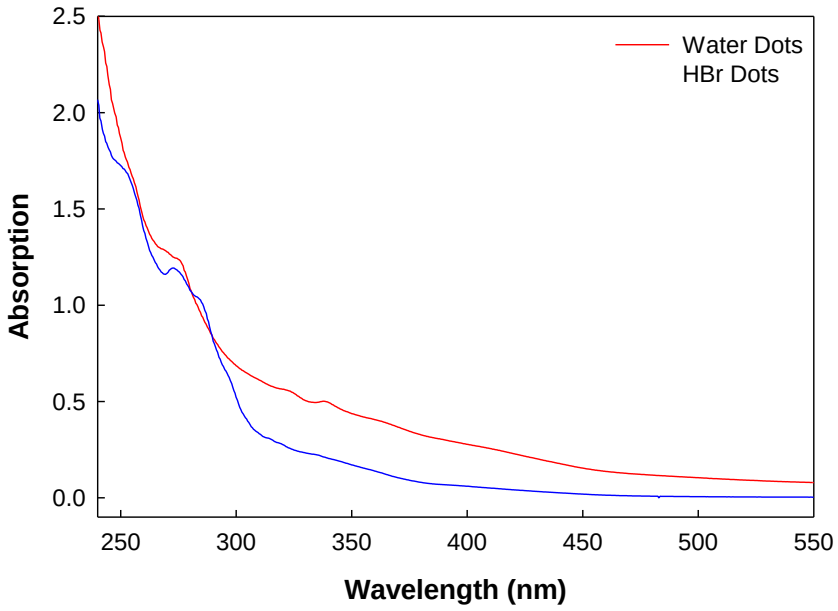


**Figure 6.3** Comparison of the absorbance spectra of water dots and HBr dots synthesized for 2 hours

Next, the absorption spectra of the HBr dots were assessed for Rayleigh light scatter to determine if HBr dots contained large amounts of scatter, like the water dots. Figure 6.4 demonstrates this comparison and shows that HBr dots do not have a significant amount of light scatter, which means the broad absorption is likely due to the nature of the carbon nanodots. This observation is different than what was seen for water dots in chapter 3 and could be the result of different solvated nanodots collected in the HBr synthesis.

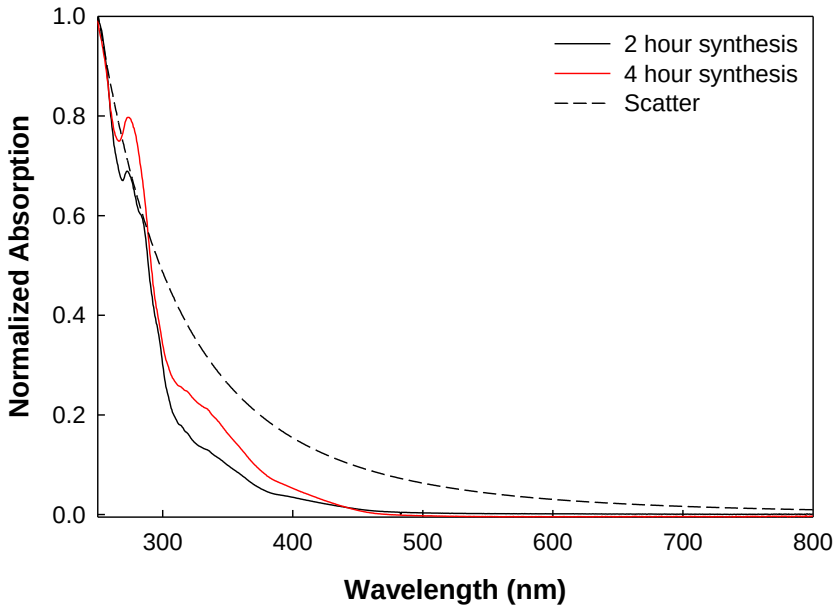


**Figure 6.4** Normalized absorption spectra of brominated carbon nanodots (Before Reflux) and Rayleigh scattering ($\lambda^{-4}$ trace). Data normalized from Figure 6.2

In order to determine if refluxing was an effective method to change the photophysical properties of HBr dots, the absorption spectra of HBr dots before and after reflux were compared (Figure 6.5). Comparing the three spectra for each synthesis time, it was observed that there are slight differences between the spectra. Based on these differences and differences seen in the emission spectra, as described in the next section, it is thought that the refluxing of the nanodots could influence the photophysical properties of HBr dots.

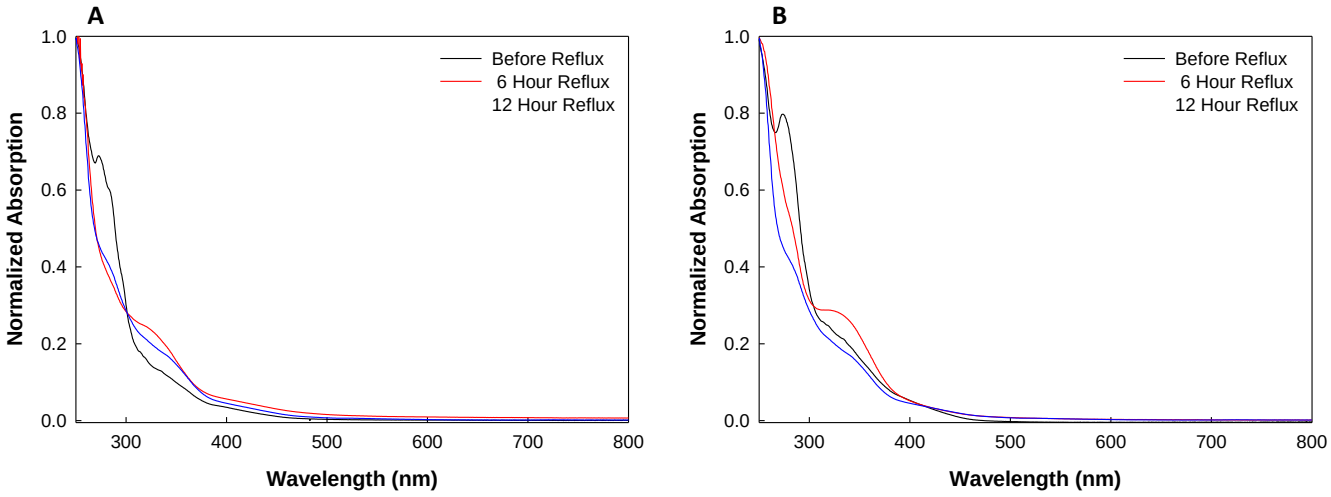


**Figure 6.5** Comparison of the normalized absorption spectra of HBr dots before reflux (Black), after 6-hour reflux (Red), and after 12-hour reflux (Blue) for A) 2-hour synthesis and B) 4-hour synthesis

## Fluorescence Characterization

### *Before Reflux*

The emission properties of HBr dots were analyzed to determine the effects of the HBr solvent on the fluorescence of carbon nanodots. Figures 6.6 and 6.7 show the emission spectra of HBr dots, before reflux, synthesized for 2 and 4 hours, respectively. First, in Figure 6.6, the contour plots display the emission spectra over multiple excitation wavelengths. When comparing the contour emission structure between the two duration times, it can be observed that they look similar, but as highlighted by the white dashed circles, there were some slight differences. These differences could be explained by a change in concentration of the nanodots in solution between the two samples. As described in Chapter 3, the longer the synthesis time, typically results in more concentrated samples and therefore, a stronger emission intensity was expected, as seen in Figure 6.6. When compared to water dots,

there are some notable differences seen in the contour plots. For water dots, the emission intensity appeared as a much broader spectra and higher intensities, whereas, HBr dots appeared to have more emission spectra structure and overall lower fluorescence emission intensity. It is hypothesized that the lower fluorescence emission intensity of HBr dots is due to the presence of phosphorescence, which will be discussed later.

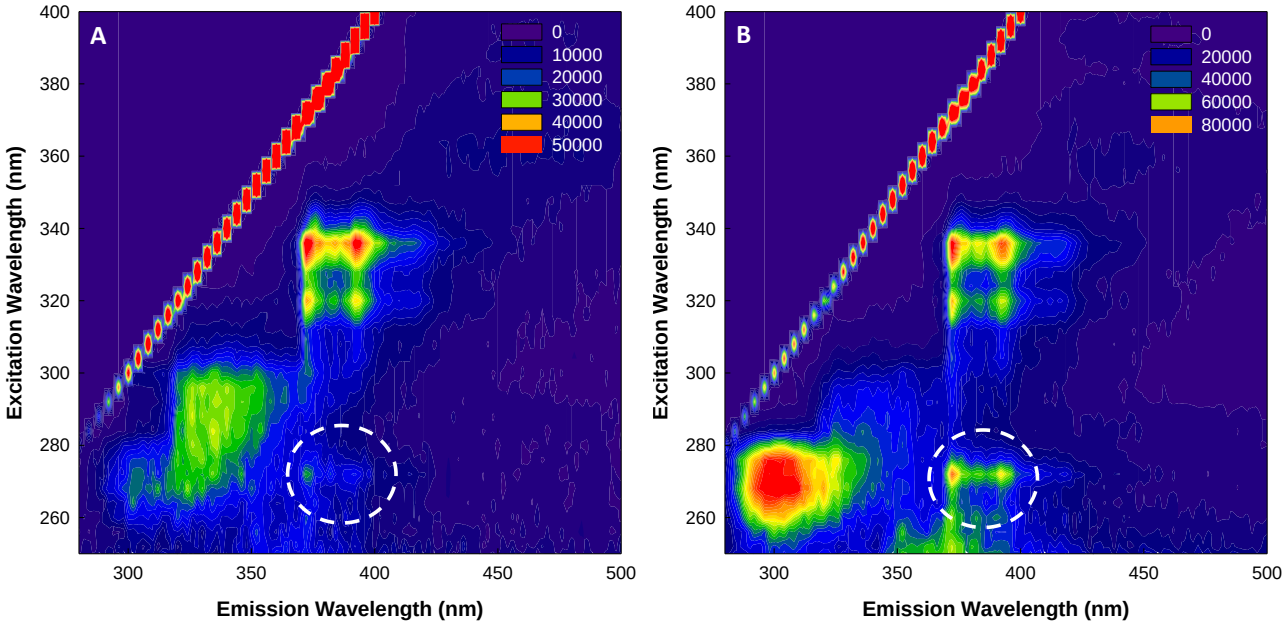


**Figure 6.6** Contour plot of HBr (before reflux) synthesized for A) 2 hours and B) 4 hours. The intensity, red band is the zero-order overtone band due to the monochromator.

Next, when examining the normalized emission plots, shown in Figure 6.7, the excitation wavelength dependent emission is present in HBr dots, before reflux, as well. Also, there is a decrease in emission intensity at longer wavelengths (Data not shown). Again, both of these observations are unique emission properties of all carbon nanodots.[2–5] From both the absorption and emission spectra of HBr dots, it can be observed that different carbon nanodots are collected within this synthesis.

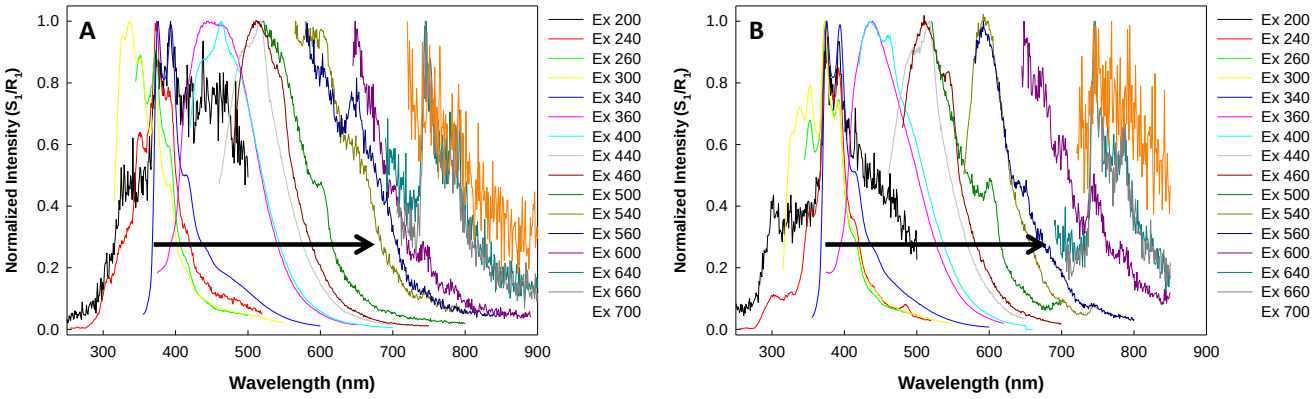


**Figure 6.7** Normalized emission spectra of HBr dots (before reflux) synthesized for A) 2 and B) 4 hours. Samples were excited from 200 nm to 700 nm with the arrow representing the increase of the excitation wavelength.

### *After Reflux*

The emission spectra for HBr dots (2-hour synthesis), after either a 6 or 12-hour reflux, are shown in Figures 6.8 and 6.9, respectively. There are significant differences between the before reflux and the after-reflux emission spectra. As shown in the contour plots (Figure 6.8), the spectra have significantly decreased in the intensity, along with a bathochromic shift (red shift) in the emission signal. In the un-refluxed samples, the emission intensity was typically centered between 370 and 410 nm and in the after-reflux samples, the emission intensity was typically centered

between 400 and 500 nm. This general trend was reproducible over several different HBr dots samples. A comparison of the normalized emission signal for before and after refluxed HBr dots is shown in Figure 6.9. All samples were excited at 300 nm and a bathochromic shift can be seen for HBr dots that were refluxed. A similar trend was observed for HBr synthesized for 4 hours as well. The purpose of refluxing the HBr dots was to increase the chances of creating phosphorescent dots. Therefore, observing a decrease in the emission intensity could be due to an increase in the triplet emission of HBr dots after reflux.

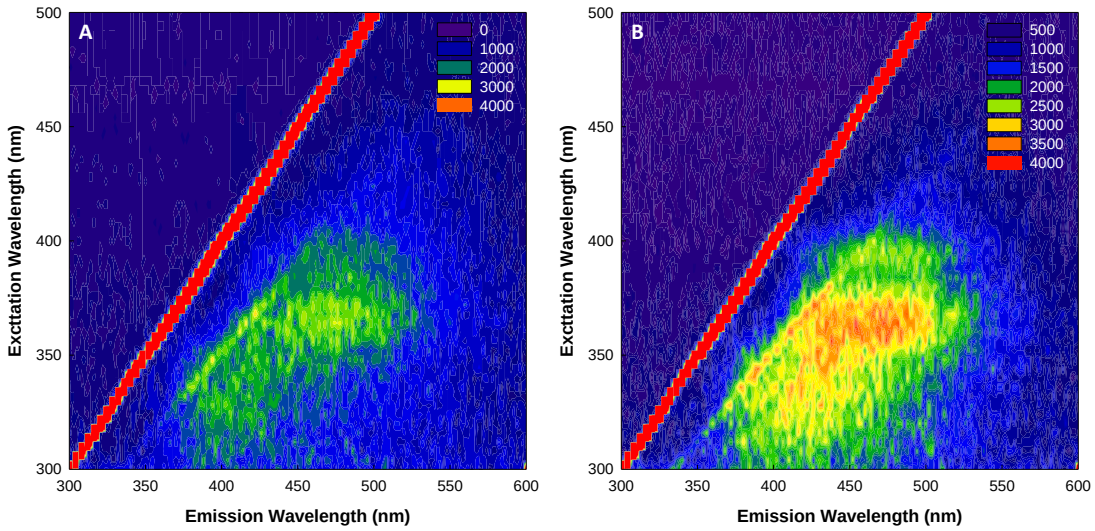


**Figure 6.8** Contour plots of HBr dots (2-hour synthesis) after being refluxed for A) 6 and B) 12 hours.

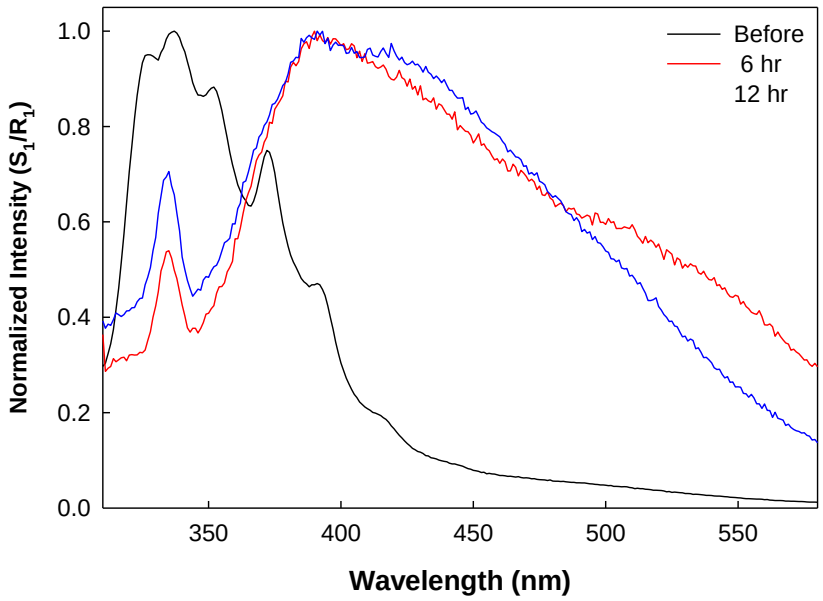


**Figure 6.9** Comparison of the normalized emission spectra of HBr dots (2 hours) before reflux (Black), after 6-hour reflux (Red) and after 12-hour reflux (Blue) excited at 300 nm.

**Fluorescence Quantum Yields Determination**

The relative fluorescence quantum yields of HBr dots were determined by using equation 2.1 and three known fluorophores standards namely, quinine sulfate, fluorescein, and rhodamine 101. The quantum yields for the 2-hour HBr dots were determined to be 2-4% when compared to quinine sulfate, however, when compared to di-sodium fluorescein the quantum yields increased to 4-6%. For the 4-hour HBr dots the quantum yields were determined to be 5.5% and 6.5%, when compared with quinine sulfate and fluorescein, respectively. When both the 2 and 4 hour HBr dots were compared to Rhodamine 101, there was a significant decrease in the quantum yields to less than 1%. Table 6.1 summarizes the average quantum yield results from three or four different measurements.

**Table 6.2** Relative approximate quantum yield calculations of HBr dots at various excitation wavelengths.

| Sample | Average Φ (%) | Average Φ (%) | Average Φ (%) |
|---|---|---|---|
| | $\lambda_{ex}$= 350 nm[1] | $\lambda_{ex}$= 496 nm[2] | $\lambda_{ex}$= 450 nm[3] |
| HBr (4hrs) | 5.47 ± 0.10 | 4.65 ± 0.64 | 0.54 ± 0.05 |
| HBr (4hrs) | 5.40 ± 0.33 | N/A | N/A |
| HBr (2hrs) | 3.58 ± 1.19 | 5.33 ± 0.57 | 0.58 ± 0.03 |
| HBr (2hrs) | 2.10 ± 0.24 | 3.98 ± 0.16 | 0.48 ± 0.03 |

[1,2,3] refer to the standards use for comparison at those excitation wavelengths, Quinine Sulfate, Fluorescein, and Rhodamine 101. *Each average quantum yield calculation is from triplicate measurements within same batch of nanodots.

When the quantum yields of HBr dots are compared to the earlier water dots, we see that there is a significant decrease in the fluorescence quantum yields. For example, for quinine sulfate, the quantum yields for the 2-hour water dots was 20% compared to the 4% for the 2-hour HBr dots. It is also worth noting that, unlike water dots, the HBr dots do not appear to have large amount of scatter light (Figure 6.4). Therefore, it is believed that relative quantum yields are not underestimated, like the water dots, in Chapter 3. The decrease in the fluorescence quantum yield suggests that the nanodots are using a different deactivation pathway to return to the ground-state. It is believed that because bromide ions are present, either in solution or on the surface of the nanodots, that the HBr dots could be phosphorescent.[49–51] The presence of phosphorescence would explain the decrease in the $S_1$ emission intensities observed and the decrease in the fluorescence quantum yields.

**Phosphorescence Characterization**

To determine if the decrease in the emission signal was due to triplet emission, phosphorescence spectra were collected for HBr dots, before and after

reflux. Since triplet states can be readily quenched by diffusing species due to their long-lived nature, samples were mixed with glycerol to slow down the diffusional quenching processes. The viscosity of water and glycerol are 1.002 m*Pa*s and 1.408 Pa*s, respectively, therefore glycerol will reduce the diffusion molecules in solution better than water.[107] phosphorescence spectra of HBr dots synthesized for 2 hours, before reflux, are shown in Figure 6.10. When comparing the fluorescence and phosphorescence spectra (Figure 6.10B), a new peak appeared in the phosphorescence spectrum that is somewhat red shifted from the fluorescence emission spectra. Since the phosphorescence spectra are collected in a gated manner and there is a red shift in the spectra, it could be concluded that the peak seen at 520 nm is due to the presence of phosphorescence.

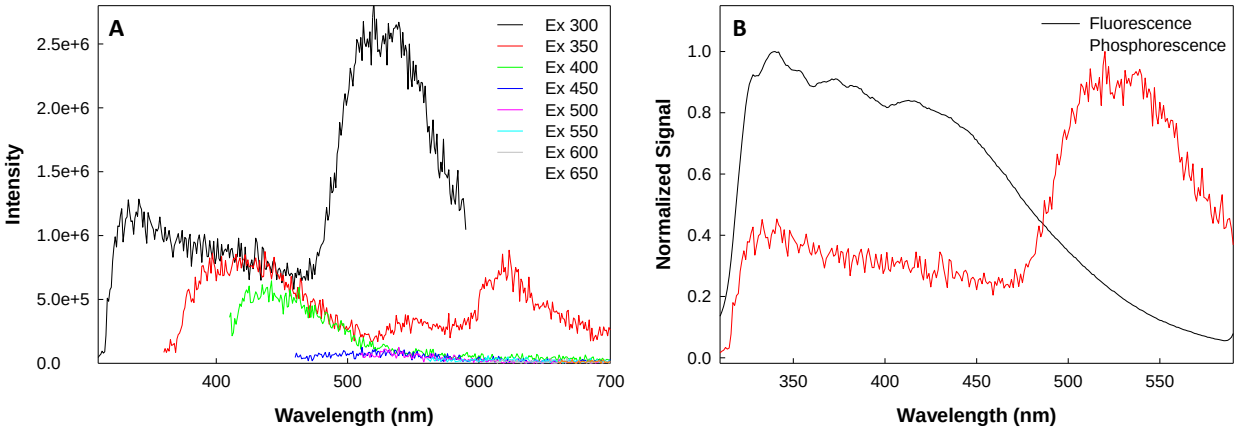


**Figure 6.10** A) Phosphorescence spectra of HBr dots (2 hours, before reflux) in glycerol and B) Normalized fluorescence and phosphorescence spectra of HBr (2 hours, before reflux) excited at 300 nm.

However, when the same experiment was completed for refluxed HBr dots, a phosphorescent peak was not observed. Figure 6.11 shows the normalized phosphorescence spectra for HBr dots before and after refluxing and it can be seen that nanodots only before the reflux have a phosphorescent peak. When examining the HBr dots synthesized for 4 hours, after the 12-hour reflux, a phosphorescent peak was observed at approximately 530 nm (Figure 6.12). The reason for these differences is still under investigation, since the it is unknown if the bromide ions were covalently added to the structure of the nanodots or if the bromide ions are electrostatically attracted, i.e. ion paired, to the charged surface of the nanodots. The strong acidic environment of the nanodots could be potentially degrading the nanodots as they are heated and refluxed, however when using a similar procedure for candle-based carbon nanodots, the acidic environment ($HNO_3$) helped to synthesis fluorescent nanodots.[13,15] It could also be reasoned that refluxing is not consistent method to incorporate halides onto the nanodots, as seen by the success of the phosphorescent peak in the 4-hour HBr versus the lack of the phosphorescent peak in the 2-hour HBr dots. Further experiments are needed to gain a better understanding of the addition of halide to the carbon nanodots.

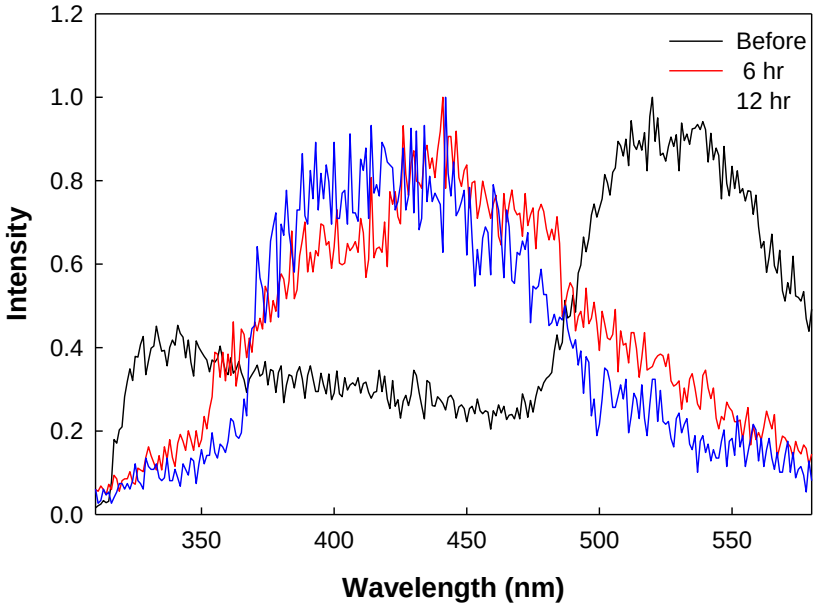


**Figure 6.11** Comparison of the normalized phosphorescence spectra of HBr dots (2 hours) before reflux (Black), after 6-hour reflux (Red) and after 12-hour reflux (Blue) excited at 300 nm.

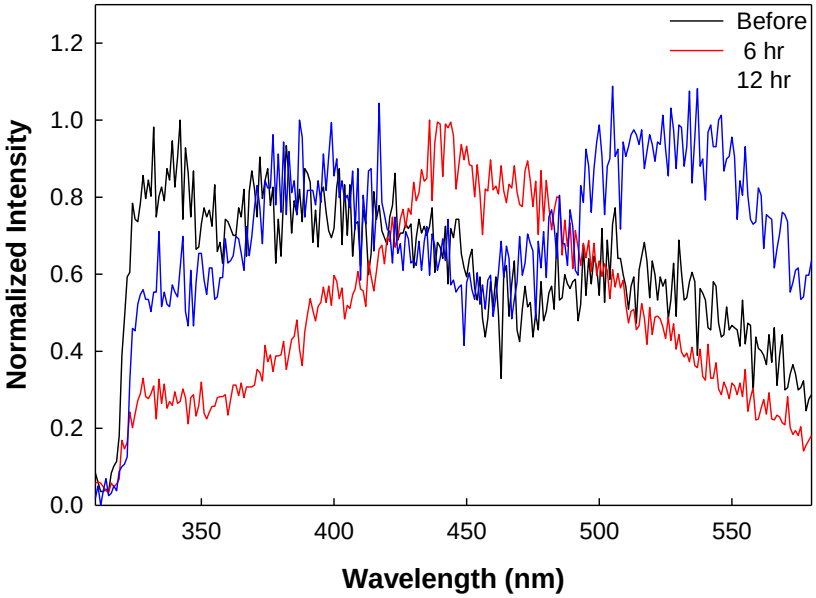


**Figure 6.12** Comparison of the normalized phosphorescence spectra of HBr dots (4 hours) before reflux (Black), after 6-hour reflux (Red) and after 12-hour reflux (Blue) excited at 300 nm.

**Dynamic Light Scattering (DLS)**

Dynamic light scattering measurements were undertaken to determine the size distributions of HBr dots. The results revealed a large distribution of sizes of HBr dots after synthesis. The HBr dots samples were studied before centrifugation and after 14,500 RPM centrifugation to determine if centrifugation could remove the large carbon nanodots from the samples. Figure 6.13 shows the DLS results before and after centrifugation for HBr dots collected for 2 hours. DLS experiments revealed that, after synthesis, there is a distribution of sizes from 1 to >1000 nm however, centrifugation can be used to some extent to separate out the smaller particles. These results are similar to the DLS results discussed in Chapter 3.

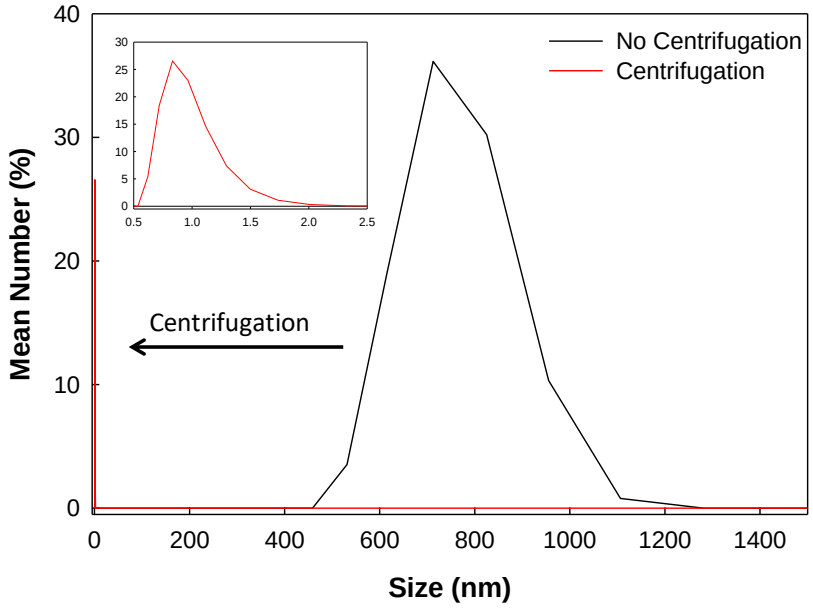


**Figure 6.13** Dynamic light scattering of HBr synthesized for 2 hours before and after centrifugation at 14,500 R. Inset. Zoomed in graph of the smaller distribution of sizes of HBr dots.

**Time-Resolved Intensity Decay Characterization**

The time-resolved intensity decay experiments were carried out to determine the average lifetime of the excite-state of the HBr dots. However, unlike the previous carbon nanodots, HBr dots appeared to have both a very short component and a longer-lived component, as shown in Figure 6.14.

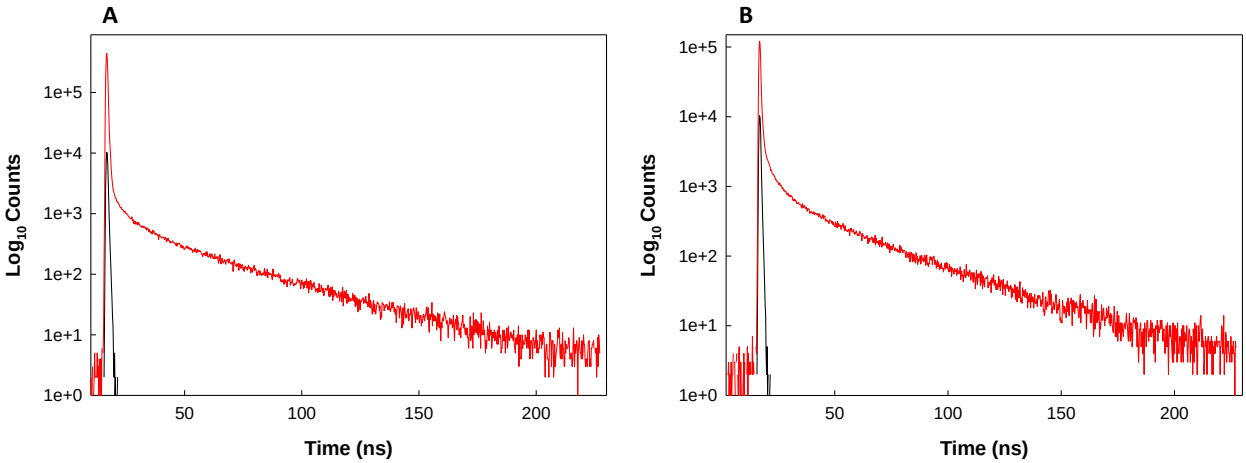


**Figure 6.14** Fluorescence intensity decay of HBr dots synthesized for 2 hours. The excitation wavelength was 351 nm and the emission was collected at A) 375 nm and B) 395 nm. (Black line- instrumental response function, Red line - fluorescence decay).

The short-lived component is speculated to be the decay of the nanodots quenched by the bromide, although we are unable to ascertain a specific value to it, as it was below the time-resolution of the instrument, i.e. ≈ <300 ps. We do not however believe that the short-lived component is a consequence of scattered light in the sample, due to the lack of notable scattering present in the absorption spectra of HBr dots (Figure 6.4). In order to determine the average lifetime of the long-lived component, a tail fit of the intensity decay was used. The average lifetime of the long-lived component was found to be 33.5 ns, which is much longer than the ~4 ns lifetimes of water dots. However, it is worth noting that the amplitude contribution of the long-lived species to the overall intensity decay of the HBr dots appears to ~5%

therefore, it does not appear to have a great influence on the overall average lifetime of the HBr dots. The origin of this long-lived fluorescence component is not known at this time.

The overall intensity decay could be approximated to a multi-exponential intensity decay using the DAS 6 Analysis software. However, in order to gain a better understanding of the long-lived components, measuring the longer lifetimes of the HBr dots would be ideal. The spectrofluorometer used for the phosphorescent measurements (FluoroMax 4P) would be capable of measuring the long lifetimes and using the FluorEssence software, it could be possible to determine the lifetime of the longer-lived component of HBr dots. Also, the use of another instrument in our labs, namely the TemPro Fluorescence Lifetime System (Horiba Scientific, Edison, NJ) could be utilized to analyze the long-lived component. This system is able to measure intensity decays of up to one second and operates relatively similar to the FluoroCube system used within this research. Further experiments utilizing the spectrofluorometer, will be able to help gain a better understanding of the long-lived lifetimes of HBr dots.

**Singlet Oxygen Generation**

As shown in the above sections, HBr dots have phosphorescence character which, in turn, makes the interaction between HBr dots and molecular oxygen a possibility. This interaction could potentially generate singlet oxygen. In order to determine if carbon nanodots are able to generate $^1O_2$, the singlet oxygen sensor green

reagent (SG), was utilized as a sensor, based on the changes in the fluorescence signal of the SG.

First, control/signal optimization experiments using methylene blue (MB) were completed to analyze SG ability to detect $^1O_2$. These experiments varied the pump duration of MB, with the expectation at longer pump times, more $^1O_2$ would be generated due to more MB being excited and available to react with molecular oxygen. Also, the experiments varied the collection times of the SG spectra to determine how long $^1O_2$ could be detected after excitation of the sensitizer. Figure 6.15 shows the results of those experiments.

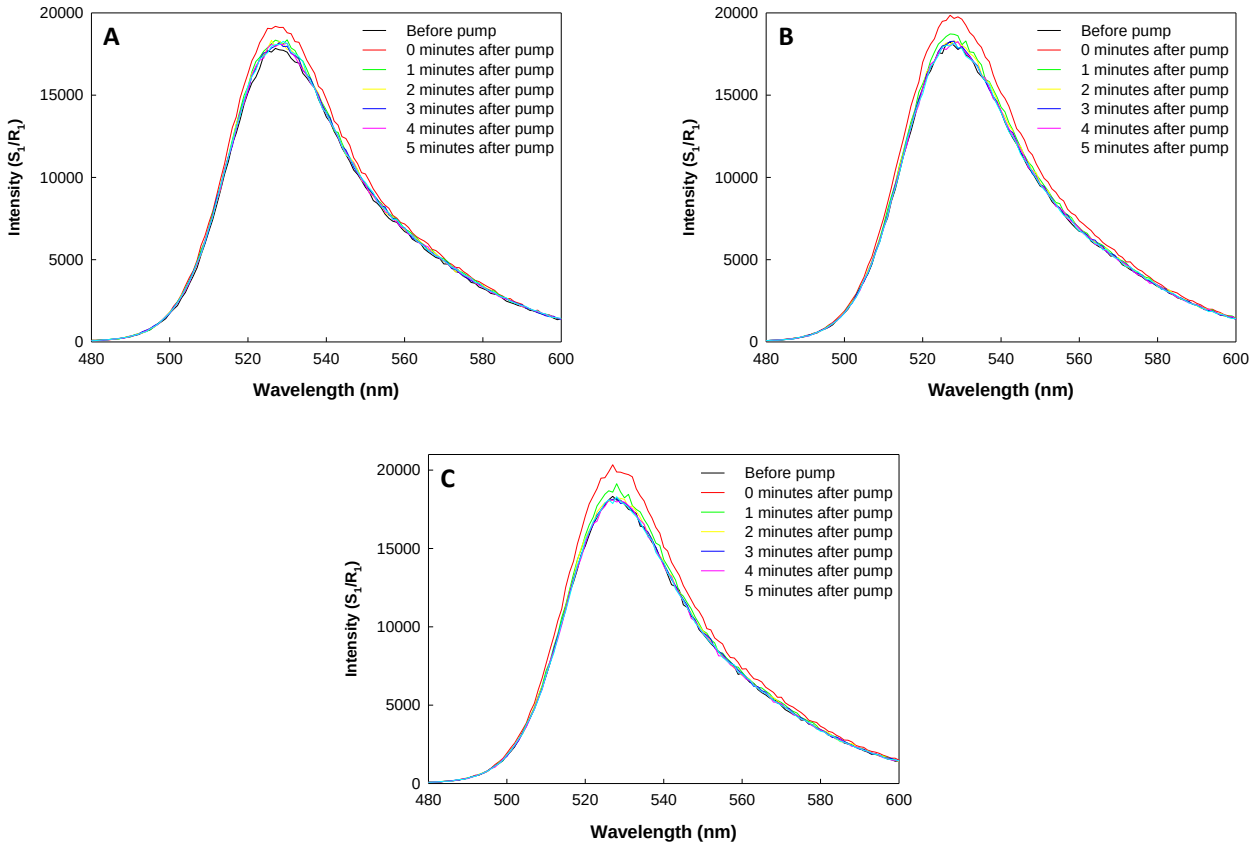


**Figure 6.15** Singlet oxygen generation from methylene blue utilizing sensor green at A) 2 minutes, B) 4 minutes, and C) 6 minutes' pump durations of MB. The pump wavelength for MB was 630 nm and the excitation wavelength for SG was 470 nm. SG spectra were collected after various times after exciting the MB ranging 0 to 5 minutes after pump.

As seen in the above figure, detection of $^1O_2$ is maximum immediately after the pump of MB which was expected given the reactivity of $^1O_2$ and its short lifetime of approximately 4 μs.[77] As time passes after the pump of MB, the amount of $^1O_2$ decreases since the $^1O_2$ has most likely already reacted and returned to the more stable ground-state. When comparing the duration of the pump of MB, it can be observed that longer pump times results in slightly more $^1O_2$ generation. The lack of a significant increase at the longer pump times, could be due to the short lifetime of $^1O_2$ in water and the time delay between pumping the MB and collecting the SG spectra (~10-20 seconds). This delay would result in only the measurement of a fraction of the $^1O_2$ generated from the MB. To further understand this process, the changes in the SG emission spectra, before and immediately after the pump, were analyzed by determining the percent change based on integrating the areas under the curves (AUC). This was carried out using SigmaPlot 11 and the AUC for the 2-minute pump (Figure 6.16A), 4-minute pump (Figure 6.16B) and 6-minute pump (Figure 6.16C) were determined to be 7.19, 9.18, and 9.68%, respectively. Based on the results of the AUC, more $^1O_2$ appeared to be generated at the longer pump times. These experiments were completed to ultimately gain an understanding of SG detection of $^1O_2$ and to see the effectiveness of SG in detecting $^1O_2$ from a well-known sensitizer. The next steps were to subsequently analyze the carbon nanodots as a possible sensitizer for $^1O_2$ generation.

Carbon nanodot $^1O_2$ experiments were carried out in a similar manner as the MB experiments with slight adjustments to the volumes of solvents and pump wavelength used, as described in the experimental section. Both water dots and HBr

dots were studied for $^1O_2$ generation using a pump wavelength of 300 nm. This wavelength was chosen based on the phosphorescent peak observed for HBr dots at 300 nm, discussed previously, which is needed for production of $^1O_2$. When analyzing water dots for singlet oxygen generation, as shown in Figure 6.16, there appeared to be no $^1O_2$ generation observed, even for the longer pump times. These results were expected due to the lack of phosphorescence present for water dots.

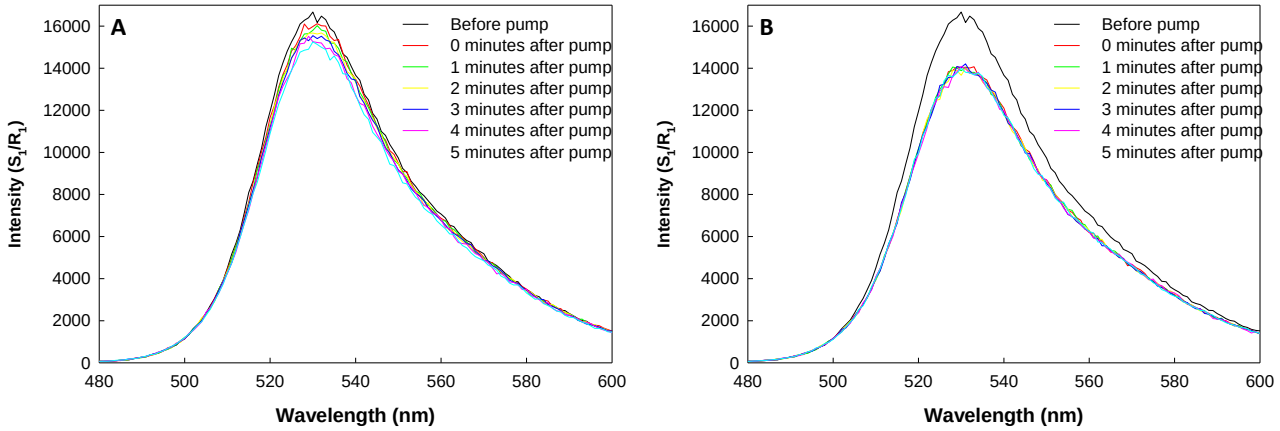


**Figure 6.16** Singlet oxygen generation from water dots utilizing senor green at different pump durations of A) 2 minutes and B) 6 minutes. The pump wavelength for water dots was 300 nm and the excitation wavelength for SG was 470 nm. SG spectra were collected after various times after exciting the water dots, ranging 0 to 5 minutes after pump.

For HBr dot, there was a phosphorescent peak observed when the nanodots are excited with 300 nm light, therefore, the triplet-state of the nanodots could interact with molecular oxygen to generate $^1O_2$. First, HBr dots were analyzed in solution (no glycerol) at the acidic pH and the signal from SG was degraded, as shown in Figure 6.17, suggesting that the SG is not stable in the harsh acidic conditions. Therefore, the HBr dots were neutralized with NaOH as described in Chapter 3, and re-analyzed for $^1O_2$ generation with SG, which is stable at the neural pH.

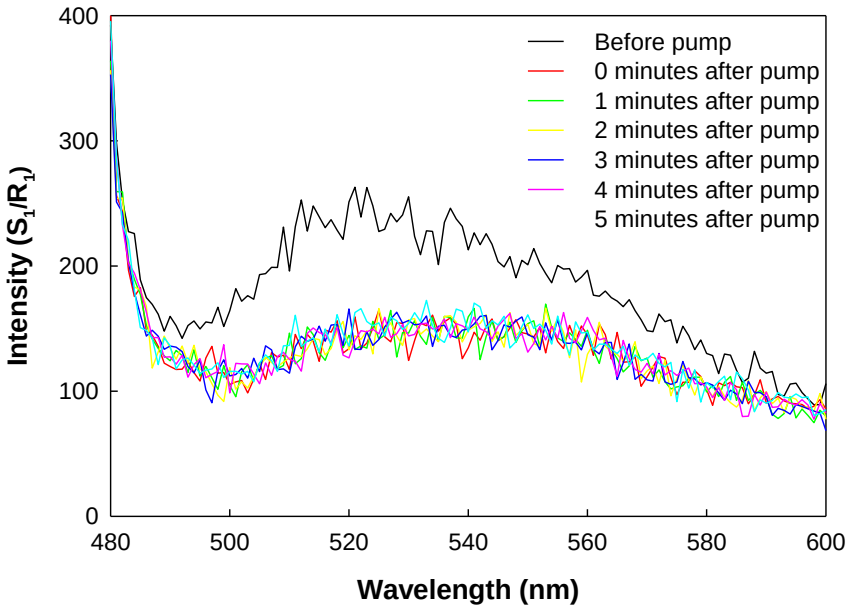


**Figure 6.17** Singlet oxygen generation from acidic HBr dots utilizing senor green pumped for 6 minutes. The pump wavelength for HBr dots was 300 nm and the excitation wavelength for SG was 470 nm. SG spectra were collected after various times after exciting the water dots, ranging 0 to 5 minutes after pump.

By neutralizing the pH of HBr dots, the fluorescence signal of SG was restored; however, when examining the spectra, it appeared that little to no $^1O_2$ was generated, even at the longer pump times for the nanodots, as shown in Figure 6.18.

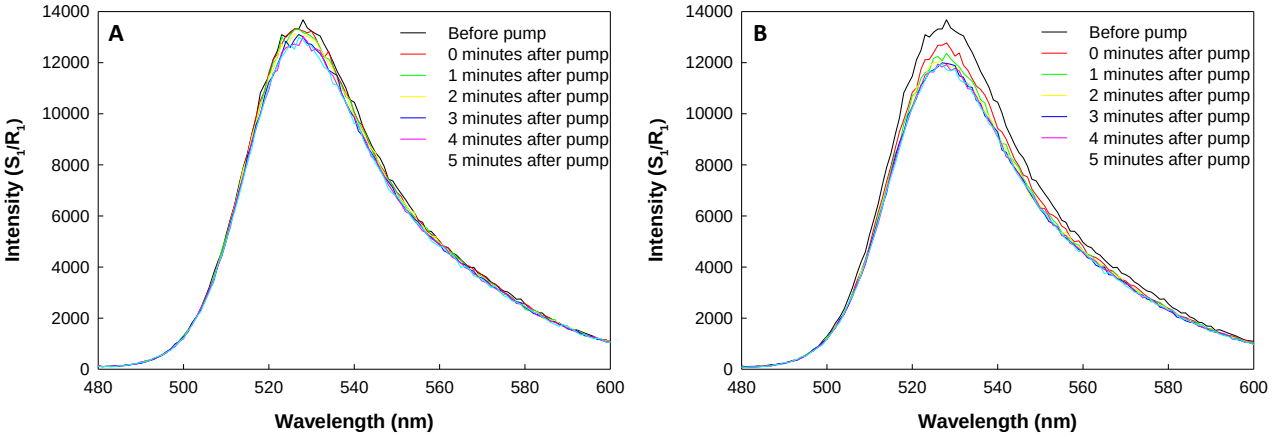


**Figure 6.18** Singlet oxygen generation from neutralized HBr dots utilizing senor green pumped for A) 2 minutes and B) 6 minutes. The pump wavelength for HBr dots was 300 nm and the excitation wavelength for SG was 470 nm. SG spectra were collected after various times after exciting the water dots, ranging 0 to 5 minutes after pump.

The HBr dots display phosphorescence when excited with 300 nm light, however in order to see the phosphorescence character, the neutralized HBr dots were mixed in glycerol. Lack of $^1O_2$, could be due to quenching of the triplet state. Therefore, the next set of experiments were completed using neutralized HBr dots mixed with glycerol and control experiments of MB in glycerol to ensure that there was no effect on the SG.

The control experiments with MB in glycerol showed the ability of MB to produce $^1O_2$ and that there was no effect on the SG spectra due to the addition of glycerol (Data not shown). When analyzing the HBr dots in glycerol, it was determined that small amounts of $^1O_2$ generation were possible (Figure 6.19) when the samples were pumped for 6 minutes. The AUCs were analyzed for the before

pump spectrum and immediately after pump spectrum to determine if singlet oxygen was generated. This analysis showed a 1.26% increase in the SG emission intensity, after the carbon nanodots were pumped, meaning that a small amount of $^1O_2$ was detected, as shown in Figure 6.19B.

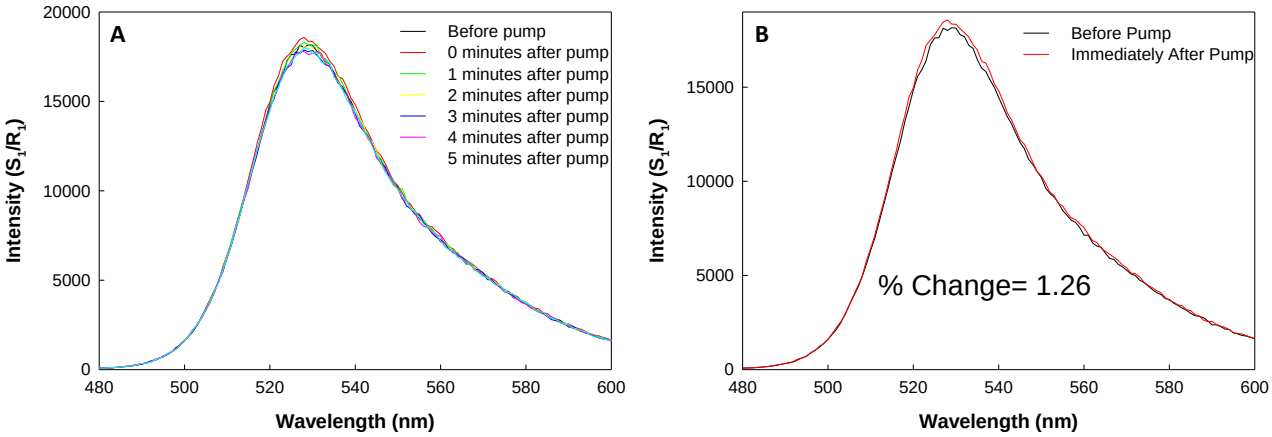


**Figure 6.19** A) Singlet oxygen generation from neutralized HBr dots utilizing senor green pumped for 6 minutes. B) Singlet oxygen generation from HBr dots utilizing sensor green pumped for 6 minutes comparing the before pump and immediately after pump spectra and the calculated percent change based on the AUC. The pump wavelength for HBr dots was 300 nm and the excitation wavelength for SG was 470 nm. SG spectra were collected after various times after exciting the water dots, ranging 0 to 5 minutes after pump.

When analyzing $^1O_2$ production of HBr dots to MB, it was determined that HBr dots are not as efficient in generating $^1O_2$ based on the AUC analysis (10% of MB compared to 1% from HBr dots). Also, when comparing multiple HBr samples, it was observed that the amounts of $^1O_2$ varied from 1-4%. This could be due to the phosphorescence differences between samples because not all of the HBr samples showed phosphorescence and the signal intensity varied from sample to sample. HBr dots with a weaker phosphorescence signal would be expected to generate less $^1O_2$ than a sample with stronger phosphorescence, similar to the comparison of MB to

HBr dots. This issue could be related to the synthetic process of HBr dots meaning that further optimization of incorporating bromide to the carbon nanodots is needed.

## 6.4 Conclusions

By using 5 M HBr as the collection solvent, carbon nanodots with phosphorescence properties were synthesized, characterized, and analyzed for $^1O_2$ generation. HBr dots showed a broad absorption spectrum, along with an excitation wavelength dependent emission, which is similar to that observed for water dots. However, some HBr dots showed phosphorescence when excited at 300 nm, which could explain the lower fluorescence quantum yield (~5%) observed for these nanodots. The time-resolved data revealed a multi-exponential decay that showed a short-lived component along with a long-lived component that was not seen in water dots however, further analysis of the long-lived component is needed.

In an effort to increase the phosphorescence of HBr dots, the nanodots were refluxed for 6 or 12 hours. It was thought that by refluxing the HBr dots, the bromide in solution could be incorporated onto/within the nanodots, similar to oxidization of the candle soot, as described in Chapter 2. However, those results were not consistent enough to draw a conclusion thus requiring further analysis and optimization.

Since phosphorescence was observed for some HBr dots, it was hypothesized that HBr dots could generate $^1O_2$. Therefore, several experiments were carried out to determine if HBr dots could be a sensitizer of $^1O_2$. These experiments analyzed water dots and neutralized HBr dots and revealed that water dots are not capable of producing $^1O_2$, but neutralized HBr dots, when in glycerol, could generate low amounts of $^1O_2$. The results for the HBr dots varied from sample to sample, therefore

further optimization of the singlet oxygen experiments and the synthetic route to produce phosphorescence dots are needed to improve the generation and consistency of $^1O_2$ generation.

# Chapter 7: Plasmonic Enhancement of Carbon Nanodots' Fluorescence and Phosphorescence

## 7.1 Introduction

In this chapter, metal-enhanced fluorescence (MEF) and phosphorescence (MEP) of candle-based and methane-based carbon nanodots will be discussed. MEF has shown the ability to enhance the emission and phosphorescence signals of fluorophores[33,59,62,65,67,75,82,108–110] and it is the goal of this chapter to use MEF and MEP to improve the weak signals of both candle-based and methane-based carbon nanodots.

These studies were carried out on three 96-well plates: uncoated, Quanta Plate 1™ and Quanta Plate 2™. The uncoated plate serves as a control sample whereas, the two silver coated plates are used to study the enhancement of emission and/or phosphorescence signals of the carbon nanodots. For candle-based carbon nanodots, all fractions were analyzed with 473 and 532 nm laser lines and a fluorometer for fluorescence, whereas, methane-based carbon nanodots (water, ethanol, methanol, HBr) were studied using 405 and 473 nm laser lines and a fluorometer in both fluorescence and phosphorescence modes. The results of those experiments are examined in the following sections.

## 7.2 Experimental Details

### *7.2.1 96-Well Plates Utilized for MEF Experiments*

Uncoated 96-well plates were purchased from Thermo Fisher Scientific (Waltham, MA) and Quanta Plates™ were supplied by Plasmonix, Inc (Baltimore, MD). Both types of plates were used as is when they were received. Figure 7.1 shows photographs of the three *plates* used for the metal-enhanced experiments.


**Figure 7.1** A) Uncoated 96-well plates, B) Quanta Plate 1™ C) Quanta Plate 2™.

### *7.2.2 Candle-Based and Methane-Based Carbon Nanodots MEF Experiments*

***Fluorescence Measurements via Laser Excitation.*** Metal-enhanced fluorescence experiments were carried out using 405, 473 or 532 nm laser sources (Lasermate, Walnut, CA) connected to an OceanOptics spectrometer utilizing the SpectraSuite software, through a bi-truncated 600 µM optical fiber. For each laser source, the appropriate notch or laser line filter was used to remove the excitation from the emission signal. Samples (80µL) were studied in a 96-well plate (Thermo Fisher Scientific, Waltham, MA) that was either uncoated or coated with silver. The experimental setup is depicted in Figure 7.2.

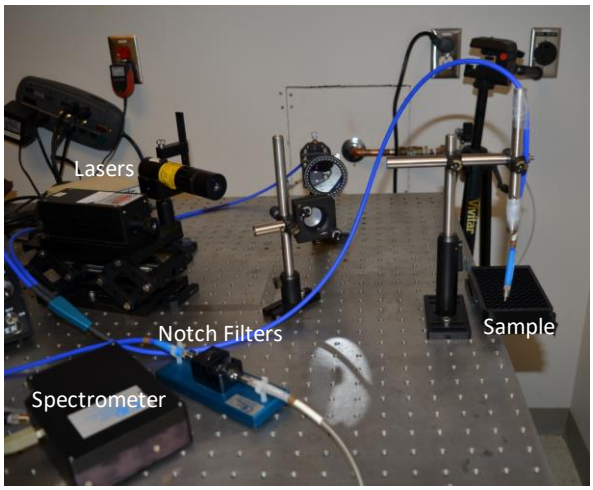


**Figure 7.2** Experimental setup of metal-enhanced fluorescence studies using laser excitation and an Ocean Optics spectrometer.

***Fluorescence Measurements using a Benchtop Fluorometer (Varian).*** Metal-enhanced fluorescence experiments were studied using a Varian Cary Eclipse fluorescence spectrophotometer (Agilent Technologies, Santa Clara, CA). The instrument is equipped with a xenon arc flash lamp, plate reader and Cary Eclipse software. Experiments were carried out on each of the 96-well plates using 80 μL of carbon nanodot sample with a scan rate of 600 nm/min. The excitation and emission monochromators were adjusted to obtain the appropriate wavelengths to collect emission data.

***Phosphorescence Measurements using a Benchtop Fluorometer (Varian).*** Metal-enhanced phosphorescence experiments were carried out on the Varian Cary Eclipse fluorescence spectrophotometer (Agilent Technologies, Santa Clara, CA) operating in phosphorescence mode with a scan rate of 600 nm/min. General parameters used for phosphorescence collection are shown in Table 7.1 and the excitation and emission monochromators were adjusted to obtain the appropriate wavelengths to collect emission data.

**Table 7.1** Experimental parameters for phosphorescence measurements.

| | |
|---|---|
| Flash Delay | 0.200 ms |
| Sample Window | 5.000 ms |
| Time per Flash | 20.000 ms |
| Flash Count | 1 |

***Synchronous Scattering Measurements.*** Synchronous spectra of the uncoated and Quanta Plates™ were measured on the Varian Cary Eclipse fluorescence spectrophotometer (Agilent Technologies, Santa Clara, CA) in the synchronous mode ($\lambda_{ex}=\lambda_{em}$). The experiments were completed on empty wells (no sample) and using the parameters shown in Table 7.2 along with a scan rate of 120 nm/min.

**Table 7.2** Experimental parameters for synchronous spectra.

| | |
|---|---|
| Delta nm | 0.00 |
| Excitation Start (nm) | 300 |
| Excitation End (nm) | 600 |
| Excitation Slit (nm) | 2.5 |
| Emission Slit (nm) | 1.5 |

## 7.3 Results and Discussion

### *7.3.1 MEF of Candle-Based Carbon Nanodots*

**Synchronous Scatter**

The synchronous spectra ($\lambda_{ex}=\lambda_{em}$) for an uncoated well and Quanta Plate 1™ are shown in Figure 7.2 with image of the plate used for the metal-enhanced fluorescence experiments inset within the figure.

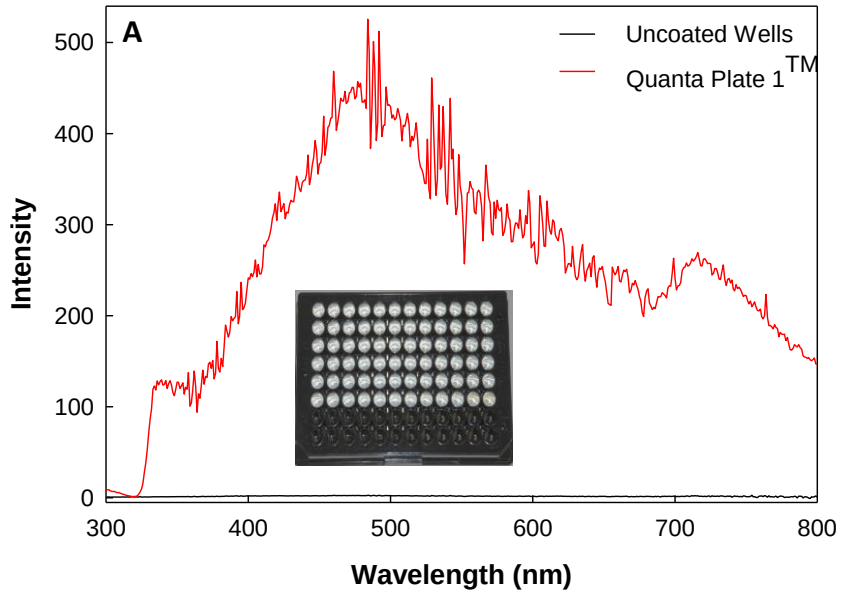


**Figure 7.3** Synchronous spectra for uncoated well (Black) and Quanta Plate 1™ (Red). Inset. Image of Quanta Plate 1™ and uncoated wells.

The above spectra show that the scattering of the Quanta Plate 1™ has a broad spectral range from the visible tailing into the near infrared with maximum scattering around 500 nm. When in the synchronous mode of the fluorometer, the excitation and emission wavelengths are scanned simultaneously in order to record the scattering properties of the surface. This spectrum describes the extinction spectrum of the surface silver coating, which is well-known to influence MEF due to the coupling and subsequent radiation of the fluorophore through the scattering mode of the surface immobilized silver nanoparticles.[59–61,71] The synchronous spectrum can also predict the wavelength dependence of the MEF enhancement factor and subsequently spectra distortions based on the overlap of the carbon nanodots emission spectrum with the scattering spectrum of the silver-coated surface.[59,71,72]

**Metal-Enhanced Fluorescence via Laser Excitation**

Two laser lines at 473 nm and 532 nm were used to study the effect of silver-coated surfaces on the emission of the carbon nanodots. Figure 7.4 shows the results of those experiments for the 10,000 RPM fraction of candle-based carbon nanodots. When in the presence of silver nanoparticles, the emission of candle-based carbon nanodots were enhanced 9.70 and 12.40 times for 473 and 532 nm laser lines, respectively at lambda maximum. The enhancement factor was calculated by dividing the coated surface signal by the uncoated surface signal at lambda maximum. Also, in order to determine the wavelength dependence of the MEF enhancement factor, a similar calculation was used, i.e. coated surface divide by uncoated surface for the entire wavelength range. It can be observed that there is spectra distortion on the red-

edge of the MEF enhancement spectra, which is thought to be due to the lack of spectra overlap between the carbon nanodots and the silver-coated surface at longer wavelengths.[72] The same wavelength dependence and enhancement trends were seen for all the carbon nanodot fractions. A summary of the enhancement for the 473 and 532 nm laser lines are portrayed in Tables 7.3 and 7.4.

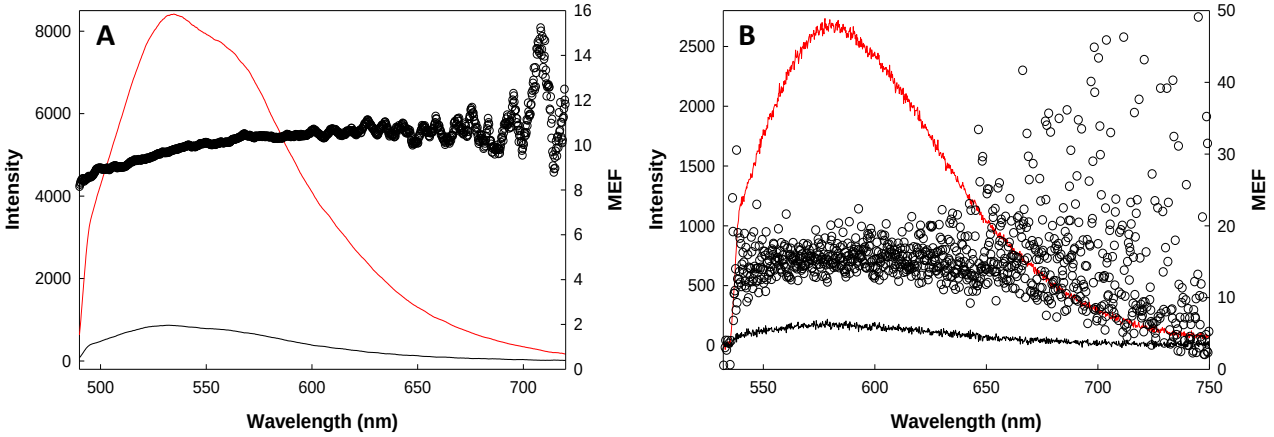


**Figure 7.4** Metal-Enhanced Fluorescence of candle-based nanodots separated at 10,000 rpm on uncoated well (Black) and Quanta Plate 1™ (Red) excited at A) 473 nm laser line with 488 nm long pass filter and B) 532nm laser line with 532 long pass filter with the wavelength dependence of the enhancement factor superimposed on the emission spectra.

**Table 7.3** Metal Enhancement of candle-based nanodots excited with 473 nm laser line.

| Sample (rpm) | MEF |
|---|---|
| 3,000 | 9.50 |
| 5,000 | 10.70 |
| 10,000 | 9.70 |
| 14,500 | 10.60 |

**Table 7.4** Metal Enhancement of candle-based nanodots excited with 532 nm laser line.

| Sample (rpm) | MEF |
|---|---|
| 3,000 | 11.70 |
| 5,000 | 11.40 |
| 10,000 | 12.40 |
| 14,500 | 11.10 |

It notable that the enhancement factor appears to be greater when using the 532-nm laser as the excitation source when compared to the 473-nm laser. This is hypothesis that since the emission signal is weaker at 532 nm, the enhancement would be greater for weaker signals.[58] This trend is further observed when candle-based carbon nanodots are compared to methane-based carbon nanodots.

**Metal-Enhanced Fluorescence on a Benchtop Fluorometer**

All fractions of the candle-based carbon nanodots were analyzed on the Varian at excitation wavelength of 482-nm. These studies require the use of excitation and emission filters to remove scattering and stray light from the spectrum. Figure 7.5 shows the enhanced emission of the carbon nanodots to be about 30 times greater at lambda max, when excited with 482 nm light, when comparing silver-coated wells to uncoated wells. There is an increase enhancement seen with using the Varian as compared to laser lines. This is thought to be due to the emission wavelength overlapping with the scattering mode of the silver. However, it has also, been hypothesis that Varian is more efficient at collecting the emitted light than the fiber used with laser set-up. Also, these spectra reveal a similar wavelength

dependence of the MEF compared to the 473-nm laser line. Similar results were seen for the other fractions of candle-based carbon nanodots.

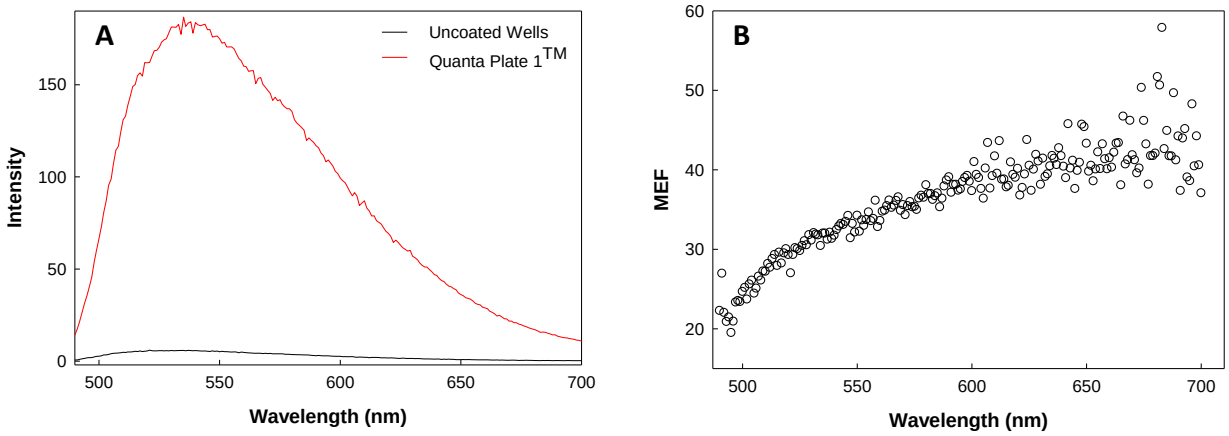


**Figure 7.5** A) Metal-Enhanced Fluorescence of candle-based carbon nanodots separated at 10,000 rpm on uncoated well (Black) and Quanta Plate 1™ (Red) excited at 482 nm B) Wavelength dependence of MEF of Candle Nanodots separated at 10,000 rpm excited at 482 nm.

### *7.3.2 MEF of Methane-Based Carbon Nanodots*

**Synchronous Scatter**

Methane-based carbon nanodots were analyzed on Quanta Plates 1 and 2™. The Quanta Plate 1™ synchronous spectrum was shown in Figure 7.3 and the Quanta Plate 2™ synchronous spectrum is shown in Figure 7.6. When comparing the scattering spectra for both plates, the appear to be similar except for overall lower scattering intensity observed for Quanta Plate 2™. This lower intensity would be expected to result in a lower enhancement effect on the emission of carbon nanodots.

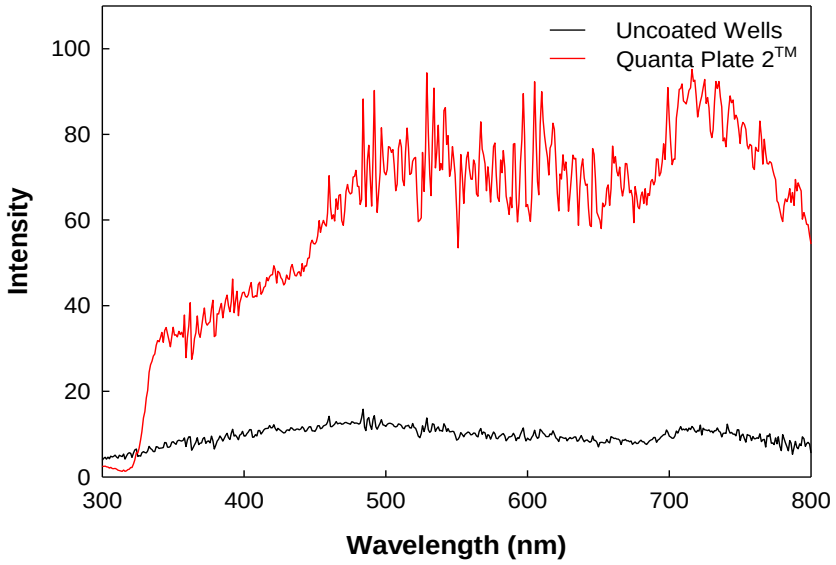


**Figure 7.6** Synchronous spectra for uncoated well (Black) and Quanta Plate 2™ (Red). The band at 700 nm is thought to be a due the grating of the monochromator.

### Metal-Enhanced Fluorescence via Laser Excitation

The MEF of water, ethanol, and methanol carbon nanodots on Quanta Plates 1 and 2™ were analyzed by 405 and 473 nm laser lines with either a 450 or 488 nm long pass filter. The results the 405 and 473 nm experiments with water, ethanol and methanol dots are shown in Figure 7.7-7.7.9 A and B, correspondingly.

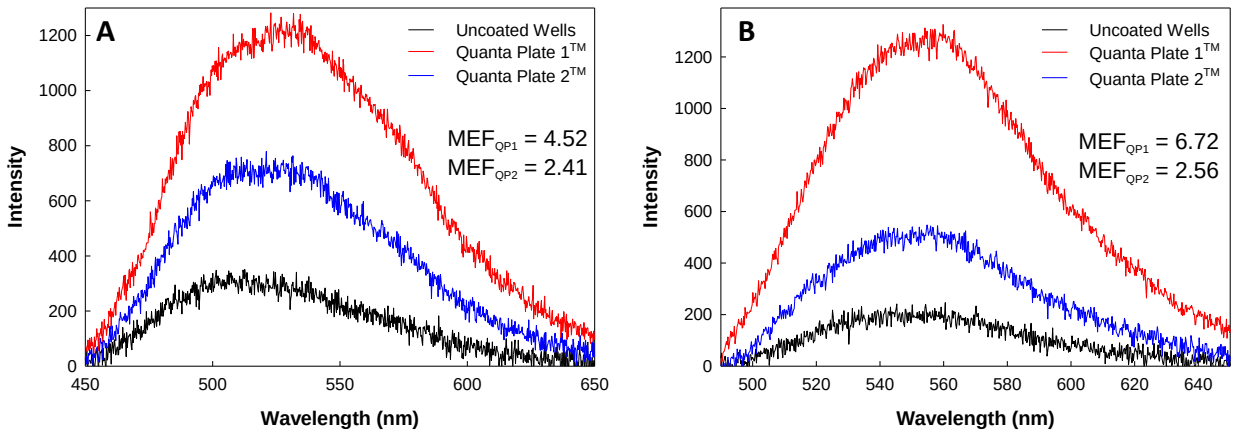


**Figure 7.7** Metal-Enhanced Fluorescence on Uncoated Wells (Black), Quanta Wells (Red) and Quanta Plates (Blue) from Water Dots synthesized for 2 hours excited with A) 405 nm laser line and B) 473 nm laser line.

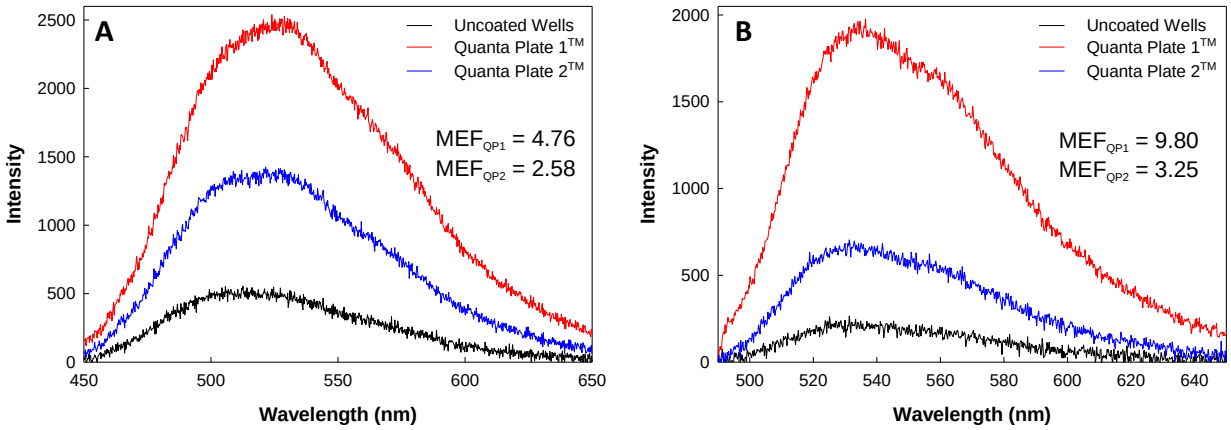


**Figure 7.8** Metal-Enhanced Fluorescence on Uncoated Wells (Black), Quanta Wells (Red) and Quanta Plates (Blue) from Ethanol Dots synthesized for 2 hours excited with A) 405 nm laser line and B) 473 nm laser line.

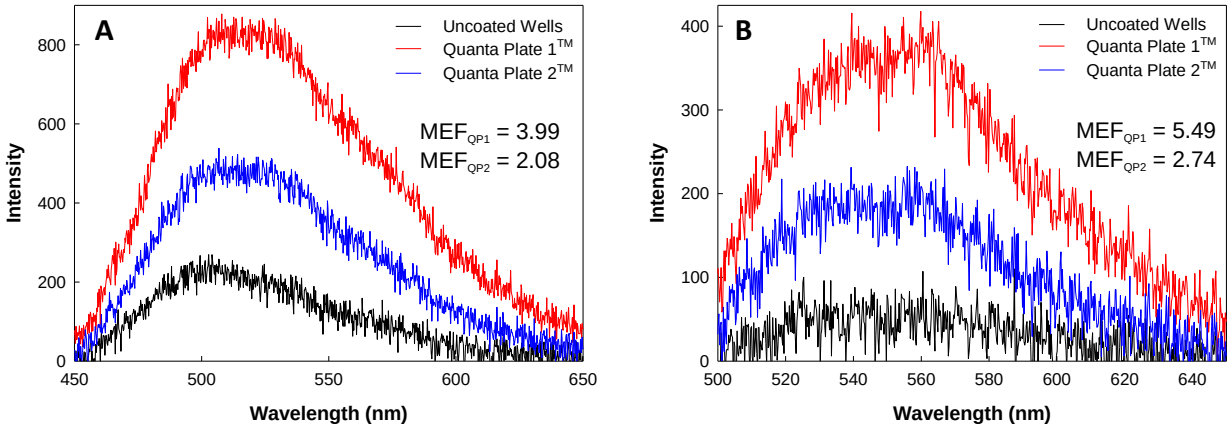


**Figure 7.9** Metal-Enhanced Fluorescence on Uncoated Wells (Black), Quanta Wells (Red) and Quanta Plates (Blue) from Methanol Dots synthesized for 2 hours excited with A) 405 nm laser line and B) 473 nm laser line

For all three solvents, it can be seen that Quanta Plate 1™ has a greater enhancement than Quanta Plate 2™. However, when comparing the enhancement for each plate against each solvent, the enhancement is not that much different when the solvent is changed. Also, when comparing the above spectra, the noise seen in each is reasoned to be due the weak emission for each sample at the excitation wavelengths. The enhancement factors for methane-based carbon nanodots, for both excitation wavelengths are shown in Tables 7.5 and 7.6. This enhancement factors show the consistent trend of Quanta Plate 1™ having a greater enhancement than Quanta Plate 2™.

**Table 7.5** Average MEF enhancement of methane-based nanodots excited with 405 nm laser.

| Sample | $MEF_{QP1}$ (average) | $MEF_{QP2}$ (average) |
|---|---|---|
| Water | 4.18 | 2.30 |
| Methanol | 3.99 | 2.08 |
| Ethanol | 3.70 | 1.86 |

**Table 7.6** Average MEF enhancement of methane-based nanodots excited with 473 nm laser line.

| Sample | $MEF_{QP1}$ (average) | $MEF_{QP2}$ (average) |
|---|---|---|
| Water | 6.25 | 2.35 |
| Methanol | 5.49 | 2.74 |
| Ethanol | 7.02 | 2.36 |

**Metal-Enhanced Fluorescence on a Benchtop Fluorometer**

Water, ethanol, and methanol dots were studied on the Varian at the excitation wavelength of 480 nm with excitation and emission filters, Figure 7.10. The

enhancement factors are observed to be greater when using the Varian to collect to spectra than using the laser sources. This observation was similar to the observation for candle-based carbon nanodots, which is reasoned to be due to the Varian having more efficiency in collecting the emitted light than the optical fiber. Also, it is noteworthy that Quanta Plate 1™, again, is observed to have a greater enhancement than Quanta Plate 2™ for methane-based carbon nanodots.

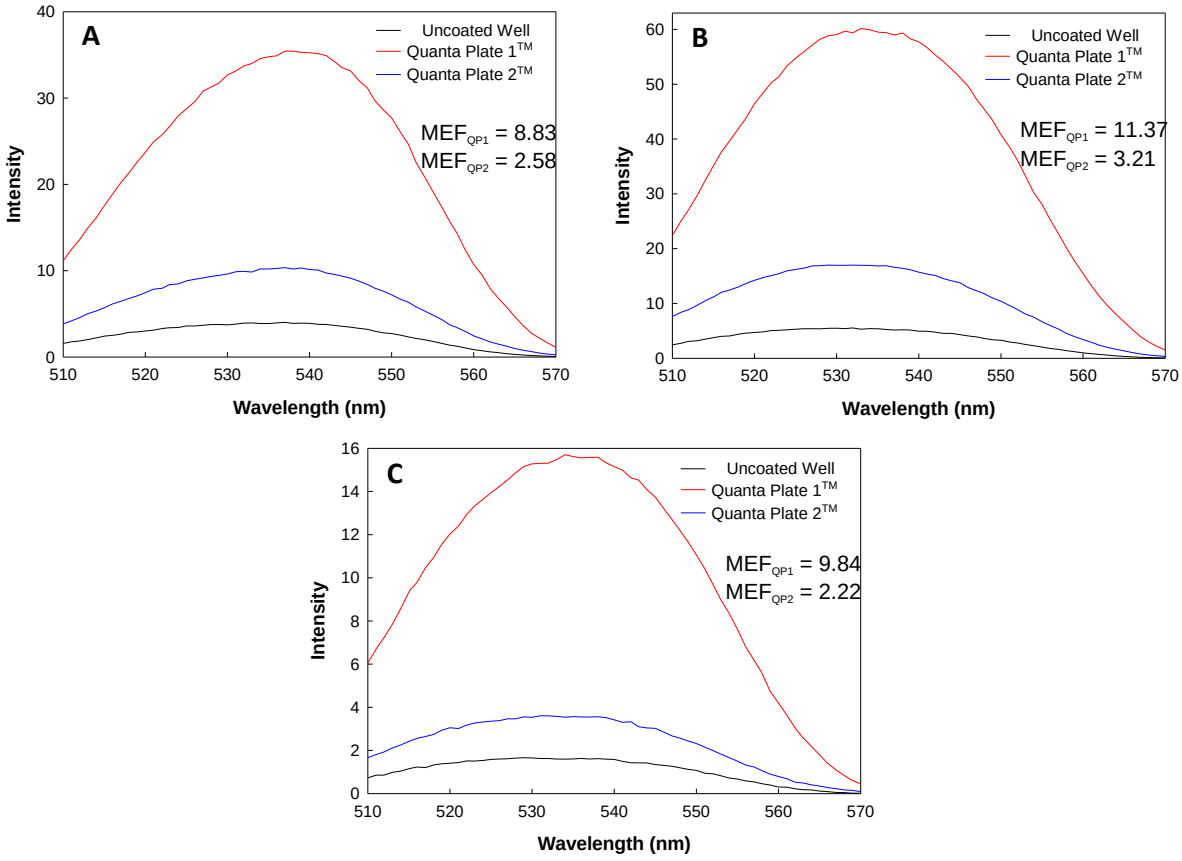


**Figure 7.10** Metal-Enhanced Fluorescence on Uncoated Wells (Black), Quanta Wells (Red) and Quanta Plates (Blue) from A) Water Dots, B) Ethanol Dots, and C) Methanol Dots synthesized for 2 hours excited at 480 nm

When comparing the candle-based carbon nanodots to methane -based carbon nanodots, it clearly seen that the candle-based nanodots have a great enhancement with 30x enhancement compared to 11x enhancement for methane-based nanodots. This difference is thought to be use to the differing free-space quantum yields of the two carbon nanodots (2% as compared to 20%).[58] Also, the different enhancement at the different excitation wavelengths would be explained by the same reasoning, as methane-based carbon nanodots have lower quantum yields at lower excitation wavelengths (Chapter 3).

### *7.3.3 MEF of HBr Methane-Based Carbon Nanodots*

**Metal-Enhanced Fluorescence via Laser Excitation**

Figure 7.11 and 7.12 show the metal enhancement of HBr dots, synthesized for 2 and 4 hours, when excited with 405 and 473 nm laser lines. There is a small enhancement for both Quanta Plates™ used, with plate 1 still having a greater

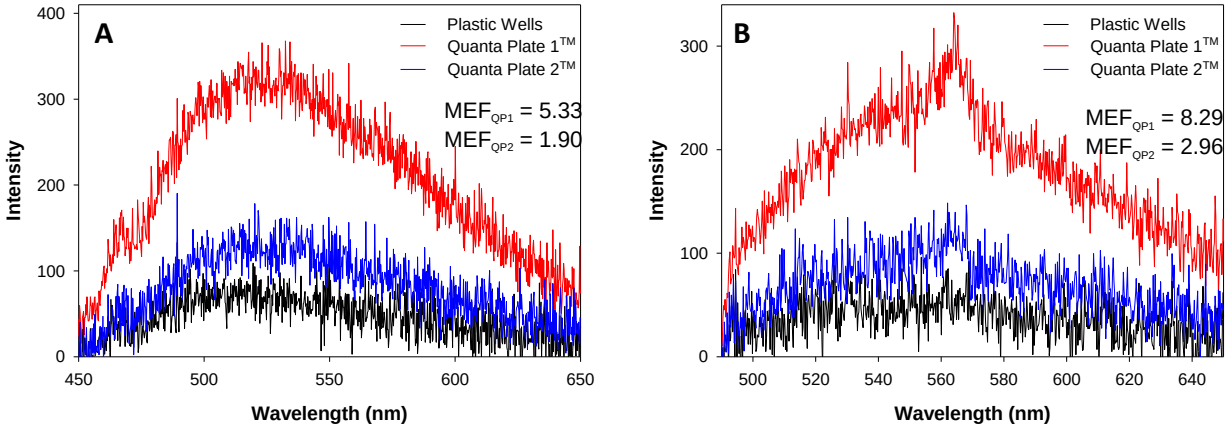


**Figure 7.11** Metal-Enhanced Fluorescence on Uncoated Wells (Black), Quanta Wells (Red) and Quanta Plates (Blue) from HBr Dots synthesized for 2 hours excited with A) 405 nm laser line and B) 473 nm laser line.

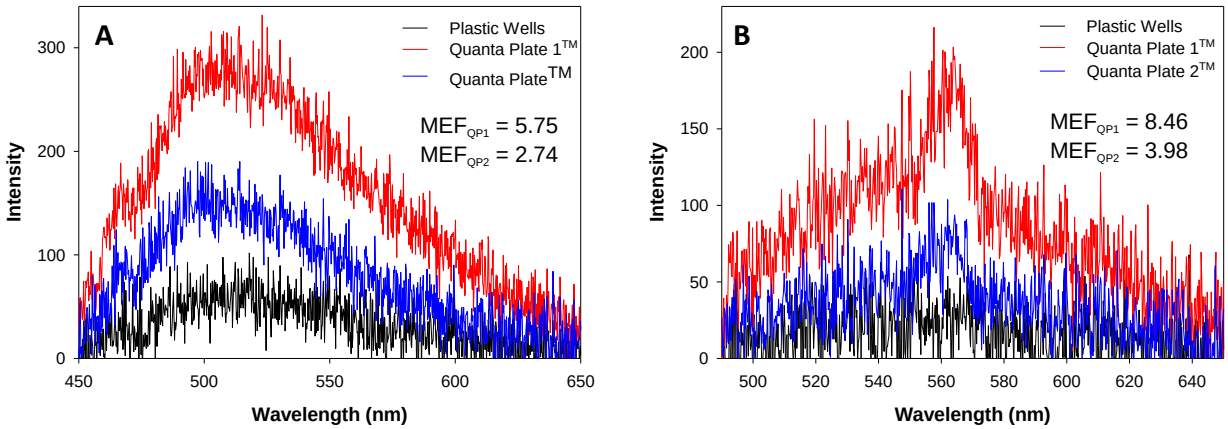


**Figure 7.12** Metal-Enhanced Fluorescence on Uncoated Wells (Black), Quanta Wells (Red) and Quanta Plates (Blue) from HBr Dots synthesized for 4 hours excited with A) 405 nm laser line and B) 473 nm laser line.

enhancement than plate 2.

The fluorescence emission signals of HBr dots were observed to be much less than the previous carbon nanodots, which is thought to be due to the fact that the HBr dots show evidence for ISC and phosphorescence. When comparing the enhancement over several syntheses the average MEF of Quanta Plates 1 and 2™ for 405 nm excitation are 4.75 and 1.75, respectively. For 473 nm excitation, the average MEF for the two are 7.29 and 2.96, respectively. Again, these enhancement factors show that Quanta Plate 1™ has a greater ability to enhance the emission signal than Quanta Plate 2™.

**Metal-Enhanced Fluorescence on a Benchtop Fluorometer**

Similar to the experiments for water, ethanol, and methanol dots, HBr dots were studied on the Varian at the excitation wavelength 480 nm. Both the 2 and 4 hour syntheses show an enhancement, with plate 1 being greater than plate 2. Figure

7.13 shows the spectra from these experiments. As seen with laser excitation, HBr dots emission signal is much lower than previous carbon nanodots samples, which is thought to be due to ISC and phosphorescence being present for these types of carbon

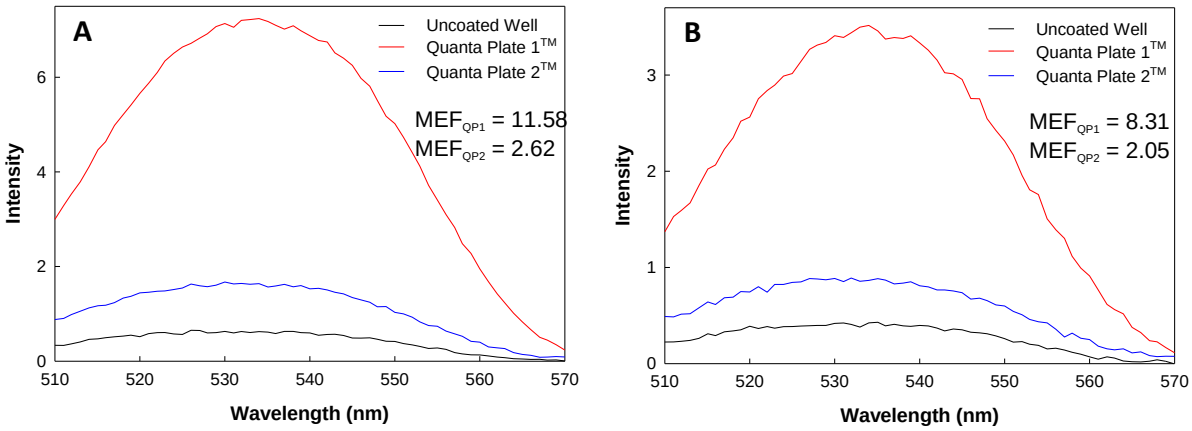


**Figure 7.13** Metal-Enhanced Fluorescence on Uncoated Wells (Black), Quanta Wells (Red) and Quanta Plates (Blue) from HBr Dots synthesized for A) 2 hours and B) 4 hours excited at 480 nm.

nanodots. Also, the Varian appears to be more efficient at collecting the emitted light than the optical fiber, thus greater enhancement factors and cleaner spectra.

**Metal-Enhanced Phosphorescence on a Benchtop Fluorometer**

Metal-enhanced phosphorescence experiments were carried out on HBr dots mixed with glycerol in order to be able to see the phosphorescence signal. Figures 7.14 and 7.15 show the MEF and MEP of HBr synthesized for 2 and 4 hours when excited at 300 nm. These figures show that the phosphorescence in present for HBr dots, but it also shows that the phosphorescence signal can be enhanced along with the emission signal. The below figures show that there is clearly phosphorescence present for HBr dots due to the Stokes shift seen between the fluorescence and phosphorescence signals. Also, when the fluorometer is in phosphorescence mode, there is a delay in signal collection so that no fluorescence signal will be recorded.

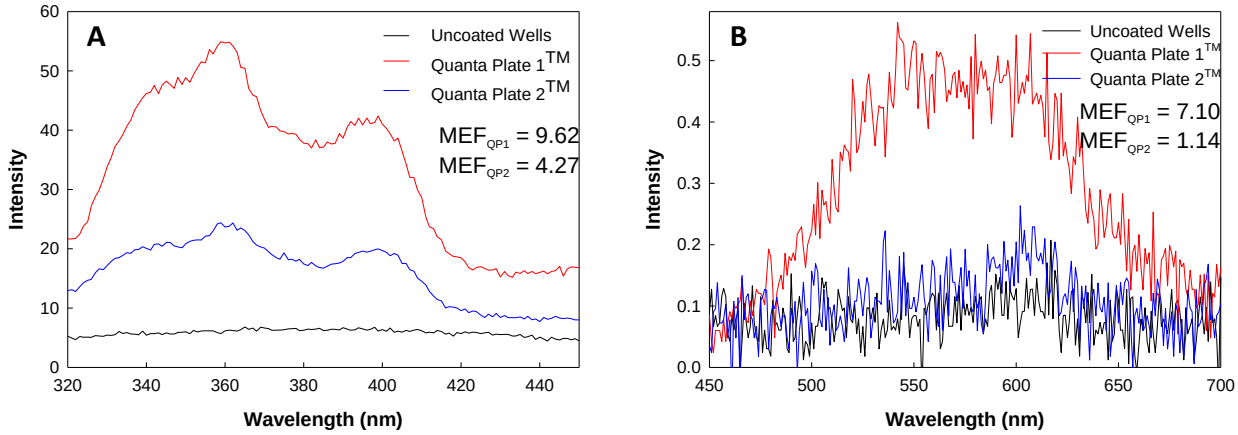


**Figure 7.14** A) Metal-Enhanced Fluorescence and B) Phosphorescence on Uncoated Wells (Black), Quanta Wells (Red) and Quanta Plates (Blue) from HBr Dots synthesized for 2 hours 80% glycerol excited at 300 nm.

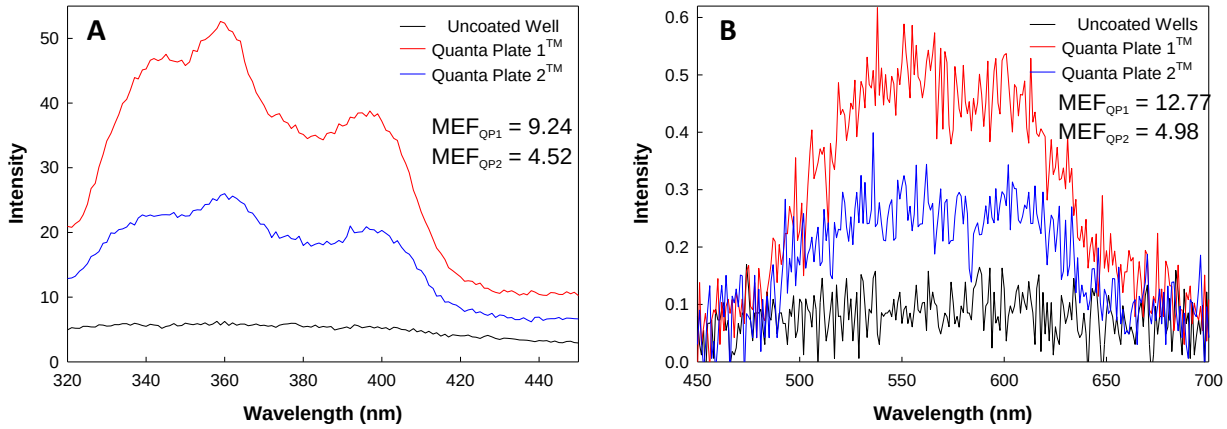


**Figure 7.15** A) Metal-Enhanced Fluorescence and B) Phosphorescence on Uncoated Wells (Black), Quanta Wells (Red) and Quanta Plates (Blue) from HBr Dots synthesized for 4 hours in 80% glycerol excited at 300 nm.

Once more, the enhancement is great for plate 1 than plate 2. This continued pattern is supported by the scattering spectrum being greater for plate 1 than plate 2. Therefore, plate 1 would be predicted to have a greater enhancement than plate 2,

which is what is being repeatedly seen. To show a better comparison of the fluorescence and the phosphorescence enhancements Figures 7.16 and 7.17 show the

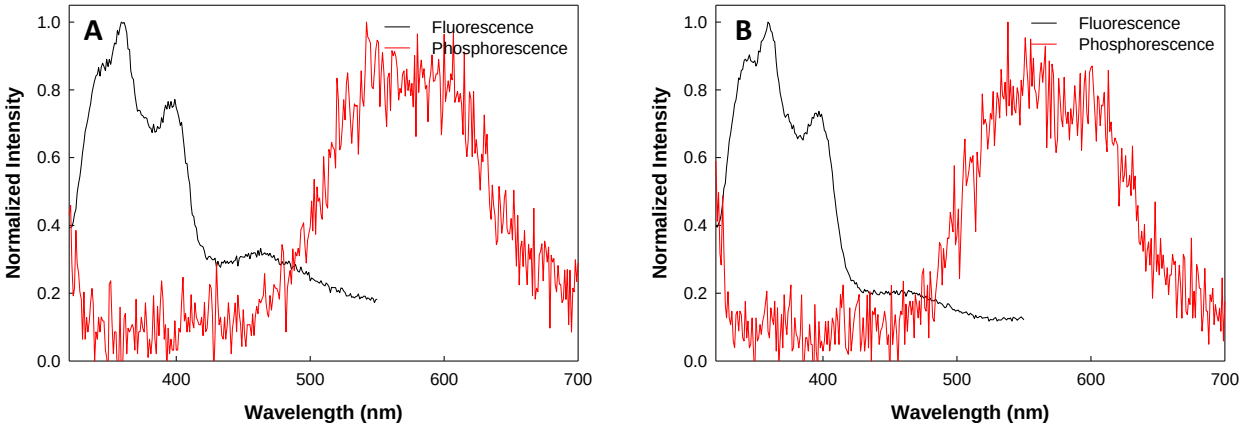


**Figure 7.16** Comparison of normalized fluorescence and phosphorescence spectra of Quanta Plate 1™ from HBr Dots synthesized for A) 2 hours and B) 4 hours in 80% glycerol excited at 300 nm.

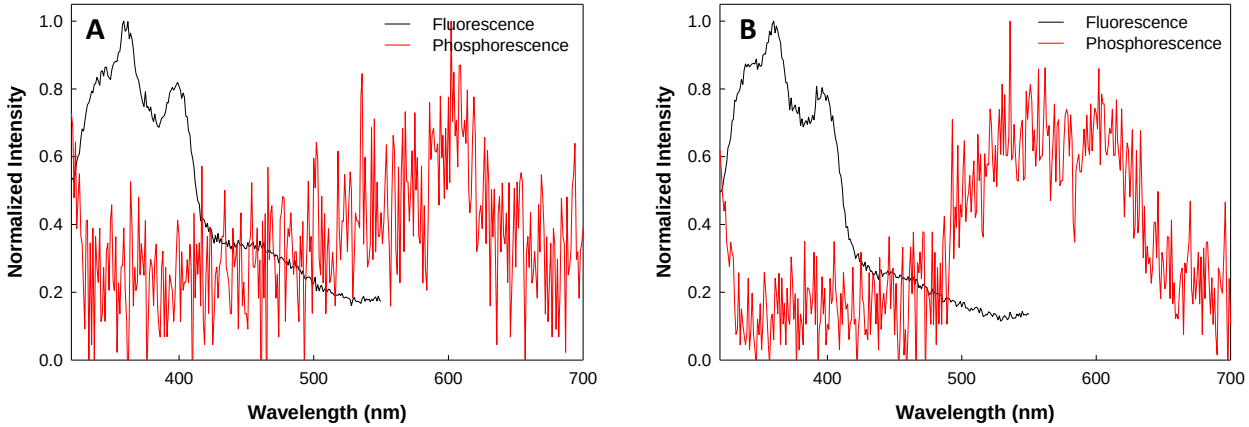


**Figure 7.17** Comparison of normalized fluorescence and phosphorescence spectra of Quanta Plate 2™ from HBr Dots synthesized for A) 2 hours and B) 4 hours in 80% glycerol excited at 300 nm.

normalized signals for fluorescence and phosphorescence of HBr dots when on Quanta Plate 1 and 2™. These figure help highlight the Stokes shift seen between the fluorescence and phosphorescence signals of HBr dots.[49–51]

## 7.4 Conclusions

In the presence of silver nanoparticles, carbon nanodots, synthesized from candle soot and methane gas, emission can be successfully enhanced. Candle-based carbon nanodots emission signals were enhanced up to 30 times when compared to the control (uncoated wells). Methane-based carbon nanodots showed a significantly lower enhancement of the emission signal at only 11 times greater than the control. This difference is due to the noteworthy difference in the quantum yields of the two synthetic methods. Metal-enhanced fluorescence is dependent on the natural quantum yield of the fluorophore and as the quantum yield increases, the coupled system enhancement factor decreases.[58] Along with metal-enhanced fluorescence, metal-enhanced phosphorescence was observed from methane HBr dots, when excited with 300 nm light. The phosphorescence is distinguishable from the fluorescence because of the red shift observed in the spectra and time-gated nature of the intensity collected. Overall, the emission and phosphorescence signals of carbon nanodots synthesized multiple ways and in various solvents, are able to be enhanced in the presence of silver-coated surfaces.

# Chapter 8: Conclusions and Future Directions

## 8.1 Conclusions

Carbon nanodots are small fluorescent nanoparticles that have several unique photophysical characteristics which makes them potentially useful as luminescent probes in multiple fields of science.[2–6] Although synthetic routes of carbon nanodots have been extensively investigated, many of them produce carbon nanodots with low fluorescence quantum yields and/or require surface modifications to become fluorescent nanoparticles.[1–4,13,15,22,23] The present research aimed to address the issue of low quantum yields by developing a simple and inexpensive combustion method to synthesize highly fluorescent carbon nanodots, followed by characterization and modifications to change their photophysical properties.

Two synthetic pathways were investigated that utilized either candle soot or ultra-pure methane gas to generate carbon nanodots. First, the candle-based carbon nanodots were synthesized and characterized. The candle-based synthetic procedures were found to be time-consuming and multifaceted and resulted in nanodots with only ~2% quantum yields. This approach required the oxidization of candle soot with nitric acid for 12 hours followed by multiple neutralization and separation steps before the nanodots could be characterized. The candle-based carbon nanodots showed an excitation wavelength dependent fluorescence, a broad absorption, good photostability, coupled with complex intensity decays. Due to the length and ineffectiveness of the synthetic procedures to produce highly fluorescent carbon nanodots, a second synthetic method was developed to produce carbon nanodots from methane gas.

The methane-based approach produced and collected the carbon nanodots directly from a sooting flame with an overall synthesis time of four hours and no further treatment of the nanodots was required. This method reduced the experimental time drastically and was able to produce nanodots with quantum yields of up to ~30%. The characterization of the methane-based nanodots revealed an excitation wavelength dependent fluorescence, a broad absorption, and complex intensity decays that were slightly different from nanodots synthesized with candle-based method. It has been reported that the synthetic pathway utilized can influence the photophysical properties of carbon nanodots, which supports the differences observed for candle-based and methane-based carbon nanodots.[2–6]

Further investigation of the methane-based carbon nanodots photophysical properties was undertaken, utilizing fluorescence quenching, to help understand the possible mechanism/origin of their luminescence. The luminescence properties of carbon nanodots are hypothesized to be due to either a core structure and surface traps or possess multiple emissive centers. However, it is also possible that the nanodots have a combination of both the core/surface traps mechanism and the multiple emissive centers.[6,42,87] The methane-based nanodots appeared to have a buried chromophore core that was inaccessible to the solvent based on the presence of vibronic structure observed in the emission spectra (Figure 3.14). The existence of both a buried core and multiple emissive centers on the surface was further supported by the fluorescence quenching experiments of methane-based carbon nanodots. These experiments showed that fluorescence of the nanodots could be quenched by negative, positive, and neutral quenchers, but that only the neutral quencher

(acrylamide) could diffuse into the core and quench the vibronic structure whereas, the charged quenchers are able to quench the luminescence due to the emissive centers on the surface. These experiments also revealed that the quenching of carbon nanodots occurred by a dynamic quenching mechanism for charged quenchers and a static quenching mechanism for the neutral quencher based on the Stern-Volmer plots.

While completing the fluorescence quenching experiments, a novel temperature dependent emission property was observed. This property resulted in the increase of the emission intensity as a function of increased temperature. The mechanism behind this property is hypothesized to be Thermally-Activated Delayed Fluorescence (TADF), which is commonly found in fullerenes.[97–102] TADF occurs through intersystem crossing from the $S_1$ state to the $T_1$ state and back intersystem crossing to the $S_1$ state, where delayed fluorescence occurs. The results obtained from this research appear to support the TADF mechanism, however, further work is needed in order to gain a full understanding of this property of carbon nanodots.

The final aspect of this research was to modify the methane-based carbon nanodots to produce phosphorescence nanodots that could be used for singlet oxygen ($^1O_2$) generation and to use Metal-Enhanced Fluorescence (MEF) to improve the fluorescence and phosphorescence signals. Brominated carbon nanodots were synthesized by using a solvent that contained bromide ions, which are known to promote intersystem crossing.[49–51] These brominated nanodots displayed similar photophysical properties as the previously synthesized methane-based nanodots, with the exception of low fluorescence quantum yields (~5%), a long-lived lifetime

component and phosphorescent peaks at certain excitation wavelengths. The low fluorescence quantum yields are attributed to the phosphorescence property of theses nanodots. As hypothesized, brominated nanodots were shown to produce low amounts of singlet oxygen, whereas, methane-based nanodots did not generate singlet oxygen. However, further studies are needed to optimize the synthesis of phosphorescent nanodots and singlet oxygen generation. Finally, the emission and phosphorescence signals of candle-based, methane-based and brominated carbon nanodots were successfully enhanced when in the presences of silver nanoparticles due to MEF.

## 8.2 Future Directions

### *8.2.1 Synthesis of Methane-Based Carbon Nanodots*

It has been previously reported and showed in this research that the solvent effects can influence the photophysical properties of the nanodots therefore, the use of other solvents should be further investigated.[30,88,89] The present research analyzed three polar solvents (water, ethanol and methanol) and one non-polar solvent (hexane), thus investigating other non-polar solvents, such as acetonitrile or dimethyl sulfoxide (DMSO) could provide more details on the luminescence origin of methane-based carbon nanodots.[30,88,89]

### *8.2.2 Temperature Dependent Emission of Methane-Based Carbon Nanodots*

An increase in the emission intensity of carbon nanodots as a function of increased temperatures is an indicator for TADF.[97–103] TADF requires a small energy gap between the triplet and singlet excited-states and high probabilities of intersystem

and back intersystem crossing therefore, determining the energy gap between the singlet and triplet states ($\Delta G_{ST}$) of carbon nanodots would provide evidence that TADF is the mechanism for these temperature observations. The standard method for determining the $\Delta G_{ST}$ involves the measurement of delayed fluorescence and phosphorescence intensities as function of temperature and using a plot of $\ln(I_{DF}/I_P)$ vs 1/T.[97,98,100,102] Due to the lack of quality phosphorescent spectra of the methane-based carbon nanodots, an alternative method utilizing the temperature dependence of the ratio of $I_{DF}/I_{F,}$ would have to be used to determine the $\Delta G_{ST}$ (equation 8.1).[97,98,100,102]

$$\ln\left[\frac{I_F}{I_{DF}} - \left(\frac{1}{\phi_T} - 1\right)\right] = \ln\left(\frac{k_P + k_{NR}^T}{k_{ISC}^{T\rightarrow S}}\right) + \frac{\Delta G_{ST}}{RT} \qquad \textbf{(8.1)}$$

In this equation, $k_P + k_{NR}$ is dominated by the non-radiative pathway and the $\Delta G_{ST}$ is determined by plotting the left side versus 1/T.[97,98,100,102] However, this method requires the quantum yield of the triplet state ($\Phi_T$), which could be determined in a similar manner as the fluorescence quantum yield by comparing the carbon nanodots to standard phosphorescence fluorophores or by determining the lifetime of the triplet state, through time-revolved techniques. By finding both of these parameters, the $\Delta G_{ST}$ of methane-based carbon nanodots could be determined.

### *8.2.3 Bromination of Methane-Based Carbon Nanodots*

Optimization of the synthesis of phosphorescent carbon nanodots is needed in order to produce carbon nanodots with more consistent phosphorescence properties. One way to achieve this would be to incorporate iodide instead of bromide into the

nanodots. The efficiency of a halide to promote intersystem crossing is based on the atomic number (Z), i.e. $Z^4$, therefore, iodide ion has a larger atomic number and could promote more intersystem crossing than the bromide ion.[49–51] The experimental parameters could be adjusted in two ways to incorporate iodide into the nanodots. First, hydriodic acid (HI) could be used in place of hydrobromic acid, and the nanodots synthesized in the same manner as described in Chapter 6. However, this method showed some ability to produce phosphorescent nanodots but, it proved to be mostly inconsistent with bromide, as shown in Chapter 6. A second method to introduce iodide ion could be to vaporize $I_2$ and combine the vapor with the methane gas. This process would make the iodide available in the flame, which could allow for the iodide to be more efficiently incorporated into the structure of the nanodots, as opposed to the nanodots interacting with a solvent after they have been synthesized.

Optimization of the singlet oxygen experiments is also needed to improve the amount and detection of singlet oxygen produced. First, several experiments that purge the carbon nanodots sample with oxygen or nitrogen should be investigated. By purging with $N_2$ gas, all the $O_2$ should be removed from the sample, thus resulting in no $^1O_2$ generation. But when purging with $O_2$ gas, there should be more $^1O_2$ generation because there is sufficient oxygen available to interact with the carbon nanodots and the sensor green. These experiments could be used to determine if the carbon nanodots are able to produce large amounts of $^1O_2$ and if the low amounts observed in this research is due to a lack of oxygen in the sample. It is also possible that the detection method of $^1O_2$ is not ideal, therefore this should be further studied. Sensor green solutions are not stable for long periods of time, i.e. stock solution must

be used with 5 days, and the emission signal can vary in intensity day to day. [64,77–79,106] This makes sensor green difficult to optimize and work with, therefore, utilizing the direct detection of the phosphorescence of $^1O_2$ at 1270 nm could be a more beneficial detection method.[64,77–79,106]

# Bibliography


(1) Xu, X.; Ray, R.; Gu, Y.; Ploehn, H. J.; Gearheart, L.; Raker, K.; Scrivens, W. a. Electrophoretic Analysis and Purification of Fluorescent Single-Walled Carbon Nanotube Fragments. *J. Am. Chem. Soc.* **2004**, *126* (40), 12736–12737.

(2) Baker, S. N.; Baker, G. A. Luminescent Carbon Nanodots: Emergent Nanolights. *Angew. Chemie - Int. Ed.* **2010**, *49* (38), 6726–6744.

(3) Li, H.; Kang, Z.; Liu, Y.; Lee, S.-T. Carbon Nanodots: Synthesis, Properties and Applications. *J. Mater. Chem.* **2012**, *22* (46).

(4) Esteves da Silva, J. C. G.; Gonçalves, H. M. R. Analytical and Bioanalytical Applications of Carbon Dots. *TrAC - Trends Anal. Chem.* **2011**, *30* (8), 1327–1336.

(5) Wang, Y.; Hu, A. Carbon Quantum Dots: Synthesis, Properties and Applications. *J. Mater. Chem. C* **2014**, *2*, 6921–6939.

(6) Cayuela, A.; Soriano, M. L.; Carrillo-Carrión, C.; Valcárcel, M. Semiconductor and Carbon-Based Fluorescent Nanodots: The Need for Consistency. *Chem. Commun.* **2016**, *52* (7), 1311–1326.

(7) Carbon Nanodots from Molasses Reactive Oxygen Species.pdf.

(8) Chen, P.-C.; Chen, Y.-N.; Hsu, P.-C.; Shih, C.-C.; Chang, H.-T. Photoluminescent Organosilane-Functionalized Carbon Dots as Temperature Probes. *Chem. Commun. (Camb).* **2013**, *49* (X), 1639–1641.

(9) Yang, S. T.; Wang, X.; Wang, H.; Lu, F.; Luo, P. G.; Cao, L.; Meziani, M. J.; Liu, J. H.; Liu, Y.; Chen, M.; Huang, Y.; Sun, Y. P. Carbon Dots as Nontoxic and High-Performance Fluorescence Imaging Agents. *J. Phys. Chem. C* **2009**,

*113* (42), 18110–18114.

(10) Li, Q.; Ohulchanskyy, T. Y.; Liu, R.; Koynov, K.; Wu, D.; Best, A.; Kumar, R.; Bonoiu, A.; Prasad, P. N. Photoluminescent Carbon Dots as Biocompatible Nanoprobes for Targeting Cancer Cells in Vitro. *J. Phys. Chem. C* **2010**, *114* (28), 12062–12068.

(11) Cao, L.; Wang, X.; Meziani, M. J.; Lu, F.; Wang, H.; Luo, P. G.; Lin, Y.; Harruff, B. a.; Veca, L. M.; Murray, D.; Xie, S. Y.; Sun, Y. P. Carbon Dots for Multiphoton Bioimaging. *J. Am. Chem. Soc.* **2007**, *129* (37), 11318–11319.

(12) Yang, S. T.; Cao, L.; Luo, P. G.; Lu, F.; Wang, X.; Wang, H.; Meziani, M. J.; Liu, Y.; Qi, G.; Sun, Y. P. Carbon Dots for Optical Imaging in Vivo. *J. Am. Chem. Soc.* **2009**, *131* (32), 11308–11309.

(13) Ray, S. C.; Saha, A.; Jana, N. R.; Sarkar, R. Fluorescent Carbon Nanoparticles: Synthesis, Characterization, and Bioimaging Application. *J. Phys. Chem. C* **2009**, *113* (43), 18546–18551.

(14) Zhu, H.; Wang, X.; Li, Y.; Wang, Z.; Yang, F.; Yang, X. Microwave Synthesis of Fluorescent Carbon Nanoparticles with Electrochemiluminescence Properties. *Chem. Commun. (Camb).* **2009**, No. 34, 5118–5120.

(15) Liu, H.; Ye, T.; Mao, C. Fluorescent Carbon Nanoparticles Derived from Candle Soot. *Angew. Chemie - Int. Ed.* **2007**, *46* (34), 6473–6475.

(16) Liu, R.; Wu, D.; Liu, S.; Koynov, K.; Knoll, W.; Li, Q. An Aqueous Route to Multicolor Photoluminescent Carbon Dots Using Silica Spheres as Carriers. *Angew. Chemie - Int. Ed.* **2009**, *48* (25), 4598–4601.

(17) Peng, H.; Travas-Sejdic, J. Simple Aqueous Solution Route to Luminescent

Carbogenic Dots from Carbohydrates. *Chem. Mater.* **2009**, *21* (23), 5563–5565.

(18) Qu, S.; Wang, X.; Lu, Q.; Liu, X.; Wang, L. A Biocompatible Fluorescent Ink Based on Water-Soluble Luminescent Carbon Nanodots. *Angew. Chemie - Int. Ed.* **2012**, *51* (49), 12215–12218.

(19) Dong, Y.; Zhou, N.; Lin, X.; Lin, J.; Chi, Y.; Chen, G. Extraction of Electrochemiluminescent Oxidized Carbon Quantum Dots from Activated Carbon. *Chem. Mater.* **2010**, *22* (21), 5895–5899.

(20) Bao, L.; Zhang, Z. L.; Tian, Z. Q.; Zhang, L.; Liu, C.; Lin, Y.; Qi, B.; Pang, D. W. Electrochemical Tuning of Luminescent Carbon Nanodots: From Preparation to Luminescence Mechanism. *Adv. Mater.* **2011**, *23* (48), 5801–5806.

(21) Vinci, J. C.; Colon, L. A. Fractionation of Carbon-Based Nanomaterials by Anion-Exchange HPLC. **2012**.

(22) Sun, Y.-P.; Wang, X.; Lu, F.; Cao, L.; Meziani, M. J.; Luo, P. G.; Gu, L.; Veca, L. M. Doped Carbon Nanoparticles as a New Platform for Highly Photoluminescent Dots. *J. Phys. Chem. C* **2008**, *112* (47), 18295–18298.

(23) Sun, Y. P.; Zhou, B.; Lin, Y.; Wang, W.; Fernando, K. a S.; Pathak, P.; Meziani, M. J.; Harruff, B. a.; Wang, X.; Wang, H.; Luo, P. G.; Yang, H.; Kose, M. E.; Chen, B.; Veca, L. M.; Xie, S. Y. Quantum-Sized Carbon Dots for Bright and Colorful Photoluminescence. *J. Am. Chem. Soc.* **2006**, *128* (24), 7756–7757.

(24) Zhou, J.; Booker, C.; Li, R.; Zhou, X.; Sham, T. K.; Sun, X.; Ding, Z. An

Electrochemical Avenue to Blue Luminescent Nanocrystals from Multiwalled Carbon Nanotubes (MWCNTs). *J. Am. Chem. Soc.* **2007**, *129* (4), 744–745.

(25) Zheng, L.; Chi, Y.; Dong, Y.; Lin, J.; Wang, B. Electrochemiluminescence of Water-Soluble Carbon Nanocrystals Released Electrochemically from Graphite. *J. Am. Chem. Soc.* **2009**, *131* (13), 4564–4565.

(26) Bourlinos, A. B.; Stassinopoulos, A.; Anglos, D.; Zboril, R.; Georgakilas, V.; Giannelis, E. P. Photoluminescent Carbogenic Dots. *Chem. Mater.* **2008**, *20* (14), 4539–4541.

(27) Zhang, B.; Liu, C. Y.; Liu, Y. A Novel One-Step Approach to Synthesize Fluorescent Carbon Nanoparticles. *Eur. J. Inorg. Chem.* **2010**, No. 28, 4411–4414.

(28) Lin, Z.; Xue, W.; Chen, H.; Lin, J.-M. Classical Oxidant Induced Chemiluminescence of Fluorescent Carbon Dots. *Chem. Commun.* **2012**, *48* (7), 1051.

(29) Bourlinos, A. B.; Zbořil, R.; Petr, J.; Bakandritsos, A.; Krysmann, M.; Giannelis, E. P. Luminescent Surface Quaternized Carbon Dots. *Chem. Mater.* **2012**, *24* (1), 6–8.

(30) Gonçalves, H.; Da Silva, J. C. G. E. Fluorescent Carbon Dots Capped with PEG 200 and Mercaptosuccinic Acid. *J. Fluoresc.* **2010**, *20* (5), 1023–1028.

(31) Zhang, W. F.; Zhu, H.; Yu, S. F.; Yang, H. Y. Observation of Lasing Emission from Carbon Nanodots in Organic Solvents. *Adv. Mater.* **2012**, *24* (17), 2263–2267.

(32) Lu, J.; Yang, J.; Wang, J.; Lim, A.; Wang, S.; Loh, K. P. One-Pot Synthesis of

Fluorescent Carbon Graphene by the Exfoliation of Graphite in Ionic Liquids. *ACS Nano* **2009**, *3* (8), 2367–2375.

(33) Zhang, Y.; Gonçalves, H.; da Silva, J. C. G. E.; Geddes, C. D. Metal-Enhanced Photoluminescence from Carbon Nanodots. *Chem. Commun. (Camb).* **2011**, *47* (18), 5313–5315.

(34) Baker, J. S.; Colón, L. A. Influence of Buffer Composition on the Capillary Electrophoretic Separation of Carbon Nanoparticles. *J. Chromatogr. A* **2009**, *1216* (52), 9048–9054.

(35) Shi, W.; Li, X.; Ma, H. A Tunable Ratiometric Ph Sensor Based on Carbon Nanodots for the Quantitative Measurement of the Intracellular pH of Whole Cells. *Angew. Chemie - Int. Ed.* **2012**, *51* (26), 6432–6435.

(36) Zhou, Y.; Xing, G.; Chen, H.; Ogawa, N.; Lin, J. M. Carbon Nanodots Sensitized Chemiluminescence on Peroxomonosulfate-Sulfite- Hydrochloric Acid System and Its Analytical Applications. *Talanta* **2012**, *99*, 471–477.

(37) Zhu, H.; Wang, X.; Li, Y.; Wang, Z.; Yang, F.; Yang, X. Microwave Synthesis of Fluorescent Carbon Nanoparticles with Electrochemiluminescence Properties. (Supporting Information). *Chem. Commun. (Camb).* **2009**, No. 34, 5118–5120.

(38) Xue, W.; Lin, Z.; Chen, H.; Lu, C.; Lin, J. M. Enhancement of Ultraweak Chemiluminescence from Reaction of Hydrogen Peroxide and Bisulfite by Water-Soluble Carbon Nanodots. *J. Phys. Chem. C* **2011**, *115* (44), 21707–21714.

(39) Han, L.; Ghosh, D.; Chen, W.; Pradhan, S.; Chang, X.; Chen, S. Nanosized

Carbon Particles from Natural Gas Soot. *Chem. Mater.* **2009**, *21* (13), 2803–2809.

(40) Kamat, P. V. Photophysical, Photochemical and Photocatalytic Aspects of Metal Nanoparticles. *J. Phys. Chem. B* **2002**, *106* (32), 7729–7744.

(41) Bruno, a.; de Lisio, C.; Iuorio, M.; Minutolo, P. Diffusivity in Water and Fluorescence Properties of Organic Nanoparticles Produced in Flames. *Appl. Phys. B* **2011**, *102* (4), 711–715.

(42) Krysmann, M. J.; Kelarakis, A.; Dallas, P.; Giannelis, E. P. Formation Mechanism of Carbogenic Nanoparticles with Dual Photoluminescence Emission. *J. Am. Chem. Soc.* **2012**, *134* (2), 747–750.

(43) Strauss, V.; Margraf, J. T.; Dolle, C.; Butz, B.; Nacken, T. J.; Walter, J.; Bauer, W.; Peukert, W.; Spiecker, E.; Clark, T.; Guldi, D. M. Carbon Nanodots: Toward a Comprehensive Understanding of Their Photoluminescence. *J. Am. Chem. Soc.* **2014**, *136* (49), 17308–17316.

(44) Marzari, G.; Gm, M.; Ms, M.; Di, G.-G.; Fungo, F. The Optoelectronic Behaviour of Carbon Nanoparticles: Evidence of the Importance of the Outer Carbon Shell. *Nanoscale* **2013**, *5* (17), 7977–7983.

(45) Ghosh, S.; Chizhik, A. M.; Karedla, N.; Dekaliuk, M. O.; Gregor, I.; Schuhmann, H.; Seibt, M.; Bodensiek, K.; Schaap, I. A. T.; Schulz, O.; Demchenko, A. P.; Enderlein, J.; Chizhik, A. I. Photoluminescence of Carbon Nanodots: Dipole Emission Centers and Electron-Phonon Coupling. *Nano Lett.* **2014**, *14* (10), 5656–5661.

(46) Tao, Y.; Yuan, K.; Chen, T.; Xu, P.; Li, H.; Chen, R.; Zheng, C.; Zhang, L.;

Huang, W. Thermally Activated Delayed Fluorescence Materials towards the Breakthrough of Organoelectronics. *Adv. Mater.* **2014**, *26* (47), 7931–7958.

(47) Wang, L.; Zhu, S.; Wang, H.; Qu, S.; Zhang, Y.; Zhang, J.; Chen, Q.; Al, W. E. T. Common Origin of Green Luminescence in Carbon Nanodots and Graphene Quantum Dots. **2014**, No. 3, 2541–2547.

(48) Frigerio, C.; Ribeiro, D. S. M.; Rodrigues, S. S. M.; Abreu, V. L. R. G.; Barbosa, J. A. C.; Prior, J. A. V; Marques, K. L.; Santos, J. L. M. Application of Quantum Dots as Analytical Tools in Automated Chemical Analysis: A Review. *Anal. Chim. Acta* **2012**, *735*, 9–22.

(49) Lakowicz, J. *Principles of Fluorescence Spectroscopy*, Third.; Springer: Baltimore, MD, 2006.

(50) Valeur, B. *Molecular Fluorescence Principles and Applications*; Wiley-VCH Verlah GmbH: Weinheim, Germany, 2001.

(51) Klessinger, M.; Michl, J. Chapter 5: Photophysical Processes. In *Excited States and Photochemistry of Organic Molecules*; VCH Publishers: New York, NY, 1995; pp 243–308.

(52) Redmond, R. Introduction to Fluorescence and Photophysics. In *Handbook of Biomedical Fluorescence*; Mycek, M.-A., Pogue, B., Eds.; Marcel Dekker, Inc: New York, NY, 2003; pp 1–27.

(53) Hahn, D. Raman Scattering Theory, University of Florida, 2007.

(54) Saidi, I. S.; Jacques, S. L.; Tittel, F. K. Mie and Rayleigh Modeling of Visible-Light Scattering in Neonatal Skin. *Appl. Opt.* **1995**, *34* (31), 7410–7418.

(55) Grabolle, M.; Spieles, M.; Lesnyak, V.; Gaponik, N.; Eychmüller, A.; Resch-

Genger, U. Determination of the Fluorescence Quantum Yield of Quantum Dots. *Suitable Proced. Achievable Uncertainties* **2009**, *81* (15), 6285–6294.

(56) Rurack, K. *Fluorescence Quantum Yields — Methods of Determination and Standards*.

(57) Geddes, C. D. Optical Halide Sensing Using Fluorescence Quenching: Theory, Simulations and Applications - a Review. *Meas. Sci. Technol.* **2001**, *12* (9), R53–R88.

(58) Geddes, C. D.; Lakowicz, J. R. Metal-Enhanced Fluorescence. *J. Fluoresc.* **2002**, *12* (2), 121–129.

(59) Zhang, Y.; Dragan, A.; Geddes, C. D. Wavelength Dependence of Metal-Enhanced Fluorescence. *J. Phys. Chem. C* **2009**, *113* (28), 12095–12100.

(60) Deng, W.; Xie, F.; Baltar, H. T. M. C. M.; Goldys, E. M. Metal-Enhanced Fluorescence in the Life Sciences: Here, Now and beyond. *Phys. Chem. Chem. Phys.* **2013**, *15* (38), 15695–15708.

(61) Dragan, A. I.; Bishop, E. S.; Casas-Finet, J. R.; Strouse, R. J.; McGivney, J.; Schenerman, M. A.; Geddes, C. D. Distance Dependence of Metal-Enhanced Fluorescence. *Plasmonics* **2012**, *7* (4), 739–744.

(62) Pribik, R.; Dragan, A. I.; Zhang, Y.; Gaydos, C.; Geddes, C. D. Metal-Enhanced Fluorescence (MEF): Physical Characterization of Silver-Island Films and Exploring Sample Geometries. *Chem. Phys. Lett.* **2009**, *478* (1–3), 70–74.

(63) Zhang, Y.; Aslan, K.; Previte, M. J. R.; Geddes, C. D. Metal-Enhanced Fluorescence: Surface Plasmons Can Radiate a Fluorophore's Structured

Emission. *Appl. Phys. Lett.* **2007**, *90* (5), 1–3.

(64) Zhang, Y.; Aslan, K.; Previte, M. J. R.; Geddes, C. D. Metal-Enhanced Singlet Oxygen Generation: A Consequence of Plasmon Enhanced Triplet Yields. *J. Fluoresc.* **2007**, *17* (4), 345–349.

(65) Golberg, K.; Elbaz, A.; Zhang, Y.; Dragan, A. I.; Marks, R.; Geddes, C. D. Mixed-Metal Substrates for Applications in Metal-Enhanced Fluorescence. *J. Mater. Chem.* **2011**, *21* (17), 6179.

(66) Siraj, N.; El-Zahab, B.; Hamdan, S.; Karam, T. E.; Haber, L. H.; Li, M.; Fakayode, S. O.; Das, S.; Valle, B.; Strongin, R. M.; Patonay, G.; Sintim, H. O.; Baker, G. A.; Powe, A.; Lowry, M.; Karolin, J. O.; Geddes, C. D.; Warner, I. M. Fluorescence, Phosphorescence, and Chemiluminescence. *Anal. Chem.* **2016**, *88* (1), 170–202.

(67) Mishra, H.; Dragan, A.; Geddes, C. D. UV to NIR Surface Plasmon Coupled and Metal-Enhanced Fluorescence Using Indium Thin Films: Application to Intrinsic (Label-Less) Protein Fluorescence Detection. *J. Phys. Chem. C* **2011**, *115* (35), 17227–17236.

(68) Zhang, Y.; Aslan, K.; Malyn, S. N.; Geddes, C. D. Metal-Enhanced Phosphorescence (MEP). *Chem. Phys. Lett.* **2006**, *427* (4–6), 432–437.

(69) Zhang, Y.; Aslan, K.; Previte, M. J. R.; Malyn, S. N.; Geddes, C. D. Metal-Enhanced Phosphorescence: Interpretation in Terms of Triplet-Coupled Radiating Plasmons. *J. Phys. Chem. B* **2006**, *110* (49), 25108–25114.

(70) Zhang, Y.; Gonçalves, H.; da Silva, J. C. G. E.; Geddes, C. D.; Aslan, K.; Malyn, S. N.; Geddes, C. D.; Previte, M. J. R.; Malyn, S. N.; Geddes, C. D.;

Golberg, K.; Elbaz, A.; Zhang, Y.; Dragan, A. I.; Marks, R.; Geddes, C. D.; Karolin, J.; Geddes, C. D.; Zhang, Y.; Dragan, A. I.; Geddes, C. D.; Mishra, H.; Mali, B. L.; Karolin, J.; Dragan, A. I.; Geddes, C. D.; Pribik, R.; Dragan, A. I.; Zhang, Y.; Gaydos, C.; Geddes, C. D.; Hamo, H. Ben; Karolin, J.; Mali, B. L.; Kushmaro, A.; Marks, R.; Geddes, C. D.; Deng, W.; Xie, F.; Baltar, H. T. M. C. M.; Goldys, E. M.; Zhang, Y.; Aslan, K.; Previte, M. J. R.; Geddes, C. D. Metal-Enhanced Fluorescence: Surface Plasmons Can Radiate a Fluorophore's Structured Emission. *Appl. Phys. Lett.* **2011**, *15* (45), 6179.

(71) Dragan, A. I.; Geddes, C. D. Author ' S Personal Copy Wavelength-Dependent Metal-Enhanced Fluorescence Using Synchronous Spectral Analysis.

(72) Karolin, J.; Geddes, C. Spectral Shifts in Metal-Enhanced Fluorescence. *Appl. Phys. Lett.* **2014**, *105* (6), 1–4.

(73) Aslan, K.; Geddes, C. D. Microwave-Accelerated Metal-Enhanced Fluorescence: Platform Technology for Ultrafast and Ultrabright Assays. *Anal. Chem.* **2005**, *77* (24), 8057–8067.

(74) Dragan, A. I.; Albrecht, M. T.; Pavlovic, R.; Keane-Myers, A. M.; Geddes, C. D. Ultra-Fast Pg/ml Anthrax Toxin (Protective Antigen) Detection Assay Based on Microwave-Accelerated Metal-Enhanced Fluorescence. *Anal. Biochem.* **2012**, *425* (1), 54–61.

(75) Dragan, a I.; Geddes, C. D. Excitation Volumetric Effects (EVE) in Metal-Enhanced Fluorescence. *Phys. Chem. Chem. Phys.* **2011**, *13* (9), 3831–3838.

(76) Hamo, H. Ben; Karolin, J.; Mali, B.; Kushmaro, A.; Marks, R.; Geddes, C. D. Metal-Enhanced Fluorescence from Zinc Substrates Can Lead to Spectral

Distortion and a Wavelength Dependence. *Appl. Phys. Lett.* **2015**, *106* (8).

(77) Ogilby, P. R. Singlet Oxygen: There Is Indeed Something New under the Sun. *Chem. Soc. Rev.* **2010**, *39* (8), 3181.

(78) Ogilby, P. R. P.; Foote, C. C. S. Chemistry of Singlet Oxygen. 42. Effect of Solvent, Solvent Isotopic Substitution, and Temperature on the Lifetime of Singlet Molecular Oxygen (1. DELTA. G). *J. Am. Chem. Soc.* **1981**, *103* (11), 3423–3430.

(79) DeRosa, M. C.; Crutchley, R. J. Photosensitized Singlet Oxygen and Its Applications. *Coord. Chem. Rev.* **2002**, *233–234*, 351–371.

(80) Zhang, Y.; Aslan, K.; Previte, M. J. R.; Geddes, C. D. Plasmonic Engineering of Singlet Oxygen Generation. *Proc. Natl. Acad. Sci. U. S. A.* **2008**, *105* (6), 1798–1802.

(81) Ragàs, X.; Gallardo, A.; Zhang, Y.; Massad, W.; Geddes, C. D.; Nonell, S. Singlet Oxygen Phosphorescence Enhancement by Silver Islands Films. *J. Phys. Chem. C* **2011**, *115* (33), 16275–16281.

(82) Karolin, J.; Geddes, C. D. Metal-Enhanced Fluorescence Based Excitation Volumetric Effect of Plasmon-Enhanced Singlet Oxygen and Super Oxide Generation. *Phys. Chem. Chem. Phys.* **2013**, *15* (38), 15740–15745.

(83) Zhao, L. Singlet Oxygen, The University of Iowa, 2001.

(84) Fletcher, R. *Practical Methods of Optimization*, Second.; John Wiley &Sons, Inc: West Sussex, England, 1987.

(85) Gill, P.; Murray, W.; Wright, M. *Practical Optimization*; Emerald Group Publishing Limited: Bingley, UK, 1982.

(86) Hock, W.; Schittkowski, K. A Comparative Performance Evaluation of 27 Nonlinear Programming Codes. *Computing* **1983**, *30*, 335–358.

(87) Li, J.; Li, W.; Qiang, W.; Wang, X.; Li, H.; Xu, D. A Non-Aggregation Colorimetric Assay for Thrombin Based on Catalytic Properties of Silver Nanoparticles. *Anal. Chim. Acta* **2014**.

(88) Reckmeier, C. J.; Wang, Y.; Zboril, R.; Rogach, A. L. Influence of Doping and Temperature on Solvatochromic Shifts in Optical Spectra of Carbon Dots. *J. Phys. Chem. C* **2016**, *120* (19), 10591–10604.

(89) Li, X.; Wang, H.; Shimizu, Y.; Pyatenko, A.; Kawaguchi, K.; Koshizaki, N. Preparation of Carbon Quantum Dots with Tunable Photoluminescence by Rapid Laser Passivation in Ordinary Organic Solvents. *Chem. Commun. (Camb).* **2011**, *47* (NOVEMBER), 932–934.

(90) Kumar, P.; Bohidar, H. B. Observation of Fluorescence from Non-Functionalized Carbon Nanoparticles and Its Solvent Dependent Spectroscopy. *J. Lumin.* **2013**, *141*, 155–161.

(91) Deng, Y.; Chen, X.; Wang, F.; Zhang, X.; Zhao, D.; Shen, D. Nanoscale Solid State Carbon Dots and Its Mechanism †. *Nanoscale* **2014**, *6* (17), 10388–10393.

(92) Maiti, R.; Mukherjee, S.; Haldar, S.; Bhowmick, D.; Ray, S. K. Novel Thermal Quenching Characteristics of Luminescent Carbon Nanodots via Tailoring the Surface Chemical Groups. *Carbon N. Y.* **2016**, *104*, 226–232.

(93) Song, Y.; Zhu, S.; Xiang, S.; Zhao, X.; Zhang, J.; Zhang, H.; Fu, Y.; Yang, B. Investigation into the Fluorescence Quenching Behaviors and Applications of

Carbon Dots. *Nanoscale* **2014**, *6* (9), 4676–4682.

(94) Wang, C.; Xu, Z.; Cheng, H.; Lin, H.; Humphrey, M. G.; Zhang, C. A Hydrothermal Route to Water-Stable Luminescent Carbon Dots as Nanosensors for pH and Temperature. *Carbon N. Y.* **2015**, *82* (C), 87–95.

(95) Song, Z.; Quan, F.; Xu, Y.; Liu, M.; Cui, L.; Liu, J. Multifunctional N,S Co-Doped Carbon Quantum Dots with pH- and Thermo-Dependent Switchable Fluorescent Properties and Highly Selective Detection of Glutathione. *Carbon N. Y.* **2016**, *104*, 169–178.

(96) Yu, P.; Wen, X.; Toh, Y. R.; Tang, J. Temperature-Dependent Fluorescence in Carbon Dots. *J. Phys. Chem. C* **2012**, *116* (48), 25552–25557.

(97) Berberan, N.; Garcia, M. M. Unusually Strong Delayed Fluorescence of C 70. *J. Am. Chem. Soc.* **1996**, *7863* (13), 9391–9394.

(98) Kropp, J. L.; Dawson, W. R. Radiationless Deactivation of Triplet Coronene in Plastics. *J. Phys. Chem.* **1967**, *71* (13), 4499–4506.

(99) Tanaka, F. Pressure and Temperature Dependences of the Rate Constant for S 1 - T ~ Intersystem. **1995**, 525–530.

(100) Baleizão, C.; Berberan-Santos, M. N. Thermally Activated Delayed Fluorescence in Fullerenes. *Ann. N. Y. Acad. Sci.* **2008**, *1130*, 224–234.

(101) Augusto, V.; Baleizão, C.; Berberan-Santos, M. N.; Farinha, J. P. S. Oxygen-Proof Fluorescence Temperature Sensing with Pristine C70 Encapsulated in Polymer Nanoparticles. *J. Mater. Chem.* **2010**, *20* (6), 1192.

(102) Salazar, F. a.; Fedorov, A.; Berberan-Santos, M. N. A Study of Thermally Activated Delayed Fluorescence in C60. *Chem. Phys. Lett.* **1997**, *271* (4–6),

361–366.

(103) Fister III, J. C.; Harris, J. M.; Rank, D.; Wacholtz, W. Molecular Photophysics of Acridine Yellow Studied by Phosphorescence and Delayed Fluorescence: An Undergraduate Physical Chemistry Experiment. *J. Chem. Educ.* **1997**, *74* (10), 1208–1212.

(104) Hou, J.; Wang, L.; Zhang, P.; Xu, Y.; Ding, L. Facile Synthesis of Carbon Dots in an Immiscible System with Excitation-Independent Emission and Thermally Activated Delayed Fluorescence. *Chem. Commun.* **2015**, *51*, 17768–17771.

(105) Foote, C. S. Photosensitized Oxygenations and the Role of Singlet Oxygen. *Acc. Chem. Res.* **1968**, *1* (6), 104–110.

(106) Ogilby, P. R. Solvent Effects on the Radiative Transitions of Singlet Oxygen. *Acc. Chem. Res.* **1999**, *32* (6), 512–519.

(107) Viscosities http://www.kayelaby.npl.co.uk/general_physics/2_2/2_2_3.html.

(108) Malicka, J.; Gryczynski, I.; Geddes, C. D.; Lakowicz, J. R. Metal-Enhanced Emission from Indocyanine Green: A New Approach to in Vivo Imaging. *J. Biomed. Opt.* **2003**, *8* (3), 472–478.

(109) Dragan, A. I.; Bishop, E. S.; Strouse, R. J.; Casas-Finet, J. R.; Schenerman, M. A.; Geddes, C. D. Metal-Enhanced Ethidium Bromide Emission: Application to dsDNA Detection. *Chem. Phys. Lett.* **2009**, *480* (4–6), 296–299.

(110) Chowdhury, M. H.; Ray, K.; Aslan, K.; Lakowicz, J. R.; Geddes, C. D. Metal-Enhanced Fluorescence of Phycobiliproteins from Heterogeneous Plasmonic Nanostructures. *J. Phys. Chem. C* **2007**, *111* (51), 18856–18863.